AD-A174 597 BEHAVIOR OF PARTIALLY RESTRAINED REINFORCED CONCRETE SLABS(U) ARMY ENGINEER WATERWAYS EXPERIMENT STATION VICKSBURG MS STRUCTURES LAB L K GUICE SEP 86 1/3

UNCLASSIFIED WES/TR/SL-86-32 F/G 13/3 NL

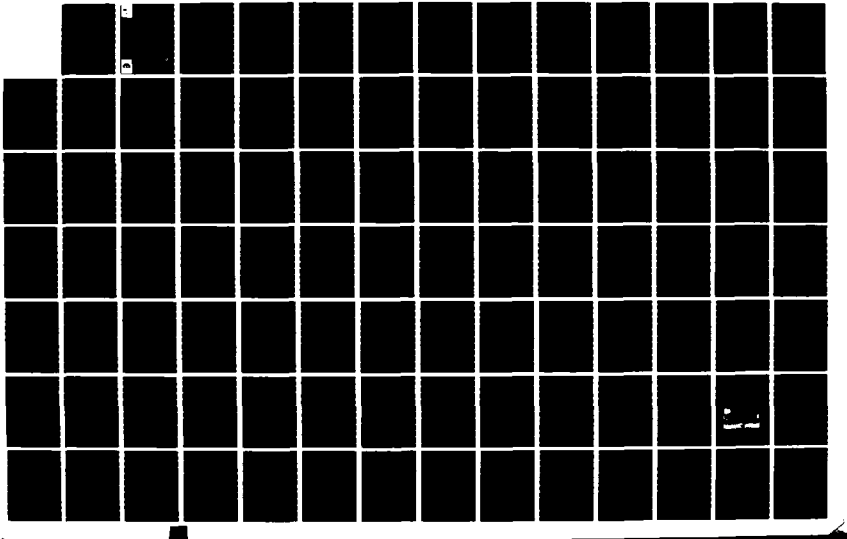

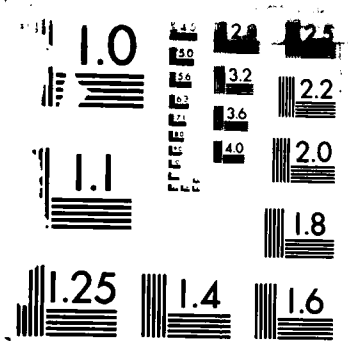

MICROCOPY RESOLUTION TEST CHART

US Army Corps of Engineers

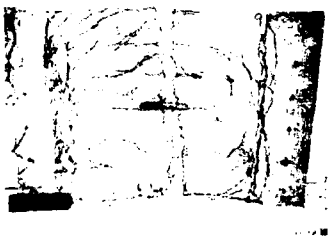

STRUCTURES LABORATORY

(12)

TECHNICAL REPORT SL-86-32

BEHAVIOR OF PARTIALLY RESTRAINED REINFORCED CONCRETE SLABS

by

L. K. Guice

Structures Laboratory

DEPARTMENT OF THE ARMY
Waterways Experiment Station, Corps of Engineers
PO Box 631, Vicksburg, Mississippi 39180-0631

September 1986
Final Report

Prepared for Federal Emergency Management Agency
Washington, DC 20472

TECHNICAL REPORT SL-86-32

BEHAVIOR OF PARTIALLY RESTRAINED REINFORCED CONCRETE SLABS

by

L. K. Guice

Structures Laboratory

DEPARTMENT OF THE ARMY
Waterways Experiment Station, Corps of Engineers
PO Box 631, Vicksburg, Mississippi 39180-0631

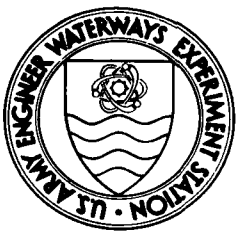

September 1986
Final Report

Prepared for Federal Emergency Management Agency
Washington, DC 20472

Unclassified
SECURITY CLASSIFICATION OF THIS PAGE

ADA174597

REPORT DOCUMENTATION PAGE

Form Approved
OMB No 0704-0188
Exp Date Jun 30 1986

1a REPORT SECURITY CLASSIFICATION Unclassified	1b RESTRICTIVE MARKINGS
2a SECURITY CLASSIFICATION AUTHORITY	3 DISTRIBUTION / AVAILABILITY OF REPORT Approved for public release; distribution unlimited.
2b DECLASSIFICATION / DOWNGRADING SCHEDULE	
4 PERFORMING ORGANIZATION REPORT NUMBER(S) Technical Report SL-86-32	5 MONITORING ORGANIZATION REPORT NUMBER(S)
6a NAME OF PERFORMING ORGANIZATION USAEWES Structures Laboratory 6b OFFICE SYMBOL (If applicable) WESSS	7a NAME OF MONITORING ORGANIZATION
6c ADDRESS (City, State, and ZIP Code) PO Box 631 Vicksburg, MS 39180-0631	7b ADDRESS (City, State, and ZIP Code)
8a NAME OF FUNDING / SPONSORING ORGANIZATION Federal Emergency Management Agency 8b OFFICE SYMBOL (If applicable)	9 PROCUREMENT INSTRUMENT IDENTIFICATION NUMBER
8c ADDRESS (City, State, and ZIP Code) Washington, DC 20472	10 SOURCE OF FUNDING NUMBERS PROGRAM ELEMENT NO / PROJECT NO / TASK NO / WORK UNIT ACCESSION NO

11 TITLE (Include Security Classification)
Behavior of Partially Restrained Reinforced Concrete Slabs

12 PERSONAL AUTHOR(S)
Guice, L. K.

13a TYPE OF REPORT	13b TIME COVERED	14 DATE OF REPORT (Year, Month, Day)	15 PAGE COUNT
Final report	FROM _____ TO _____	September 1986	197

16 SUPPLEMENTARY NOTATION
Available from National Technical Information Service, 5285 Port Royal Road, Springfield, VA 22161.

17 COSATI CODES			18 SUBJECT TERMS (Continue on reverse if necessary and identify by block number)
FIELD	GROUP	SUB-GROUP	Blast effect Concrete slabs Reinforced concrete construction

19 ABSTRACT (Continue on reverse if necessary and identify by block number)

This study was performed in conjunction with a Federal Emergency Management Agency program to plan, design, and construct Keyworker blast shelters. Keyworker shelters are box-type shelters in which damage is more likely in the roof slab than in the walls or floor. This study investigates the effect of partial edge restraint on the strength, ductility, and failure mechanisms of a slab.

Sixteen one-way, reinforced concrete plate elements were tested in a specially designed reaction structure under uniform static water pressure. Facilities were designed and constructed to measure the slab end actions, including thrusts, moments, and rotations. The primary parameters investigated included the span-thickness ratio, reinforcement ratio, and degree of edge restraint. Most slabs were loaded until significant tensile membrane forces developed.

(Continued)

20 DISTRIBUTION / AVAILABILITY OF ABSTRACT	21 ABSTRACT SECURITY CLASSIFICATION
☒ UNCLASSIFIED/UNLIMITED ☐ SAME AS RPT ☐ DTIC USERS	Unclassified
22a NAME OF RESPONSIBLE INDIVIDUAL	22b TELEPHONE (Include Area Code) / 22c OFFICE SYMBOL

DD FORM 1473, 84 MAR — 83 APR edition may be used until exhausted. All other editions are obsolete.

SECURITY CLASSIFICATION OF THIS PAGE
Unclassified

19. ABSTRACT (Continued).

Rotational restraint significantly influenced overall slab behavior. If a slab is to develop significant compressive membrane forces, both lateral and rotational restraint must be provided. Small rotational freedoms had a relatively small effect on the slab's compressive membrane response. With large rotational freedoms, however, the slabs generally snapped through to the tensile membrane stage before significant thrusts were developed. Thin slabs generally exhibited a much better tensile membrane response than thicker slabs and underwent larger deflections before collapse.

Recommendations are presented and an analytical procedure which considers nonlinear geometric behavior is proposed for investigating total slab response.

Keywords: Blast effect, Concrete slabs.

PREFACE

The research reported herein was sponsored by the Federal Emergency Management Agency (FEMA) through the US Army Engineer Division, Huntsville (HND).

Construction and testing were conducted by personnel of the Structural Mechanics Division (SMD), Structures Laboratory (SL), US Army Engineer Waterways Experiment Station (WES), under the general supervision of Mr. Bryant Mather, Chief, SL, and Mr. J. T. Ballard, Assistant Chief, SL, and under the direct supervision of Dr. J. P. Balsara, Chief, SMD. The project was managed by Dr. S. A. Kiger, and Mr. S. C. Woodson supervised the experiments. This report was prepared by Mr. L. K. Guice, who worked for SMD at the time of this investigation. This document was submitted in similar form to Texas A&M University as a Ph.D. dissertation. This report is a more comprehensive version of WES Technical Report SL-86-2, "Effects of Edge Restraint on Slab Behavior."

COL Allen F. Grum, USA, was the previous Director of WES. COL Dwayne G. Lee, CE, is the present Commander and Director. Dr. Robert W. Whalin is the Technical Director.

CONTENTS

LIST OF FIGURES

LIST OF TABLES

CONVERSION FACTORS, NON-SI TO SI (METRIC)
UNITS OF MEASUREMENT

Non-SI units of measurement used in this report can be converted to SI (metric) units as follows:

Multiply	By	To Obtain
degrees	0.01745	radians
feet	0.3048	metres
inches	2.54	centimetres
inch-pounds	0.1129848	newton-metres
kips (force) per inch	175.1268	kilonewtons per metre
kips per square inch	6.894757	megapascals
pounds (force)	4.448222	newtons
pounds (force) per square inch	6.894757	kilopascals
square inches	6.4516	square centimetres

CHAPTER I

INTRODUCTION

BACKGROUND

Fundamental Slab Behavior.-A reinforced concrete slab is one of the most common types of structural elements. Slabs are found in practically every type of structural system, whether steel or concrete, single-story or highrise, or shortspan or longspan. Yet the actual behavior of slabs under increasing loads is rather poorly understood. As a result, most practitioners use simplified analytical techniques which have proven to yield safe and conservative designs.

However, researchers have provided an abundance of data from which more reliable analyses can be derived. The behavior of reinforced concrete slabs has been investigated since the first of the century. Classical elasticity and plasticity theories have both been applied to the analysis of slabs. But the complexity of elasticity theory and difficulties in defining deflection functions compatible with boundary conditions have limited the direct applicability of the theory. Because of the nature of reinforced concrete slabs, accurate evaluations of stresses, strains, and deflections are difficult to make by elasticity concepts,

particularly at higher load levels. However, conservative assumptions and approximations to the theory have led to the general acceptance of elasticity theory by the design community. The methodology of design presented in the Building Code Requirements for Reinforced Concrete [6] defines distributions of moments based on elasticity theory.

In recent years, plasticity theories [27] have become the most predominant methods of slab analysis because of the need to provide more realistic factors of safety and because of the general trend toward limit state analysis. Johansen's yield line plasticity theory [17] has offered a means for determining the ultimate capacity of slabs. The yield line theory is based on the plastic moment capacities along a slab's critical cross-sections, i.e., yield lines. When the moment capacities of enough sections have been exceeded to permit a mechanism to form, the slab is considered to have achieved its limiting capacity. For many years, the method was theoretically recognized as an upper bound approach because it was assumed to predict an ultimate capacity for a slab which is either correct or too high [27,36].

More recently, tests by numerous investigators [34] have confirmed that the yield line theory significantly underpredicts the strength of slabs, particularly if the slabs are laterally restrained. The enhancement in strength over the yield line capacity is attributable to compressive membrane action. Compressive thrusts resulting from the restricted movement of the slab's edges increase the moment

capacities of the critical cross-sections and, consequently, enhance the total capacity of the slab. The generation of thrusts as the slab undergoes small deflections and the effect of arching in the slab are illustrated in Fig. 1.1.

Although most attention has been given to investigating slab behavior during small and moderate deflections, there has been a growing interest in understanding slab behavior throughout large deflections. Fig. 1.2 illustrates the three distinct phases of behavior which are evident in the load versus deflection curve for a restrained concrete slab. Initially, the load increases with deflection until the maximum load is reached. This initial portion of the curve is referred to as the compressive membrane stage because of the presence of in-plane compressive forces. Some writers [3,4] denote this as the elastic stage since the material behaves elastically and elasto-plastically.

At point A, a mechanism forms and the load decreases with increasing deflection until the whole section is fully cracked in depth at point B. This transition region, sometimes referred to as the decay region, is characterized by gradually decreasing in-plane forces and could still be considered to be part of the compressive membrane stage. However, resultant tensile forces may actually be present in some parts of the slab as the slab goes through this transition stage. For thick slabs, the drop in load during the transition stage is due to decreasing thrusts resulting

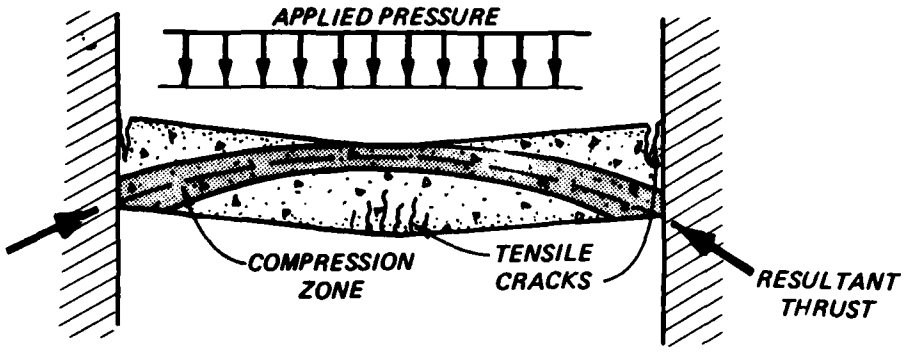

FIG. 1.1.-Compressive Membrane Action

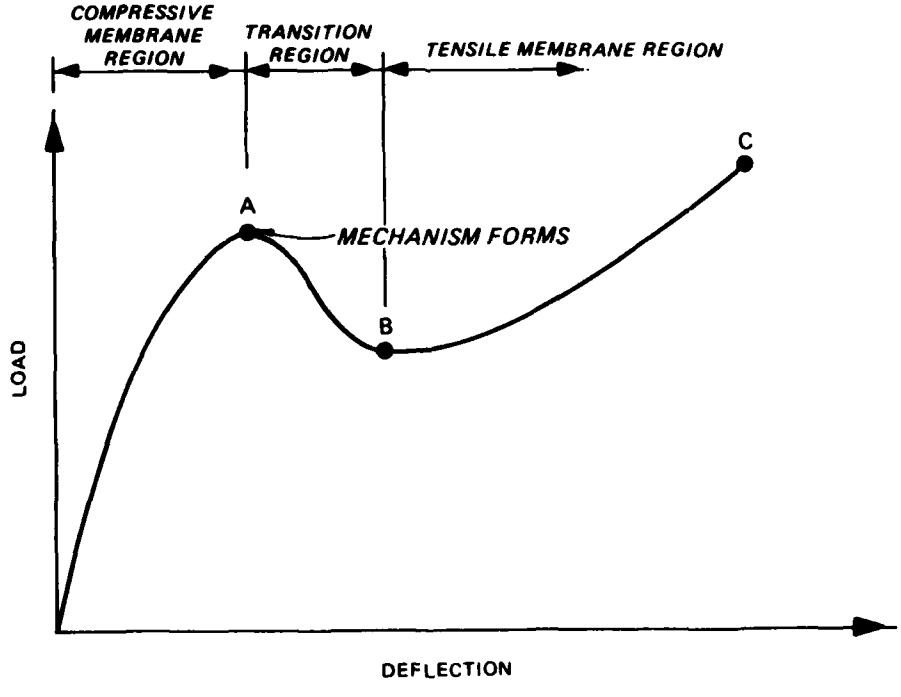

FIG. 1.2.-Load-Deflection Relationship for Restrained Slabs

from crushing of the concrete. For thin slabs, geometric instability may lead to a drop in the load-carrying capacity following point A.

With further deflection beyond point B, the load is carried almost entirely by tension in the reinforcement. As illustrated in Fig. 1.3, full-depth cracks usually appear throughout the slab and the slab generally takes a shape resembling a net or a catenary. Hence, the region from point B to C is known as the tensile membrane stage. If load is continued in the tensile membrane stage, the slab undergoes larger deflections until the reinforcement reaches its breaking strain at point C. The deflection at C is called the incipient collapse deflection.

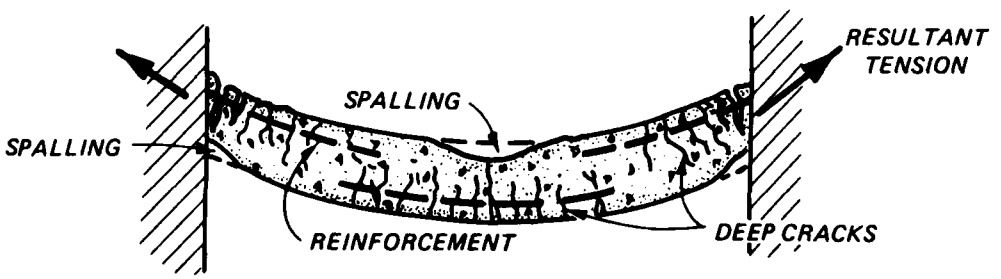

FIG.1.3.-Tensile Membrane Action

Compressive Membrane Action.-The enhancement in flexural capacity for restrained slabs is attributed to two actions. First, axial compressive forces in some cases can increase the moment capacity of a section beyond its normal flexural capacity. This enhancement in capacity is particularly apparent as long as the magnitude of the compressive force is less than the balanced thrust. The influence of axial thrusts on the failure criterion for a reinforced concrete cross-section can be seen in the moment-thrust interaction diagram of Fig. 1.4. Second, because the thrusts act within the compression zone of the cross-section and away from the plastic centroid, an internal couple is generated providing additional resistance to the load. In other words, it is not only the magnitude of the compressive force but its location that can serve to enhance the flexural capacity of a section.

Compressive membrane action in slabs is frequently referred to as arch, vault, or dome action because of the self-generated (passive) thrusts. Although all laterally restrained slabs generate passive compressive forces, the presence of active forces such as blast, wind, and soil pressures can also enhance the membrane capacity.

Most analyses of compressive membrane behavior in reinforced concrete slabs have been concerned with determining the ultimate capacity because that is what is of primary importance from the standpoint of design. However, there have been some efforts, e.g., Braestrup and Morley [3], Desayi and Kulkarni [9], and Jacobson [16], to define the

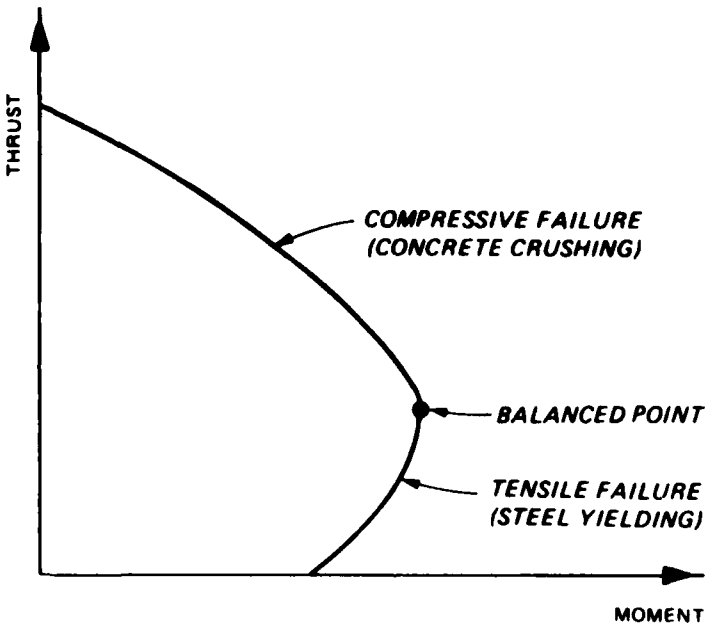

FIG. 1.4.-Moment-Thrust Interaction Diagram for a Reinforced Concrete Cross-Section

load-deflection behavior prior to the peak capacity by using various elastic and elasto-plastic theories. It should be noted that although the tensile membrane capacity may actually be greater than the peak flexural capacity referred to in this section, the terms membrane capacity, peak capacity, and ultimate capacity are used synonymously in reference to the initial peak as shown in Fig. 1.2 (p. 4).

Several theories have been developed to predict the capacity of slabs with compressive membrane forces [5,24,28]. However, those theories usually require a pre-existing knowledge of the relationship between deflection and peak capacity. Using empirical relationships, the existing theories have generally been in close agreement with test results. Keenan [18,19] derived an expression for computing the ultimate deflection, i.e., peak capacity deflection, using rigid-plastic theory. The theory was shown to provide reasonable results under certain conditions.

Several investigators have confirmed the existence of compressive membrane action in both models and actual structures [5,22,31]. Most investigations have involved parametric studies of two-way slabs. A limited number of the tests have included aspect ratios and orthotropic reinforcement patterns which are considered to be representative of one-way slabs. A review of related analytical and experimental investigations is provided in subsequent sections.

Tensile Membrane Action.-Another phenomenon of slab behavior that has received considerable attention in recent years is tensile membrane action or catenary action. Such action typically occurs after the slab has exceeded its compressive membrane capacity and has begun to undergo large deflections. If sufficient lateral restraint is provided, the tensile strength of the steel can supply a reserve capacity that will defer the progressive collapse of the slab. Tensile membrane action is usually accompanied with full-depth cracking and inward support movement. The largest deflection that a slab can withstand before there is a loss in tensile membrane capacity is referred to as the incipient collapse deflection. The collapse condition is associated with tensile rupture of the flexural reinforcement.

Provided there is sufficient ductile reinforcement, the tensile membrane capacity can actually exceed the compressive membrane capacity. Such behavior can provide the necessary strength and ductility to prevent a structure from collapsing under accidental overload.

Several investigators [5,18,19,28] have recorded tensile membrane action in two-way slabs. However, many of the records were results of studies of compressive membrane action, and the tensile membrane behavior received only secondary attention. Relatively few tests have been carried

to the point of incipient collapse deflection. Of the tests that have been carried into the tensile membrane stage, standard plastic membrane theory has been shown to provide reasonable predictions of the response.

Role of Membrane Behavior in Design.-Restrained slabs are capable of developing compressive and tensile membrane stresses provided premature failure does not occur. An enhancement of both the compressive and tensile membrane capacities of slabs can provide an optimal combination of strength and ductility. However, design criteria which are governed by a consideration of only one type of membrane action may lead to uneconomical or unsafe designs. Although the tensile membrane capacity can exceed the compressive membrane capacity, design criteria based entirely on tensile membrane action would be unacceptable because of the associated large deflections, and would be too costly because of the lack of consideration for the energy absorption capacity in the compressive membrane stage.

Since membrane behavior is a phenomenon that has received considerable attention only in the past few years, relatively few of the associated concepts have been incorporated into conventional design codes. There are some current attempts to verify and include membrane design criteria in military-based design guides. However, the

incorporation of such criteria into any governing document, particularly one that is used by the general engineering community, must be preceded by:

1. a thorough review of experimental and analytical investigations;

2. a reconciliation of voids, ambiguities, and contradictions in the experimental data; and

3. a theoretical explanation and experimental verification of various parametric contributions to fundamental slab behavior.

Although significant progress has been made toward satisfying these prerequisites, a concerted effort to extend the knowledge of membrane behavior into applications for the design profession has yet to be made. This study will contribute to the base of information for those who are investigating the role of membrane behavior in design. However, the real intent of this study was to evaluate the role of certain parameters on membrane behavior in protective structures.

Role of the Membrane Behavior in Protective Structures.- The impact of membrane research has had the most immediate effect on the members of the military and private sectors who are involved with the analysis and design of protective structures. Since these structures are considered to have a

high probability of receiving unusually large loads, conventional analyses which ignore membrane effects are too conservative to lead to economical designs. Generally, the rationale for the design of protective structures is to design for no damage under normal loads and for moderate damage under the most severe loading. Hence, ductility plays as an important of a role as strength in the design criteria for protective structures. Consequently, it is necessary to understand the behavior of slabs throughout the total range of loading, both experimentally and analytically.

The need to improve our ability to design structures for moderate damage was the fundamental purpose of the research presented in this paper. A statement of the problem and its relationship to previous research follows.

STATEMENT OF PROBLEM

The Federal Emergency Management Agency (FEMA) has established a program to plan, design and construct thousands of keyworker blast shelters throughout the United States. These shelters will be used as control centers and housing facilities for personnel operating critical industries within high-risk areas of the country during and after a nuclear attack.

Economic considerations in the design of these structures are very important. Design alterations that result in a reduction of materials or a simplification in construction can have a significant impact on the total cost of the program. However, design modifications which reduce the structural capacity below a specified safety threshold are not considered to be valid.

Both conventional and nuclear blast simulation procedures are used to evaluate the structural capacity of these facilities. The conventional design criteria have undergone repeated verification through laboratory experimentation and through the construction of facilities by the public sector. However, nuclear design procedures have not been as rigorously verified. Methods have been developed to analyze the response of structures under the exponentially-decayed pressure histories produced by nuclear weapons, but those methods are not consistently in agreement

with the test data for simulated low-yield nuclear weapons effects.

For box-type structures such as the keyworker blast shelters, the roof slab is much more likely to see significant structural damage than the walls or floor. Attenuation of the blast load and favorable soil-structure interaction characteristics minimize the amount of load received by the walls and floor. As a consequence, analytical and experimental investigations of the overall structural behavior are generally not necessary. Models which accurately represent the response of the roof slab should sufficiently represent the controlling response of the whole structure.

The construction details of slabs which are designed to resist blast loads are significantly different from conventional slab details. Blast resistant slabs are typically reinforced with relatively high percentages of reinforcement in both the tension and compression zones. Most reinforcement is run continuously throughout the slab, with little splicing and with substantial development lengths provided at the supports. Either stirrups or lacing reinforcement are use to separate the two mats of primary steel and to provide confinement for the concrete. Both stirrups and principal steel are usually closely spaced to minimize fragmentation and spalling of the concrete. Also,

blast resistant slabs are generally somewhat thicker than conventional slabs.

Predicting the flexural response of structural slabs under blast loads requires a thorough understanding of their behavior under similarly distributed static loads. Unless an alternate mode of response is invoked, e.g., shear, the dynamically loaded slab is typically assumed to provide a similar pattern of response as a statically loaded slab. However, some differences in the magnitudes of resistance may be noted because of strain-rate effects in the material properties.

Static tests of slabs are not only necessary to understand fundamental slab behavior, but are an economical way to investigate parametric effects on dynamic slab response. Both the quantity and quality of data are generally better in static tests.

REVIEW OF INVESTIGATIONS

Recent Experimental Investigations at WES.-There have been numerous static and dynamic tests conducted at WES on one-way slabs with characteristics similar to those discussed in the previous section. A summary of those tests [11] provides details of the basic design parameters and test results. The purpose of most of the dynamic tests was to investigate the effects of different weapon simulations on slab response. The purpose of the static tests was to investigate the effects of geometric and material parameters. Major parameters which were investigated in the static tests included the span-thickness ratio, reinforcement ratio, material properties, reinforcement spacing, and other reinforcement details. Most of the tests were conducted in a rigid reaction structure which provided both lateral and rotational restraint. As a result of the restricted lateral movement, a significant enhancement in the flexural capacity of each slab was noted.

The rigid reaction structure used in the WES tests also permitted the development of tensile membrane action in the slabs. As the slabs underwent large deflections, the compressive membrane thrusts were transformed into tensile forces which made the slabs respond somewhat as a net. Most slabs were loaded until collapse was imminent, providing an abundance of data in an area of slab response which had not been previously investigated to any great extent.

Compressive Membrane Tests.-The compressive membrane behavior noted in the previous static slab tests at WES has been well-documented in both experimental and analytical investigations over the past three decades. Ockleston [22] has generally been given credit for being the first to observe an increase in capacity by arching action due to the development of compressive membrane forces. His tests of continuous floor panels in existing buildings revealed that the yield line plasticity theory significantly underpredicted the capacities of the slabs. Previously, yield line theory had been considered to be an upper-bound solution in the analysis of plates.

Braestrup [2,3] noted that compressive membrane behavior did not receive much attention before Ockleston's tests because most experimental investigations were designed to verify yield line theory and test plans were developed to insure that membrane forces did not develop. Consequently, Ockleston's tests which recorded collapse loads several times greater than yield line theory attracted the attention of many engineers and resulted in a flurry of investigation into restrained slab behavior.

Since that time, tests by several other investigators have confirmed the existence of compressive membrane forces in laterally restrained slabs. Most of the tests have been conducted on conventionally-reinforced, two-way slabs with either rigidly-clamped or simple supports.

Powell [28] conducted the first laboratory tests of

isotropic slabs with fully restrained edges. Results of those tests revealed that the failure loads were significantly greater than the loads predicted by yield line theory. The enhancement in load-carrying capacity was dependent on the percentage of reinforcement and was most significant for slabs with smaller steel percentages.

Wood [36] conducted tests on five two-way slabs with isotropic reinforcement patterns and variable boundary conditions. In addition to slabs with simple and rigid supports, one test was conducted on a slab supported on encased steel beams. Each of the slabs had capacities which were significantly greater than predicted by yield line theory. Even though the rigidly restrained slabs showed the greatest enhancement in capacity, all slabs exhibited compressive membrane behavior.

Park [25] extended the studies of Powell and Wood to consider slabs with different boundary conditions along different edges. Some of the edges were fixed while others were simply allowed to rest on the support. Again it was shown that yield line theory was not a good predictor of the peak capacity.

Hung and Nawy [15] and Nawy and Blair [21] conducted tests on ninety slabs with various combinations of pinned and clamped boundaries to consider the limit strength and serviceability aspects of slabs with compressive membrane stresses. Partial restraint along the hinged boundaries

caused significant differences in tests and theory.

Approximately forty-five tests were conducted on two-way slabs by Brotchie and Holley [4] and Brotchie, Jacobson, and Okubo [5]. Three types of boundary conditions were considered in these tests of isotropically reinforced slabs: (a) restraint to elongation only, (b) fully clamped edges, and (c) no lateral or rotational restraint. In addition to boundary conditions, both the span-thickness ratio and the reinforcement ratio were varied. The magnitude and character of the lateral restraining force was measured in some of the tests.

Correlations between the tests with different boundary conditions were only partially conclusive. Results demonstrated that even unreinforced laterally restrained slabs are stronger than unrestrained slabs with normal steel ratios. Consequently, lateral restraint was concluded to be the most important parameter for an enhancement due to membrane action. In addition, full restraint provided the greatest enhancement in capacity for slabs with the largest span-thickness ratio.

Datta and Ramesh [8] investigated compressive membrane behavior in isotropically reinforced, two-way square slabs supported on edge beams. Approximately half of the nineteen test specimens were constructed with the slab at the center of the edge beams and the rest with the slab at the top of the edge beams. Both conditions provided sufficient lateral restraint to develop an enhanced flexural capacity. However,

the capacities were approximately twenty percent greater for the latter condition because of T-beam action. In other words, compressive stresses in the top of the edge beam provided a greater resistance to lateral movement of the slab. The deflection at which the maximum load occurred increased as the degree of edge restraint increased. No conclusions were made regarding the effects of variable rotational restraint in the slabs.

As stated previously, most investigations have been focused on two-way slabs. Other than the tests conducted at WES, only three investigators have studied the behavior of one-way slabs or slab strips. One-way slabs are slabs with dimensions such that bending primarily occurs in the short direction. An aspect ratio, i.e., ratio of long dimension of slab to short dimension, of at least two would be required for the slab to be considered as one-way. If the aspect ratio is greater than about four, then bending in the long direction is usually neglected altogether. In such a case, the slab can be adequately represented by a slab strip, i.e., a slab of narrow width and supported at two ends. A slab strip differs from a beam in that (1) lateral stability is insignificant, (2) shear stresses and deformations are relatively small, (3) some flexibility is present across the strip, and (4) transverse reinforcement is provided.

Christianson [7] and Roberts [31] tested laterally restrained, conventionally reinforced slab strips. Keenan

[18] tested one heavily reinforced, laced, one-way slab strip in a rigid reaction structure. The ratio of slab capacity to Johansen's load varied from approximately 1.5 to 17 in the tests of one-way slab strips. The enhancement in capacity was shown to increase as the strength of the concrete increased and as the reinforcement ratio decreased.

Analytical Studies of Compressive Membrane Behavior.- Wood [36] was the first to develop an analytical procedure for considering the effects of compressive membrane action in reinforced concrete slabs. By considering the material to be rigid-plastic and using large deflection plate theory, he derived the load-deflection relationship for a restrained isotropic circular slab subjected to a uniform loading. Because it neglected the effects of elastic bending, the theory erroneously predicted a maximum load at zero deflection as illustrated in Fig. 1.5. In reality, elastic deformations cause the maximum load to occur at some deflection larger than zero.

It was a relatively straight-forward task for Wood to apply his theory to uniform isotropic circular slabs. However, the presence of significant torsional moments in rectangular slabs created problems which were more difficult to handle.

Christianson [7] and Roberts [31] isolated the primary flexural action of slabs from the torsional moments by analyzing and testing one-way slab strips. Using geometric

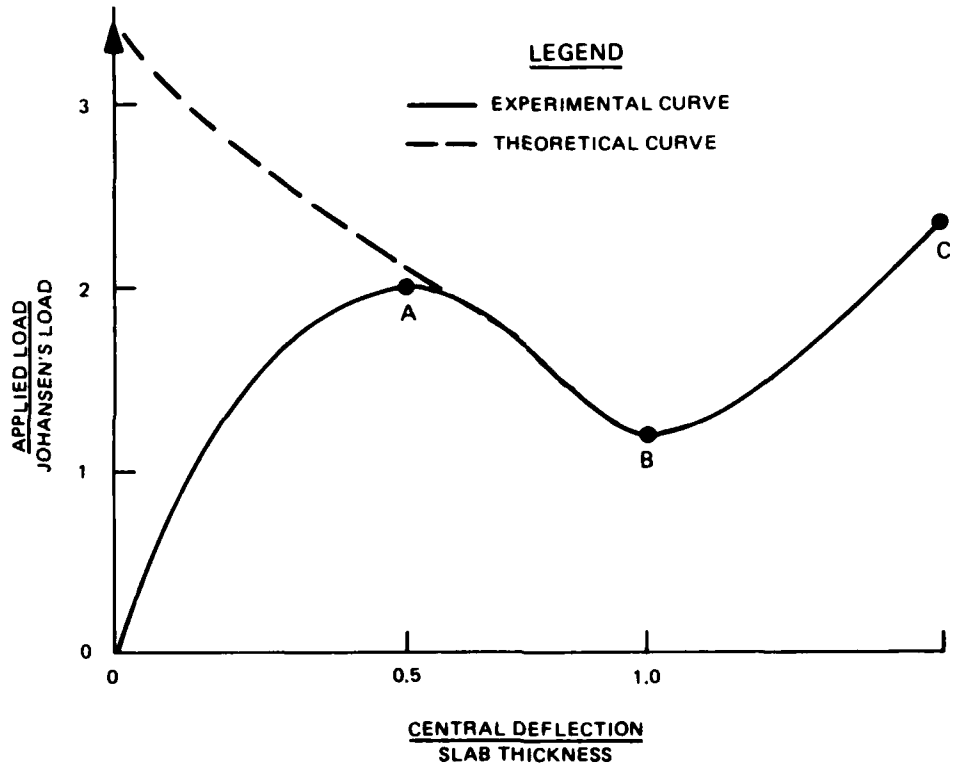

FIG. 1.5.-Relationship Between Experimental and Theoretical Curves Based on Rigid-Plastic Theory

and kinematic relationships for an idealized rigid-plastic strip similar to Fig. 1.6, they determined the depths of the compression zones at the midspan and support hinges. The depths were assumed to be dependent on the outward support movement, elastic shortening of the slab strip, and lengthening of the strip due to rotations at the yield sections. Resultant compressive forces and moments were computed by considering equilibrium of the strip.

Park [24] extended the compressive membrane strip theory to the analysis of two-way rectangular slabs. He used a virtual work approach to obtain the ultimate load of a slab by summing the contributions of rigid-plastic strips running in the short and long directions. The decomposition of a two-way slab into a series of slab strips is illustrated in Fig. 1.7. Although Park concluded that the theory satisfactorily predicted the ultimate load for actual tests, it was necessary to know the deflection at which the ultimate load occurred in order to get good results. Based on his own tests and those of Powell [28], Park recommended that the ultimate deflection be set equal to half the slab thickness.

Later, Park [25] made further enhancements in his theory to include the effects of sustained loadings and partial lateral restraint. Two effects were considered to reduce the capacity, (1) a lateral movement of the support, and (2) a loss of lateral stiffness due to shortening of the member from longitudinal strains. Ramesh and Datta [29] extended his work to account for the bowing action of edge beams.

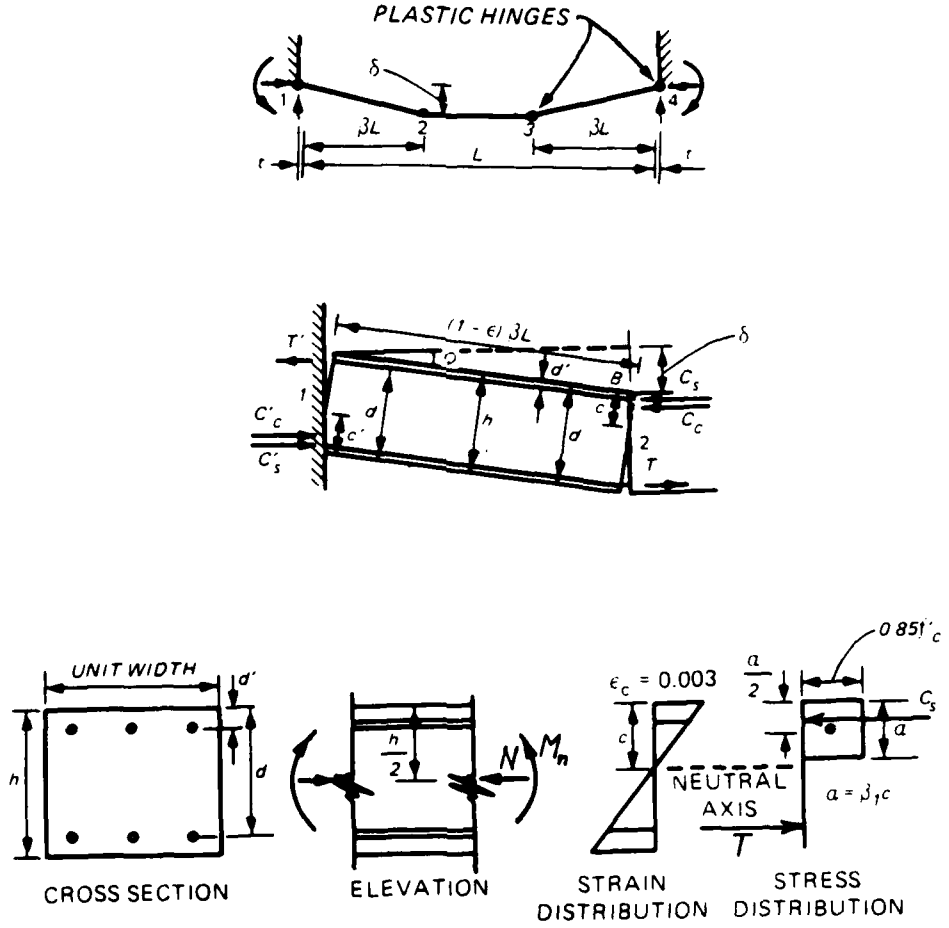

FIG. 1.6.-(a) Geometry of Deformation of Restrained Strip,
(b) Portion of Strip Between Yield Sections,
(c) Assumed Conditions at Yield Section

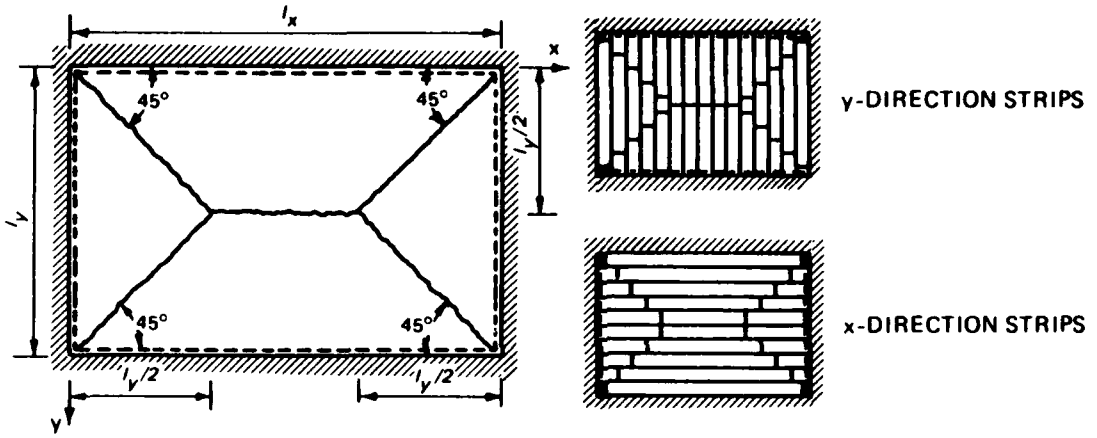

FIG. 1.7.-Idealization of a Two-Way Slab Using Strips

Sawczuk [32,33] used an energy approach for the plastic analysis of laterally restrained, simply supported slabs. He derived an equation which expressed the total energy due to plastic motion in terms of the energy dissipated along the yield lines as a result of bending and membrane stresses. The resulting load-deflection relationship was similar to that of Park. It also required an empirical value for the deflection at ultimate load.

Hung and Nawy [15] extended the work by Sawczuk to consider slabs with full restraint as well as slabs with either fixed or hinged conditions along different boundaries. Rather than using a value of deflection at ultimate load of 0.5 times the slab thickness as recommended by Park, they used the actual experimental values corresponding with the tests of their program. They demonstrated that the ultimate deflection varied from 0.4 to 1.0 times the slab thickness and was dependent on several slab parameters.

Keenan [19] made a comprehensive parametric study of restrained square slabs as a basis for developing design criteria for slabs with significant membrane forces. Parameters which were included in the analytical study were the span-thickness ratio, reinforcement ratio, ultimate strength and crushing strain of the concrete, yield strength of the reinforcement, and lateral restraint.

The basis for Keenan's analytical procedure was similar to Park's with the exception that it did not account for the effects of strain shortening. However, Keenan made a

significant contribution to the procedure by developing an expression for computing the deflection required to crush the concrete along the yield lines. This was the first approach that did not require the use of an empirical relationship for the deflection at ultimate capacity in order to determine the ultimate capacity. It was implied in the formulation that initiation of the collapse mechanism was dependent upon crushing of the concrete and that the failure did not occur because of geometric instability. Based on his own experimental work and also the tests of Wood [36] and Brotchie and Holley [4], Keenan established empirical relationships for determining whether slabs would fail by material or geometric instability. However, those relationships were based on a relatively small group of tests and were not theoretically verified.

Morley [20] used a different approach to the rigid-plastic analysis of slabs to arrive at a load-deflection relationship. The method was adapted from conventional yield line theory and accounted for membrane forces by considering displacement rates and in-plane equilibrium along the yield lines of the assumed mechanism. Although the formulation of the problem resulted in a relationship very similar to the one by Park, it was limited to isotropic slabs and did not account for elastic shortening and lateral support movement.

Braestrup [2] noted that the theory presented by Morley was fundamentally different from the theory used by the other

investigators in that it was based on plastic flow theory and not deformation theory. Flow theory considers strain increments as opposed to the total strains used by deformation theory. Consequently, flow theory can account for elastic unloading paths as strains decrease. The result is that flow theory predicts thrusts which decrease more rapidly with increasing deflection than does deformation theory. Similarly, the slope of the load-deflection curve is steeper for flow theory. However, flow theory does not predict a significantly different ultimate capacity than deformation theory.

Studies of Tensile Membrane Action.-Very few investigators have investigated the tensile membrane action in slabs as a primary objective of their study. However, the reasons for the apparent neglect of attention are understandable. First of all, designers consider any slab that reaches the tensile membrane stage to have failed the serviceability requirements of design. Consequently, there is little interest in studying the effects of various parameters on tensile membrane response. Second, the tensile membrane behavior is somewhat dependent on the extent of damage which occurs in the compressive membrane stage. Thus, the latter stage of response cannot be studied independently. Finally, it is difficult to devise an apparatus which is physically capable of loading a slab during very large deflections. The problem is even compounded more as the slab

approaches the incipient collapse deflection.

Tensile membrane action has attracted the attention of a few investigators, in particular those involved in the analysis and design of protective structures. The energy absorption capacity resulting from large deflections can provide protection against collapse in the case of a single catastrophic loading. Black [1], Keenan [18,19], and various WES investigators [11] have studied tensile membrane behavior from this point of view.

Park [23], Keenan [19], and Black [1] have made the most notable contributions in the area of tensile membrane analysis. Park used classical membrane theory to develop a linear relationship between load and deflection in the tensile membrane region. The theory assumes that the concrete does not contribute to the capacity. It also implies that the reinforcement reaches its yield stress throughout the slab and neglects the effects of strain hardening.

By comparing the experimental and analytical load-deflection curves, Park concluded that the theory leads to a conservative estimate of the tensile membrane response. One reason for the conservativeness of the solution is that the theory neglects the effects of strain hardening. Also, because pure membrane theory is used, no consideration is given to the combined action of flexure and tension. Flexural contributions to the capacity are likely to be much more significant in lightly reinforced slabs. Black and

Keenan suggested an empirical modification to Park's formulation to account for these effects.

Some of the previously mentioned investigators have proposed empirical relationships for determining the tensile membrane limiting deflection, i.e., incipient collapse deflection, by relating it to the short span length. Park and Keenan both suggested a safe value of a tenth of the span. However, Black suggested that their value was too conservative. Herzog [14] derived an expression for the incipient collapse deflection which was dependent on the short span length and rupture strain of the principal reinforcement. Takehira, Derecho, and Iqbal [34] followed a similar approach to arrive at recommended design criteria for the Naval Facilities Engineering Command. However, the number of slabs tested to incipient collapse deflection has been too small to confidently establish design criteria.

NEED FOR RESEARCH

Past studies have led to a significantly better understanding of membrane behavior in slabs. Some of the major conclusions which investigators have drawn with regard to restrained slabs include: (1) behavior prior to initial failure, i.e., ultimate capacity, is a combination of elastic and elastic-plastic and is influenced by restraining forces; (2) deformations associated with initial failure are primarily concentrated along yield lines; (3) the ultimate strength is much higher than predicted by yield line theory; (4) the ultimate strength is a function of the moment capacities and the interaction of thrusts and moments along yield lines; (5) the ultimate strength can be reasonably predicted by a rigid-plastic analysis, but is dependent upon knowledge of a deflection at which the ultimate capacity is reached; (6) a loss in load-carrying capacity beyond the peak capacity is associated with material instability for thick slabs and geometric instability for thin slabs; (7) flow theory provides a good representation of the load-deflection behavior in the transition region; (8) at large deflections, the reinforcement will act as a net and provide a reserve capacity; and (9) standard plastic membrane theory provides a good, but conservative, estimation of the load-deflection behavior in the tensile membrane stage.

These conclusions have been based on the previously mentioned investigations, most of which involved tests of rigidly clamped, conventionally reinforced, two-way slabs. A

few tests were conducted on simply-supported slabs with restraint to horizontal movement and a few tests have been conducted on slabs supported on edge beams. For the tests with less than full restraint, some differences in behavior were noted. In particular, the slabs had larger deflections and lower capacities. The need exists for a better understanding of slabs with partial restraint.

Deformational geometries induce complex behavioral characteristics in two-way slabs which are difficult to analyze. By testing slab strips, more information on fundamental behavior can be obtained. Consequently, there need to be more tests conducted on slab strips to establish and verify the effects of various construction parameters.

Although numerous geometric and material parameters need to be investigated, the span-thickness ratio and reinforcement ratio have been determined to be the most influential on slab behavior. Each of these parameters can also have a significant effect on the cost of a slab.

Finally, it is important that each of these parameters, i.e., restraint, span-thickness ratio, and reinforcement ratio, can be correctly modeled and included in an analytical procedure. At present, there is no single analytical procedure for predicting the entire load-deflection relationship.

OBJECTIVES

The major purpose of this program was to investigate the effects of edge restraint on slab behavior. In the past, both static and dynamic analyses have been based on the idealized conditions of perfect lateral and rotational restraint. However, prototype structures are seldom adequately represented by the idealized boundary conditions used in analytical and experimental models. In fact, even researchers have frequently been unable to obtain the degree of idealization represented by their theory.

Recent static tests [11] of rigidly restrained, one-way reinforced concrete slab strips at WES have produced some behavioral patterns which in some ways were considered to be undesirable. For example, those slabs typically failed with relatively narrow crack bands, and with little, if any, tensile membrane capacity. Although the peak flexural capacities were quite predictable using compressive membrane theory, the unpredictable behavior beyond the point of maximum capacity led to a lack of confidence in the existing analytical capabilities for determining overall slab strength and ductility. Consequently, one of the major objectives of this investigation was to improve the understanding of the load-deflection relationships for slabs with geometric proportions, reinforcement patterns and boundary conditions similar to those used in the keyworker blast shelter design.

It was anticipated that slabs with partial rotational restraint would not have significantly different initial

behavior than slabs with rigid restraint, but that the failure mechanisms could be different, particularly if rotations were significant enough to induce structural instability. If this were true, and if the structural configuration of the keyworker blast shelter did permit sufficient rotations, then analytical models could be improved to provide a more realistic analysis. An improvement in analytical capabilities always leads to a greater confidence in the integrity of design and provides a basis for making design alterations.

Certain geometric slab parameters, such as the reinforcement ratio and span-thickness ratio, were also known to have a significant effect on slab behavior. Observations of previous tests had revealed that some minimum reinforcement ratio was required in order to achieve an enhanced tensile membrane capacity. There was also a suggestion that slabs with smaller span-thickness ratios would generally have a better tendency to exhibit reserve strength. Because both of these parameters were under investigation in the final design of the shelters, it was considered necessary to bound the most probable solution with the slabs used in this experimental program.

Finally, in order to properly evaluate the effects of each parameter on the behavior of the slabs, an instrumentation program was needed which would provide accurate measurements of slab end actions. Measurements of

end rotations, moments and thrusts were considered necessary to suitably define the boundary conditions of the slab.

In summary, the objectives of this investigation were:

1) To determine the effects of partial rotational restraint on slab strength, ductility, and failure mechanism.

2) To determine the behavioral characteristics of slabs with different reinforcement ratios and span-thickness ratios.

3) To improve analytical procedures for predicting slab resistance.

4) To validate and/or enhance design criteria for slabs used in the keyworker blast shelters.

In addition to providing a better understanding of partially restrained slabs throughout all stages of loading, one of the major contributions of this work was a methodology for testing slabs with partial rotational restraint. The ability to design for a particular rotational freedom and stiffness offers a new domain for investigation.

SCOPE

Sixteen one-way reinforced concrete plate elements were loaded in a reaction structure under uniform static water pressure. The slabs were approximately 1:4 scale models of slabs with geometric parameters similar to the prototype keyworker blast shelters. Overall dimensions of the slabs were 24 in. x 36 in. with an effective loaded area of 24 in. x 24 in. All slabs had the same percentage of steel in compression as in tension.

The span-thickness ratio, reinforcement ratio and degree of rotational restraint were the primary parameters varied in the tests. Tests were conducted on eight slabs with span-thickness ratios of approximately 10.4 and reinforcement ratios of 0.52%, 0.74% and 1.06% in each face. The eight remaining slabs had span-thickness ratios of 14.8 and reinforcement ratios of 0.58%, 1.14% and 1.47%.

The reaction structure was designed to permit partial rotation at the supports. Rotations were varied within a range expected to simulate rotations in a box-type structure. Average support rotations were varied between approximately 0.4 to 2.8 degrees.

CHAPTER II

EXPERIMENTAL INVESTIGATION

OVERVIEW

The experimental phase of the project consisted of the testing of 16 scaled models of one-way reinforced concrete slabs. Slabs with an effective loaded area of 24 inches by 24 inches but supported on only two edges were tested under uniform static pressure. The intent of performing tests on slab strips was to isolate the primary flexural action of one-way slabs and eliminate any contributary effects due to two-way action. Also, the choice of slab strips enabled the tests to be conducted on much larger models than would otherwise have been possible.

All slabs had equal percentages of steel in the top and bottom faces. Temperature steel was provided in the transverse direction. Single-leg stirrups were spaced along the length of the longitudinal bars at the locations of the transverse reinforcement. This steel configuration resulted in a structural cage which provided confinement for the inner core of concrete. A study of the effects of shear stirrup details on slab behavior was presented by Woodson [37]. That report and recommendations from the shelter design group were used as a basis for the selection of the reinforcement configurations for this program.

It was necessary to design and construct a reaction

structure which would meet the objective of permitting partial rotational restraint as established for this program. It was also deemed necessary to provide additional capabilities for measuring the resultant actions at the ends of the slab. A reaction structure was constructed which allowed the slab to be mounted in rigid steel support racks and those racks were permitted to rotate within the confines of a solid steel reaction structure. Efforts were made to eliminate undesirable friction forces and to isolate the various member-end actions of the slab. Figs. 2.1 and 2.2 illustrates the overall design of the reaction structure in its test configuration.

Measurements of support displacements, thrusts, and moments were made to allow accurate evaluations of the slab behavior. Recorded data also included water pressure, steel strains, concrete strains, and slab deflections.

Descriptions of the element construction details, material properties, test configuration, instrumentation, and test procedure are provided in the following sections.

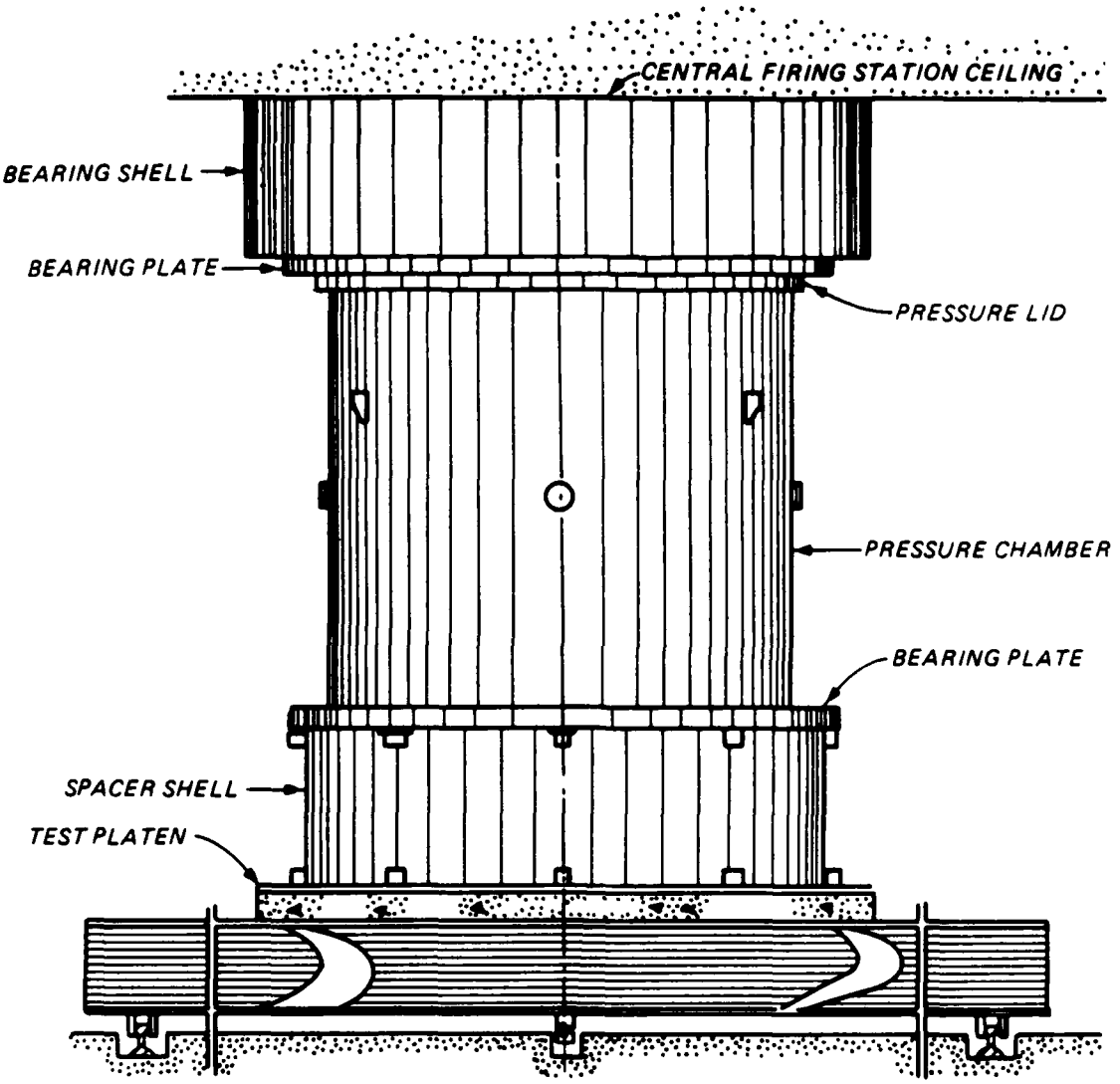

FIG. 2.1.-Elevation of Load Generator Facility

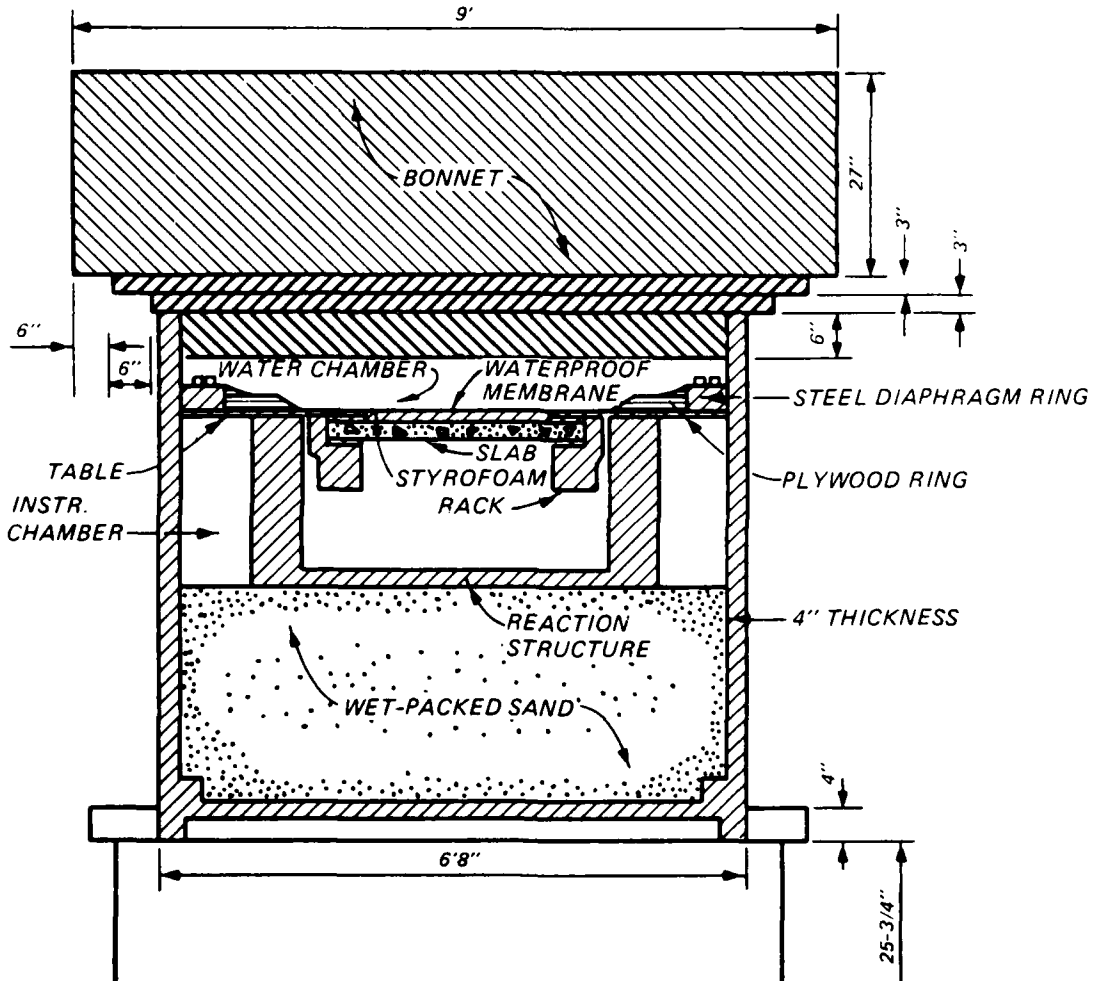

FIG. 2.2.-Cross-Section of Reaction Structure in Test Configuration

SLAB CONSTRUCTION DETAILS

One-half of the 16 slabs were constructed with a span-thickness ratio of 10.4 providing a direct correlation with previous tests performed for the prototype structure. The rest of the slabs were constructed with a span-thickness ratio of 14.8, representing more recent enhancements to the design of the prototype slabs.

Actual dimensions of the slabs were 24 inches by 36 inches However, 6 inches on each supported end of the slab were clamped between flat plates to provide continuity between the slab and support racks. Since the ends of the slabs acted integrally with the supports, only 24 inches by 24 inches of the slabs were effectively loaded by the surface pressure.

The slab thickness was 2-5/16 inches for the thick slabs and 1-5/8 inches for the thin slabs. The distance from outer face of the slab to the center of the reinforcement was held to 3/8 inch in every case, resulting in effective depths of 1-15/16 inches and 1-1/4 inches, respectively.

Three steel percentages were selected for each of the two slab groups. The slabs with the larger span-thickness ratio had steel ratios of 0.52%, 0.74% and 1.06%. The slabs with the smaller span-thickness ratio had a higher limiting steel ratio of 1.47%, and other steel ratios of 0.58% and 1.14%. The actual variances in design parameters are specified in Table 2.1. Slab construction details are listed in Table 2.2 and illustrated in Fig. 2.3.

TABLE 2.1.-Slab Design Parameters

Slab	Span-Thickness Ratio	Longitudinal Steel Percentage	Bar Type (1)	Bar Spacing, inches
1	10.4	0.52	D3	3
2	10.4	0.52	D3	3
3	10.4	0.74	No. 2	3.75
4	10.4	0.74	No. 2	3.75
4A	10.4	0.74	No. 2	3.75
4B	10.4	0.74	No. 2	3.75
5	10.4	1.06	No. 2	2.5
6	10.4	1.06	No. 2	2.5
7	14.8	0.58	D2.5	3.75
8	14.8	0.58	D2.5	3.75
9	14.8	1.14	No. 2	3.75
9A	14.8	1.14	No. 2	3.75
10	14.8	1.14	No. 2	3.75
10A	14.8	1.14	No. 2	3.75
11	14.8	1.47	No. 2	3.75
12	14.8	1.47	No. 2	3.75

Notes:
(1) Steel percentages were the same in top and bottom.
(2) Corresponding areas and diameters of bars are:
D3; area = 0.030 sq. in.; diameter = 0.195 in.;
D2.5; area = 0.025 sq. in.; diameter = 0.178 in.;
No. 2; area = 0.049 sq. in.; diameter = 0.250 in.

TABLE 2.2.-Slab Construction Details

Slab	Thickness t, inches	Depth d, inches	Bar Diameter db, inches	Spacing s, inches	Edge Spacing se, inches
1	2-5/16	1-15/16	0.195	3	1-1/2
2	2-5/16	1-15/16	0.195	3	1-1/2
3	2-5/16	1-15/16	0.25	3-3/4	3/4
4	2-5/16	1-15/16	0.25	3-3/4	3/4
4A	2-5/16	1-15/16	0.25	3-3/4	3/4
4B	2-5/16	1-15/16	0.25	3-3/4	3/4
5	2-5/16	1-15/16	0.25	2-1/2	3/4
6	2-5/16	1-15/16	0.25	2-1/2	3/4
7	1-5/8	1-1/4	0.178	3-3/4	3/4
8	1-5/8	1-1/4	0.178	3-3/4	3/4
9	1-5/8	1-1/4	0.25	3-3/4	3/4
9A	1-5/8	1-1/4	0.25	3-3/4	3/4
10	1-5/8	1-1/4	0.25	3-3/4	3/4
10A	1-5/8	1-1/4	0.25	3-3/4	3/4
11	1-5/8	1-1/4	0.25	2-3/4	1
12	1-5/8	1-1/4	0.25	2-3/4	1

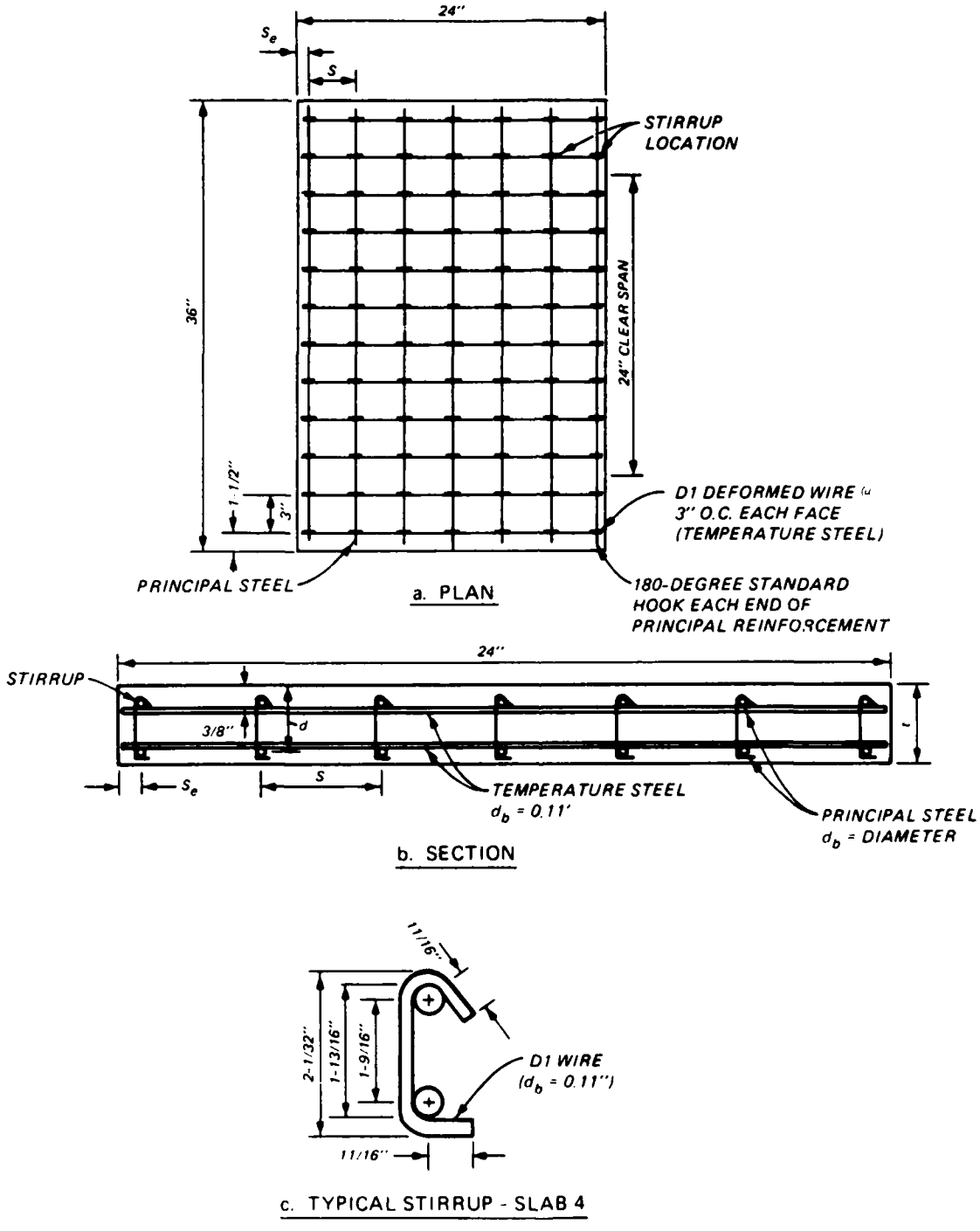

FIG. 2.3.-Slab Construction Details

Selection and placement of reinforcement were based on an objective to achieve the specified steel percentages while minimizing the variance of bar size and spacing. Recent tests at WES [38] have indicated that bar spacings greater than the slab thickness do not have a significant effect on slab behavior. Consequently, primary reinforcement spacings were controlled within the limits of 1 to 2.5 times the slab thickness. Bar diameters for the principal reinforcement were varied from 0.183 inch to 0.25 inch, with the latter diameter being used for 75% of the slabs.

Small diameter wire was used for temperature steel in all slabs and was equally spaced at 3 inches along the top and bottom mats. Both mats were tied together with single-leg, 0.11-inch-diameter wire stirrups placed at the locations where the temperature steel crossed the longitudinal steel. This configuration resulted in temperature steel ratios of 0.27% and 0.41% of the total thickness for both slab thicknesses. Shear steel percentages varied according to the spacing of the longitudinal steel. Small gage tie wire was used to hold the stirrups, temperature steel and primary steel into position.

REACTION STRUCTURE DETAILS

The reaction structure was designed with the objective of permitting partial rotations at the supports while satisfying the constraints of (1) using the standardized slab size of 24 inches by 36 inches, and (2) using the existing 6-foot-diameter load-generator facility. Other major considerations in the design of the structure were to keep the size of the gaps between the slab and the reaction structure as small as possible, to provide adequate room for the adjustment of instrumentation, to provide for the capability to test slabs of various thicknesses, and to use the the most readily available construction materials.

Six-inch-thick plate steel was selected as the construction material for the reaction structure because of its strength, stiffness, adaptability, and availability. Because high stress concentrations were expected in the areas of localized support reactions and because numerous openings for instrumentation were required, the choice of steel for construction of the structure was considered to be more acceptable than a composite of steel and concrete. Also, facilities were available for cutting, welding, and machining of heavy steel plate, making the selection of the material even more appropriate. Detailed drawings of the reaction structure are provided in Appendix I.

Rigid steel support racks were designed to transmit slab reactions to the major portion of the reaction structure through symmetrically placed shafts and spring assemblies as illustrated in Fig. I.1 and Fig. I.2. The large diameter cylindrical shafts located at each end of the support racks were machined and fitted into roller bearings (Fig. I.6). The spring assemblies were mounted to the long edge of each support rack through ball-and-socket connectors, and then fitted into slots of the reaction structure (Fig. I.1).

The spring assemblies were conceptually designed as soft load cells. By using disk springs as illustrated in Fig. I.5, each assembly could be controlled to deflect by a predetermined amount and with a given stiffness. This particular design offered the advantage of providing the capability to alter the assembly deflection and stiffness, and consequently, the rack rotation parameters, simply by modifying the configuration of the disks. Also, load washers inserted with each group of disk springs were capable of monitoring the magnitude of the load passing through the assemblies.

In addition to the load washers used in the spring assemblies, other load washers were used between the support racks and the reaction structure at the location of the cylindrical shafts (Fig. I.6). These load washers, located on each side of the shafts, were used to measure the thrusts and tensile forces generated from the restrained lateral movement of the slab.

Thrusts and moments were transmitted from the slab to the support racks by bearing and friction forces developed along the steel plate and concrete slab interfaces. High-strength steel bolts were countersunk into steel plates on top of the slab, inserted through small holes at the end of the slab, and screwed into threaded openings in the support racks. Small steel plates were also inserted between the ends of the slab and the support racks to provide bearing resistance to lateral movement of the slab.

The design of the reaction structure allowed the use of variable slab thicknesses and permitted relatively large tolerances in construction of the slabs. In anticipation of future tests on slabs with different geometric proportions, the support racks were designed to handle slabs with thicknesses up to 4 inches.

INSTRUMENTATION

Approximately 30 channels of analog data were recorded on magnetic tape for each test. The data for each channel were later digitized, processed, and plotted. Most of the channels were used to record data from instruments which were common to all tests. However, some channels were varied from test to test in an effort to obtain a broader range of data and still remain within the limits of the 32-channel recorder. A summary of the recorded channels and related instrumentation is provided in Table 2.3. Fig. 2.4 shows the location of the instrumentation in the test configuration.

Two water pressure gages (Kulite Model HKM-375) were mounted inside the bonnet of the load-generator facility to record the pressure applied to the slab. One of those gages served as a reference channel for all subsequent data.

Position/displacement transducers (Celesco Model PT-101) with a full-scale range of 10 inches and an accuracy of 0.1% were used to record the quarterspan and midspan slab deflections. These transducers measured the displacement of the slab by means of a potentiometer which detected the extension and retraction of a cable attached to a spring inside the transducer. The body of each transducer was mounted to the floor of the reaction structure and the cable was attached to a wire projecting from the bottom of each slab.

TABLE 2.3.-Instrumentation Details

	Slab															
Channel	1	2	3	4	4A	4B	5	6	7	8	9	9A	10	10A	11	12
1	P1	P1	P1	P1	P1	P1	P1	P1	P1	P1	P1	P1	P1	P1	P1	P1
2	P2	P2	P2	P2	P2	P2	P2	P2	P2	P2	P2	P2	P2	P2	P2	P2
3	D1	D1	D1	D1	D1	D1	D1	D1	D1	D1	D1	D1	D1	D1	D1	D1
4	D2	D2	D2	D2	D2	D2	D2	D2	D2	D2	D2	D2	D2	D2	D2	D2
5	D3	D3	D3	D3	D3	D3	D3	D3	D3	D3	D3	D3	D3	D3	D3	D3
6	D4	D4	D4	D4	D4	D4	D4	D4	D4	D4	D4	D4	D4	D4	D4	D4
7	LW1	LW1	LW1	LW1	LW1	LW1	LW1	LW1	b	b	LW1	LW1	LW1	LW1	LW1	LW1
8	LW2	LW2	LW2	LW2	LW2	LW2	LW2	LW2	LW2	LW2	LW2	LW2	LW2	LW2	LW2	LW2
9	LW3	LW3	LW3	LW3	LW3	LW3	LW3	LW3	LW3	LW3	LW3	LW3	LW3	LW3	LW3	LW3
10	LW4	LW4	LW4	LW4	LW4	LW4	LW4	LW4	b	LW4	LW4	LW4	LW4	LW4	LW4	LW4
11	LW5	LW5	LW5	LW5	LW5	LW5	LW5	LW5	b	LW5	LW5	LW5	LW5	LW5	b	LW5
12	LW6	LW6	LW6	LW6	LW6	LW6	LW6	LW6	LW6	LW6	LW6	LW6	LW6	LW6	LW6	LW6
13	LW7	LW7	LW7	LW7	LW7	LW7	LW7	LW7	LW7	LW7	LW7	LW7	LW7	LW7	LW7	LW7
14	LW8	LW8	LW8	LW8	LW11	LW8	LW8	LW8	LW8	LW8	LW8	LW8	LW8	LW8	LW8	LW8
15	LW9	LW9	LW9	LW9	ST1	LW9	LW9	LW9	LW9	LW9	LW9	LW9	LW9	LW9	LW9	b
16	LW10	LW10	LW10	LW11	ST2	LW11	LW10	LW10	LW10	LW10	LW10	LW10	LW10	LW10	LW10	LW10
17	LW11	LW11	LW11	LW12	ST3	LW12	LW11	LW11	LW11	LW11	LW11	LW11	LW11	LW11	LW11	LW11
18	LW13	LW12	b	LW13	SB1	LW13	LW13	LW12	LW13	LW12	LW13	LW13	LW12	LW12	LW13	LW12
19	LW14	LW14	LW13	LW15	SB2	ST1	LW14	LW13	LW14	LW13	LW14	b	LW13	LW13	LW14	LW13
20	LW15	LW14	LW14	ST1	SB3	ST2	LW15	LW14	LW15	LW14	LW15	LW15	LW14	LW14	LW15	LW14
21	ST1	LW15	LW15	ST2	b	ST3	ST1	LW15	ST1	LW15	ST1	ST1	LW15	LW15	ST1	LW15
22	ST2	LW16	ST1	ST3	D3S	SB1	ST2	LW16	ST2	LW16	ST2	ST2	LW16	LW16	ST2	b
23	ST3	ST1	ST2	SB1	D4S	SB2	ST3	ST1	ST3	ST1	ST3	ST1	ST1	ST1	ST3	ST1
24	SB1A	ST2	ST3	SB2	b	SB3	SB1	ST2	SB1	ST2	SB1	SB1	ST2	ST2	SB1	ST2
25	SB2	ST3	SB1	SB3	b	D3S	SB2	ST3	SB2	ST3	SB2	SB2	ST3	ST3	SB2	ST3

TABLE 2.3.- (Cont.)

	Slab															
Channel	1	2	3	4	4A	4B	5	6	7	8	9	9A	10	10A	11	12
26	SB3	SB1	SB2	SB2	ST1S	D4S	SB3	SB1	SB3	SB1	SB3	SB3	SB1	SB1	SB3	SB1
27	CT1	SB2	SB3	SB3	ST3S	ST1S	CT1	SB2	ST1A	SB2	CT1	CT1	SB2	SB2	CT1	SB2
28	CB3	SB3	CT1	CT1	SB1S	ST3S	CB3	SB3	ST3A	SB3	CB3	CB3	SB3	SB3	CB3	SB3
29	CB3P	b	CB3P	ST3S	SB3S	SB1S	CB3P	b	CT1	CB3	ST1A	ST1A	ST1A	b	SB1A	CB3
30	ST1A	b	CB3	CB3	b	SB3S	ST1A	b	CB3	CT1	SB1A	SB1A	SB1A	SB1A	SB3A	CT1
31	b	b	ST1A	ST1A	b	b	b	b	SB3A	CT1P	ST3A	SB3A	SB3A	SB3A	ST3A	CT1P

Notes: (1) Prefix Descriptors:
- P - water pressure gage
- D - displacement transducer
- LW - load washer
- ST - steel strain gage in top of slab
- SB - steel strain gage in bottom of slab
- CT - concrete strain gage on top of slab
- CB - concrete strain gage on bottom of slab

(2) Suffix Descriptors:
- A - alternate strain gage
- P - strain gage perpendicular to major slab axis
- S - split calibration step channel

(3) b - indicates non-instrumented channels

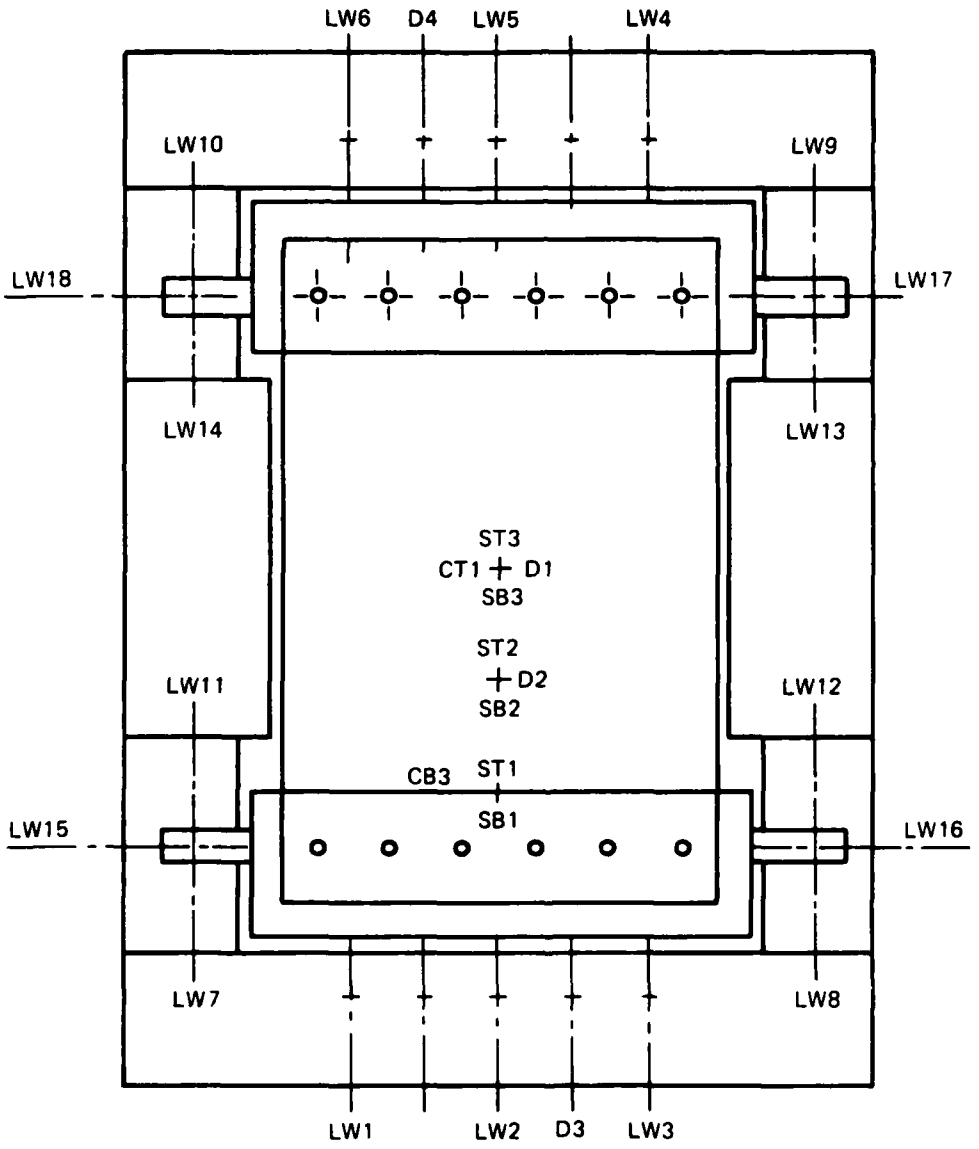

FIG. 2.4.-Instrumentation Layout

Linear variable differential transformers (LVDTs) (Trans-Tek Model 244-000) were used to measure the lateral movement of the bottom portion of the support racks. One LVDT was mounted to each end of the reaction structure with the probe attached to the associated support rack. Rotations were computed from the measured displacements and known geometries. Fig. I.4 (b) illustrates the position of the LVDT with respect to the support rack.

Two types of load washers were used in the tests. Eaton Model 3711-500 load sensors were used in the spring assemblies which were attached to the support racks. These 20,000-pound-capacity sensors had a maximum calibrated nonlinearity of 3.4%. Large diameter and high capacity force washers (Houston Scientific Model 2054V-100) were used to measure the thrusts transmitted to the reaction structure at the location of the large shafts at the ends of the support racks. A maximum calibration nonlinearity of 12.4% was computed within the working range of the 100,000-pound-capacity washers. At least one high capacity washer was placed in a position to measure the vertical load being transmitted through the support racks in each test.

Single-axis, metal-film, 350-ohm strain gages (Micro-Measurements Model EA-06-125 BZ-350) were mounted on the principal reinforcement at the midspan, quarterspan and support. In every slab, two pairs of bars (two at the top and two at the bottom) were instrumented with strain gages. However, only one pair was monitored for strains during each

test, except for the cases in which duplicate bars were tested for verification.

Epoxy-coated concrete strain gages (Tokyo Sokki Kenkyujo Types PML-60 and PMC-60) were mounted on the surface of several slabs in the compression zones at midspan and near the support. The latter type of concrete gage had filaments in mutually perpendicular directions and was used to provide information on the biaxial stresses in the concrete.

In addition to the electronic data, visual data were recorded in several of the tests with the use of a remotely-controlled camera. The camera was mounted in the bottom of the reaction structure and focused on the bottom of the slab to provide information on the sequence of formation of cracks. All slabs were painted white and marked with a reference line at quarterspan to enhance visibility and establish orientation.

PROCEDURE

The steel reinforcement for all slabs was measured, cut, bent, and formed into a cage. The cage was then placed into wood forms which had been coated with a thin film of oil. All reinforcement was adjusted and tied into position. Next, the concrete was mixed and placed into the forms. A vibrating table was used to support the forms and compact the concrete during placement. The slabs were finished with hand trowels and placed under wet burlap. Water was applied to the burlap for approximately 7 days. Finally, the forms were removed and the slabs were stacked into position until the time of testing.

Tests were performed over a period of approximately 6 weeks beginning on August 13, 1984, nearly 75 days after the date of concrete placement. Slabs were tested in somewhat of a random order with several of the thick slabs tested first, followed by some of the thin slabs and then the remainder of both slab groups.

It was intended to conduct the tests with prescribed controls on the degree of rotational restraint for each slab. However, the control of rotations was found to be more difficult than originally expected because of construction tolerances in the reaction structure. Although the reaction structure had been designed to allow for adjustments to the support racks to eliminate any gaps which were present prior to testing, the minor adjustments needed for precise control

of the supports could not be made. Hence, the rotational restraint could not be as closely controlled as desired during testing, but could be accurately evaluated after testing.

In preparation for the test series, the load-generator facility was filled with sand to within about 40 inches from the top. Then the reaction structure was carefully positioned into the generator. The support racks were put in place and the spring assemblies were installed. Instrumentation which was to remain in position for all tests was connected to the main instrument panel. The LVDTs and load washers were installed as semipermanent instrumentation for all of the tests.

For each test, a slab was placed into the support racks and held in position by partially tightening the bolts which passed through the holes in the ends of the slab. All strain gages were connected and verified at the instrument panel. For most of the tests, the assemblies at the ends of the support racks which provided lateral restraint were preloaded to about 20,000 pounds to insure that full lateral restraint would be provided. After the assemblies were preloaded, the support rack bolts were tightened and all of the instrumentation channels were balanced to zero.

A specially constructed table (Fig. I.7) was placed around the reaction structure to provide support for the water pressure. A 1/2-inch thick rubber mat and three 1-1/2-inch thick layers of styrofoam were cut to be approximately

the same size as the loaded area of the slab. The purpose of these mats was to raise the height of the loading surface and, consequently, minimize the amount of stretching in the rubber membranes.

Two thin, fiber-reinforced, rubber membranes were used to isolate the slab and reaction structure from the volume of water in the upper cavity of the generator. The membranes were clamped between two steel rings which perfectly fit the inside diameter of the generator. Slack was placed in the membranes to prevent the development of any significant tensile loads during the stage of large slab deflections.

After the rings and membranes were placed into the generator, the bonnet was lowered into position and the generator facility was moved into the central firing station. All instrumentation channels were taken through a final verification of calibration and then water was pumped into the upper cavity of the generator. Approximately 20 minutes were required to fill the chamber with water and raise the bonnet to bear against the massive portion of the central firing station. During that time the pressure was gradually increased to about 10 psi. Until the bonnet was firmly seated against the central firing station, a constant pressure of about 10 psi was maintained inside the chamber. As the pressure began to increase again, the pumping rate was reduced. Pumping rates were selected to control the rate of deflection to be slow and uniform throughout the test.

The load-deflection behavior of each slab test was monitored on a plotter which was receiving signals from the reference water pressure gage and midspan deflection transducer. The rate of loading was governed by a visual inspection of the plotted load-deflection curve.

After each slab had progressed significantly into the tensile membrane stage, the test was halted. Upon completion of each test, the bonnet was taken off, all remaining water was discharged, and the membranes were removed. Posttest activities included an inspection of crack and spall behavior, the recording of steel rupture, and photography. Results of the individual tests are presented in the next chapter.

The reaction structure was generally not moved between tests. Consequently, most of the instrumentation did not have to be dismantled then reassembled for subsequent tests. However, the instrumentation was inspected for physical damage and carried through another verification of calibration before the next test was conducted.

MATERIAL PROPERTIES

The design compressive strength of the concrete was selected to be 4,000 psi. A mix was designed using Portland cement type I, a 3/8-inch maximum size limestone coarse aggregate, and a manufactured limestone sand fine aggregate. Two batches were prepared, one for each of the different thickness slab groups. A total of 38 four-inch-diameter cylinders were collected from the two batches. The average 28-day compressive strength for the first batch was 3,420 psi and for the second batch was 4,760 psi. The remaining cylinders were tested at approximately the same time as the slab elements. Results of those compressive tests are provided in Table 2.4.

A regression analysis was performed on each batch of concrete cylinder data. The method of least squares was used to establish a second-order regression equation for the first batch and a linear regression equation for the second batch. Higher order equations were generated for each batch but those equations did not sufficiently characterize the behavior of concrete. The relationships between the equations and the raw data are illustrated in Figs. 2.5 and 2.6.

TABLE 2.4.-Experimental Concrete Properties

Cylinder	Compressive Strength, psi	Age When Tested, days	Average Strength, psi
	Batch 1		
1	3,420	29	
2	3,420	29	3,420
3	3,950	75	
4	4,220	75	4,090
5	4,340	77	
6	4,140	77	4,240
7	4,610	82	
8	3,920	82	4,270
9 *	4,230	88	
10 *	4,720	88	
11 *	4,160	88	4,370
12	4,220	103	
13	4,550	103	
14	4,610	103	
15	4,720	103	
16	4,140	103	
17	4,310	103	
18	4,500	103	4,440
	Batch 2		
19	4,770	29	
20	4,750	29	4,760
21	3,700	12	3,700
22	3,840	14	3,840
23	5,290	89	
24	5,390	89	5,340
25	4,380	106	
26	4,130	106	
27	5,210	106	4,570
28	4,380	109	
29	5,500	109	
30	4,770	109	4,880
31 *	5,180	110	
32 *	5,230	110	
33 *	5,030	110	5,150
34	5,510	111	
35	5,230	111	
36	4,660	111	5,130
37	5,110	112	
38	5,270	112	5,190

Note:
* Indicates cylinders instrumented with strain gages.

Six of the cylinders were instrumented with strain gages to allow the constitutive relationships of the concrete under uniaxial compression to be evaluated. The modulus of elasticity and Poisson's ratio were determined for each cylinder according to the American Society for Testing and Materials Standards (ASTM C469). The average moduli of elasticity for Batches 1 and 2 were 3.98×10^6 psi and 4.92×10^6 psi, respectively. The average Poisson's ratio for each group was determined to be 0.19 and 0.21, respectively.

Most of the slabs were reinforced with standard No. 2 deformed reinforcing bars. However, in order to provide the desired steel percentages and to maintain appropriate bar spacings, a few of the slabs were constructed with small-diameter, heat-treated, deformed wire. The heat treatment of the wire was performed at WES. By controlling oven temperatures and time of heating, a steel wire was produced with a substantially lower but more definitive yield point and with an increased ductility. The yield point and ultimate strength were the primary parameters which were observed during the initial heat treatment trials. Because of malfunctioning instrumentation, measurements of the ultimate deformations could not be made during the treatment process. The treated wire was later found to have a significantly lower rupture strain than No. 2 reinforcing bars.

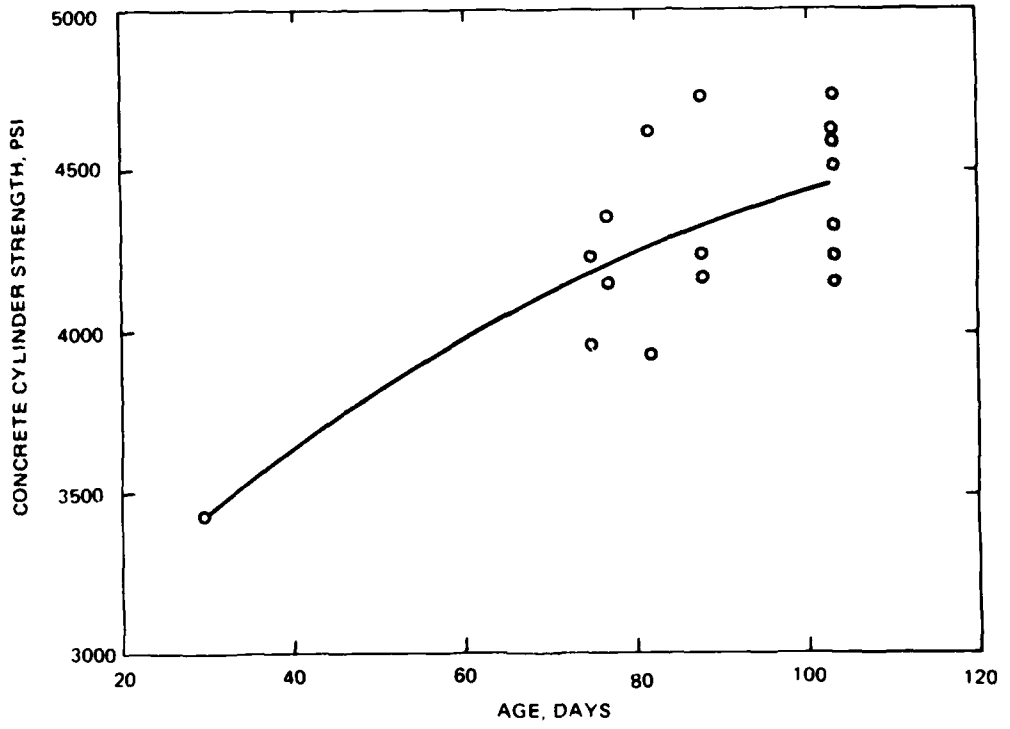

FIG. 2.5.-Relationship Between Experimental Concrete Strengths and Regression Curve for Batch 1

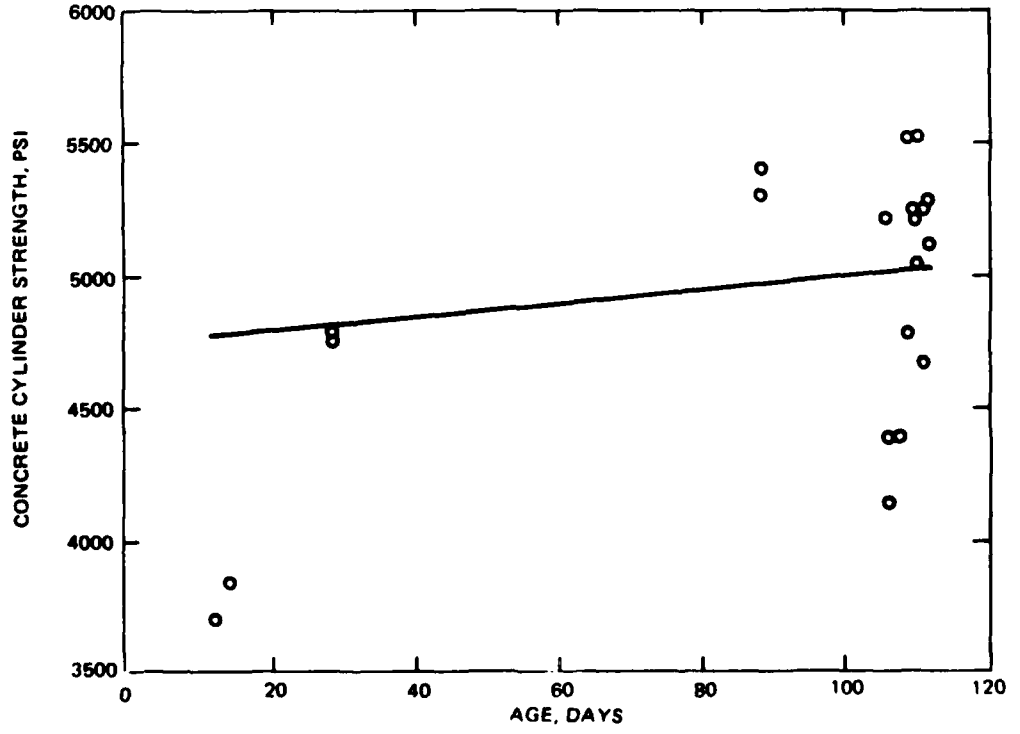

FIG. 2.6.-Relationship Between Experimental Concrete Strengths and Regression Curve for Batch 2

Random samples of all reinforcement were tested to rupture in an Instron tensile testing apparatus. An extensometer was used to monitor the deformation of each specimen. Plots of the load-deformation characteristics of the specimens were generated. The yield and ultimate strengths of the reinforcement were computed by dividing the appropriate load by the original cross-sectional area. The corresponding strains were determined by dividing the measured deformations by the gage lengths. A comparison of typical curves from the deformed bar group and the heat-treated wire group is illustrated in Fig. 2.7. Tabular results from the steel reinforcement tests are presented in Table 2.5.

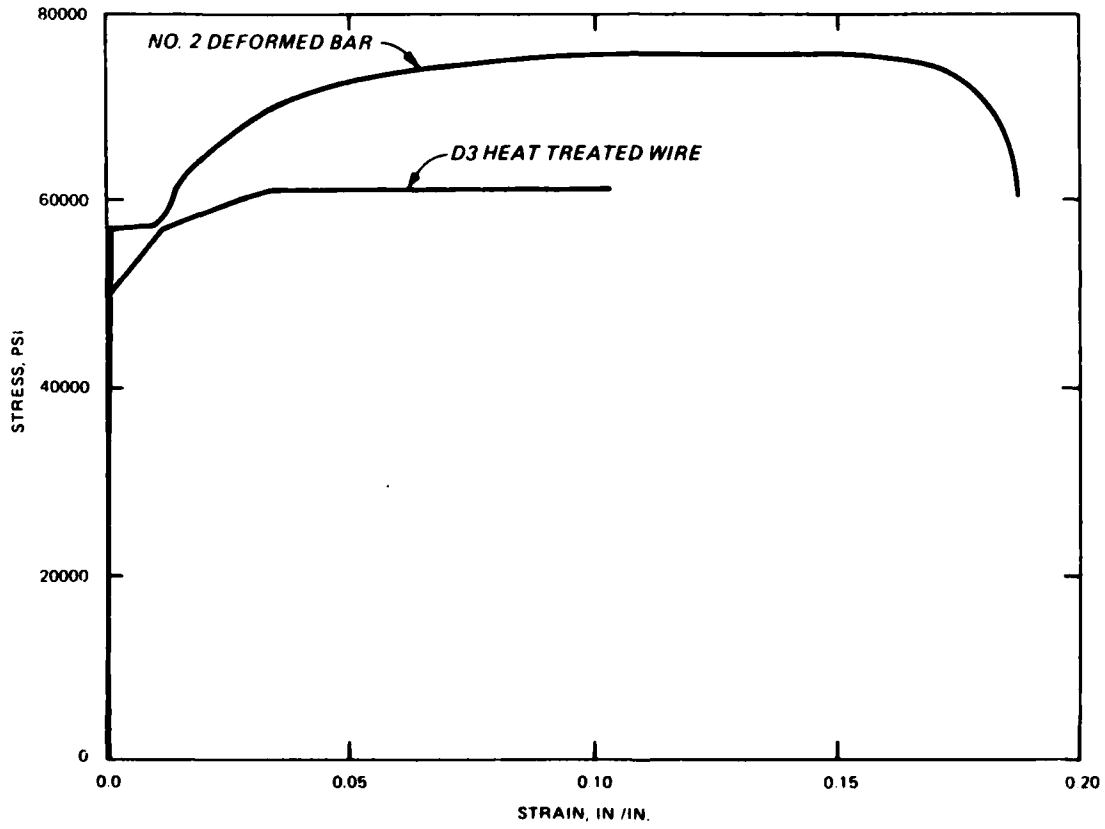

FIG. 2.7.-Representative Steel Curves for Deformed Bar and Wire Groups

TABLE 2.5.-Experimental Steel Properties

Bar Type (1)	Yield Load, pounds	Yield Stress, psi	Yield Strain, in/in	Ultimate Load, pounds	Ultimate Stress, psi	Rupture Strain, in/in
No. 2	2,920	59,590	0.0020	3,880	79,180	0.165
	2,780	56,730	0.0015	3,700	75,510	0.188
	2,880	58,780	0.0017	3,700	75,510	0.135
	2,880	58,780	0.0015	3,750	76,530	0.170
Average	2,865	58,470	0.0017	3,760	76,680	0.174
D3	1,600	53,330	0.0015	1,950	65,000	0.091
	1,180	39,330	0.0015	1,520	50,670	0.198
	1,500	50,000	0.0016	1,780	59,330	0.039
	1,720	57,330	0.0014	2,120	70,670	0.075
Average	1,500	50,000	0.0015	1,840	61,420	0.101
D2.5	1,600	64,000	0.0019	1,900	76,000	0.053
	1,900	76,000	0.0020	2,060	82,400	0.109
	1,550	62,000	0.0019	1,870	74,800	0.073
Average	1,680	67,330	0.0019	1,940	77,730	0.078
D1	950	95,000	0.0028	970	97,000	0.058
	870	87,000	0.0028	860	86,000	0.029
	860	86,000	0.0038	860	86,000	0.017
	890	89,000	0.0028	890	89,000	0.020
	960	96,000	0.0030	970	97,000	0.015
Average	906	90,600	0.0030	910	91,000	0.028

Notes:

(1) Corresponding areas and diameters of bars are:
D3; area = 0.030 sq. in.; diameter = 0.195 in.;
D2.5; area = 0.025 sq. in.; diameter = 0.178 in.;
D1; area = 0.010 sq. in.; diameter = 0.110 in.;
No. 2; area = 0.049 sq. in.; diameter = 0.250 in.

(2) Failure occurred outside the gage length in the third sample of No. 2.

CHAPTER III

EXPERIMENTAL RESULTS

PHYSICAL OBSERVATIONS

Physical posttest observations can be as important as instrumented data in evaluating the overall results of a test. A careful inspection of the test specimen can provide either a verification or contradiction of the recorded data. Also, the use of certain analytical procedures or the disallowance of others may be evident from posttest observations of the specimens. For those reasons, both descriptive and photographic records of all slabs have been provided for this program.

Crack patterns and failures of reinforcement were the most significant behavioral characteristics to be observed from the slab specimens. Descriptions of the posttest observations for each slab are provided in Table 3.1.

The bottoms of all slabs were painted white and marked with a quarterspan reference line prior to testing. Immediately after each test, all visible cracks in the slabs were highlighted with markers. Records were kept of the widths of the crack bands in the tensile zones at midspan and supports, and the width of the spall band in the compression zone at midspan. Approximate dimensions for the bands of spalling and cracking were computed by taking the average widths of the patterns measured at 6-inch intervals across

TABLE 3.1.-Posttest Observations of Slab Behavior

	Ruptured steel percentage, in percent			Average crack zone, in inches		Average spall zone, in inches
	Midspan		Support	Midspan	Support	Midspan
Slab	Top	Bottom	Top	Bottom	Top	Top
1	100.0	100.0	87.5	4	1/2 to 1	4
2	87.5	100.0	87.5	3	1/2 to 1	3
3	0.0	71.4	28.6	12	1/2 to 1	2
4	0.0	42.9	14.3	8	1/2 to 1	1
4A	0.0	57.1	0.0	8	2 to 2-1/2	2-1/2
4B	0.0	28.6	0.0	6	1/2 to 1	1-1/2
5	0.0	30.0	40.0	12	1 to 2	1-1/2
6	0.0	20.0	0.0	10	2 to 2-1/2	1-1/2
7	85.7	85.7	92.9	10	1/2 to 1	3
8	85.7	100.0	92.9	4	1/2 to 1	2-1/2
9	0.0	0.0	14.3	20	1 to 2	1-1/2
9A	0.0	0.0	14.3	20	1 to 2	2
10	0.0	0.0	0.0	12	1 to 2	1-1/2
10A	0.0	57.1	0.0	8	1/2 to 1	1-1/2
11	0.0	0.0	0.0	18	1 to 2	1-1/2
12	0.0	0.0	0.0	12	2 to 2-1/2	2-1/2

the span. Since some very small cracks developed over nearly the whole slab in practically every case, the computed widths were determined from what were considered to be the most significant flexural cracks. In most tests, the widths of the crack patterns were substantially greater at the edges of the slabs than near the center. To minimize the effect of biased data due to edge effects, only crack dimensions in the center portion of the slab were used to determine band widths. A graphical representation of the damage assessment criteria as recorded in Table 3.1 is presented in Fig. 3.1.

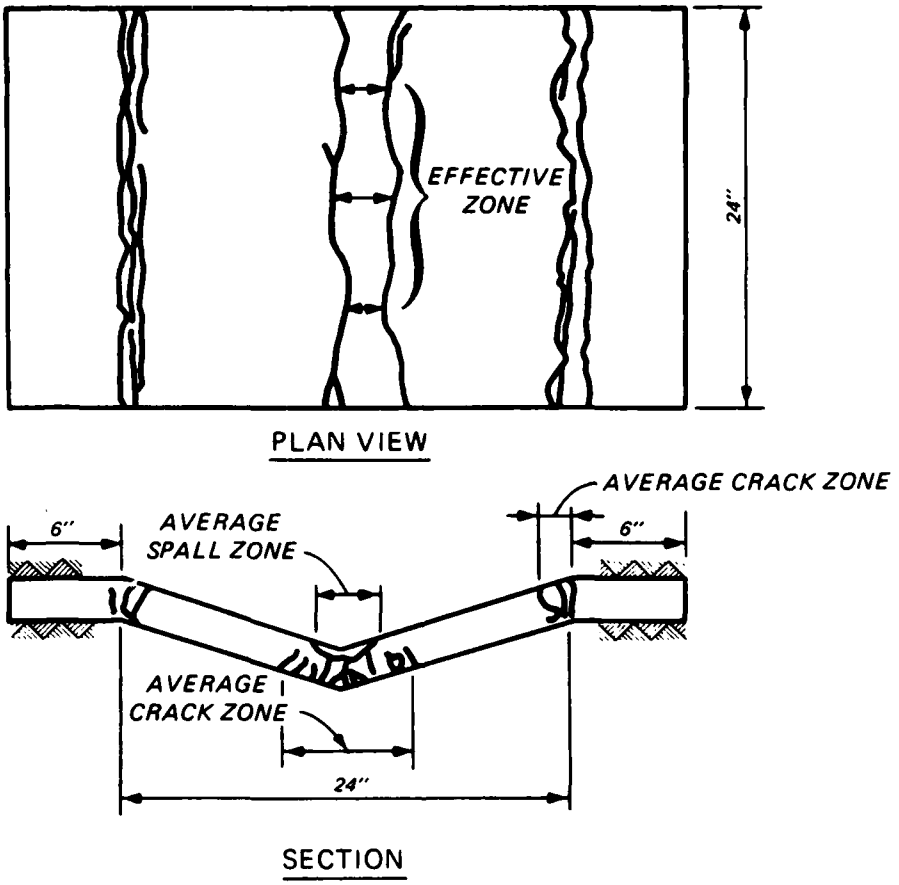

FIG. 3.1.-Crack Damage Assessment Criteria

The reader should be advised to use the approximations of the dimensions of the crack bands only as a measure of the relative damage of each slab as measured by the investigator.

The percentage of ruptured steel was recorded at both midspan and supports. Percentages were computed at midspan by dividing the number of broken bars by the total number of bars in each layer. At the supports, the average number of broken bars for both sections was divided by the number of bars at one section. No results were included in the table for ruptured steel at the location of the bottom bars at the supports since none of the bottom support bars were ruptured in any test. Although the broken bar counts were taken from careful examinations of the slabs, some of the reinforcement was still covered by the concrete and could not be observed.

Photographs were taken of both sides of each slab and have been included in Appendix II. In addition to the individual slab photographs, group pictures were taken of each slab series and of the total collection. A posttest view of the bottoms of all slabs is provided in Fig. 3.2.

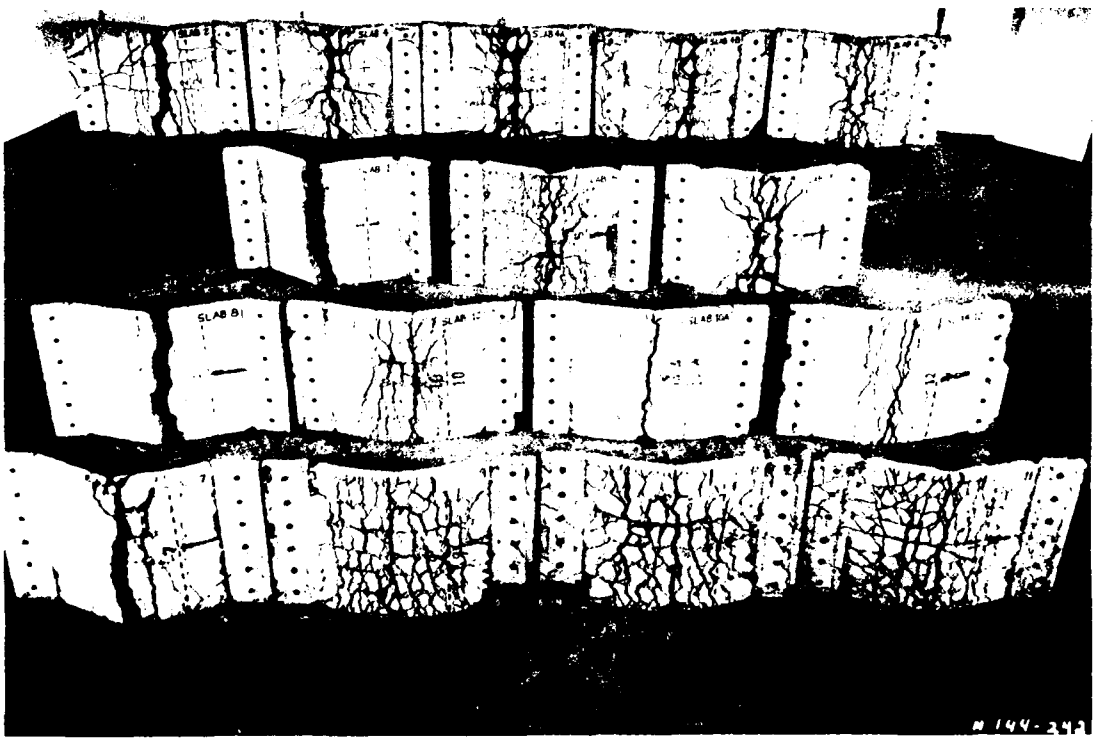

FIG. 3.2.-Posttest View of Undersurface of Slabs

INSTRUMENTED DATA

As stated previously, all of the analog signals which were received from the instrumentation during each test were recorded on magnetic tape, digitized by computer, and output on a plotter. The analog-digital sampling rate for digitization of the data was established by the acquisition of 1,000 points selected at equal time intervals over the duration of each test. In some instances where there were sudden changes in the response, e.g., following steel breakage, digitized points were sparsely distributed. Otherwise, the plots provide an accurate representation of the recorded data.

The results of the instrumented data are discussed in this chapter and the plotted data are presented in Reference 10. More detailed discussions of the experimental results and comparisons with the analytical results are presented in Chapter 4.

LOAD-DEFLECTION DATA

The midspan deflection was plotted with respect to the reference channel water pressure for each test, resulting in a load-deflection curve. Because fundamental behavior of each slab could be readily interpreted through a careful examination of the load-deflection curve, those data were plotted and monitored as each test progressed. Decisions to change the rate of loading and to terminate each test were based on observations of the real-time load-deflection curve.

The termination of each test was, in general, based on the objective to observe the state of the slab just prior to the incipient collapse deflection. However, the actual decision to terminate a test was governed by one or more of the following criteria:

1. Large decreases in pressure with little, if any, increase in deflection, indicating significant deterioration of slab capacity.

2. Very large deflections, approaching the limits of which the rubber membranes could be stretched.

3. Very high pressures, significantly exceeding the calibrated limits of the instrumentation.

4. Malfunction of equipment or instrumentation.

The character of the load-deflection data was, in general, similar to the idealized curve illustrated in Fig. 3.3(a). The typical curve exhibited a peak in load capacity

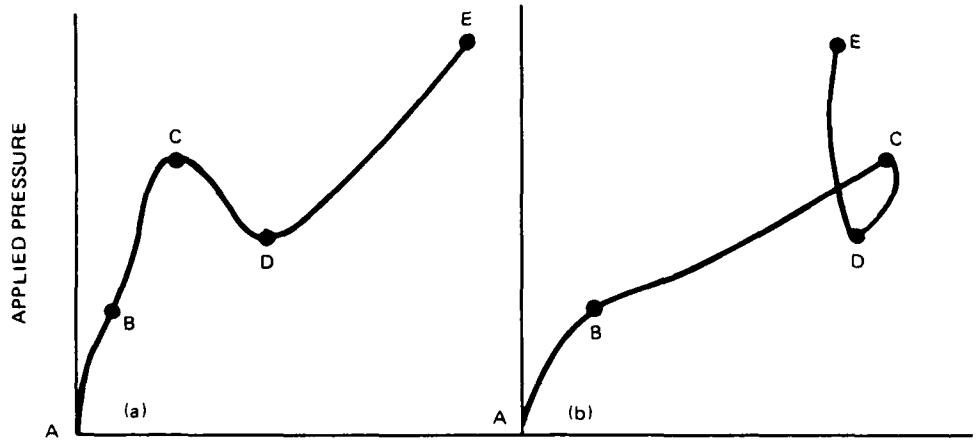

PHASE	SLAB BEHAVIOR
A-B	COMPRESSIVE MEMBRANE; MAJOR SUPPORT ROTATIONS
B-C	COMPRESSIVE MEMBRANE; MINOR SUPPORT ROTATIONS
C-D	PLASTIC DECAY
D-E	TENSILE MEMBRANE

FIG. 3.3.-Typical Relationship Between Experimental Deflections and Coupling Forces

at relatively small deflections, followed by a sharp decline in capacity with still larger deflections, and then another increase in capacity until the incipient collapse deflection was approached. The initial rise in load was primarily due to flexural action. However, the flexural stiffness of the slab, i.e., the slope of the load-deflection curve, was enhanced by thrusts generated from the restricted lateral movement of the ends of the slab. An increase in the peak capacity also resulted from the presence of compressive membrane forces. The ensuing decline in capacity corresponded with a reduction in thrust and instabilities of the slab. Because the ends of the slab were restrained from lateral movement in either direction, tensile stresses could be developed throughout the slab at very large deflections. That action, known as tensile membrane behavior, resulted in both the top and bottom layers of reinforcement acting as a tensile net with a capacity primarily determined by the rupture strength of the steel.

The slabs which had substantially different behavior than that described above can be divided into two groups. First, the slabs with the smallest reinforcement ratio in each span-thickness group (slabs 1,2,7,8) did not demonstrate an enhanced capacity in the tensile membrane stage. Second, two thin slabs with large support rotations (slabs 10,10A) did not exhibit a definitive compressive membrane peak. An

analysis of the behavior of each of these slabs is in the following chapter.

One characteristic feature of the load-deflection curves for this test program which distinguishes them from the previous tests of fully restrained slabs was a noticeable change in slope at relatively small deflections. That change correlated with an increase in support rotations and resulted in a decrease of slab stiffness. In nearly every test, the most substantial portion of the support rotations occurred prior to the initial peak in capacity. As planned, the full effects of support rotations were felt before any significant damage occurred to the slabs. Although this type of response was not a perfect idealization of the partial restraint provided by flexible supports in actual slabs, it was not assumed to produce significant differences in behavior in the latter stages of the load-deflection curves.

SUPPORT ROTATIONS

Support rotations were computed by measuring the lateral movement of a particular point located on the side and near the bottom of the support rack. As illustrated in Fig. 3.4, support rotations could be approximated by using trigonometric relationships and by knowing the center of rotation, the geometry of the support rack, and a component of displacement.

As stated before, it was very difficult to provide accurate control of support rotations. However, the amount of rotation which did occur could be accurately evaluated after each test was completed and the results processed. In some cases, rotations at one support were substantially different than at the other.

As a point of reference, rotations for each support were computed at the time each slab reached its compressive membrane capacity. Only minor support rack rotations occurred in most of the slabs after that point. Subsequent support rotations were primarily due to plastic rotations in the slabs. The measured and computed results for support rack rotations are presented in Table 3.2.

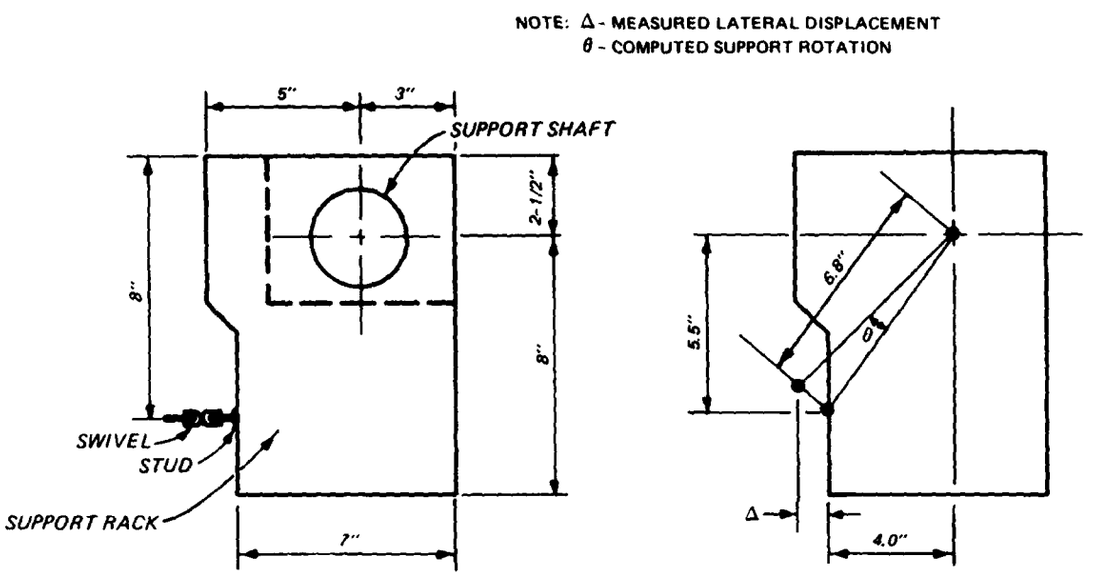

(a)

Actual Support Rack Configuration

(b)

Support Rack Geometry for Computing Rotations

FIG. 3.4.-Method of Approximating Support Rotations

TABLE 3.2.-Support Rotations

	Lateral deflection, in inches			Rack rotation, in degrees		
Slab	D3	D4	Average	at D3	at D4	Average
1	0.14	0.20	0.17	1.50	2.14	1.82
2	0.10	0.19	0.145	1.08	2.04	1.56
3	0.01	0.22	0.115	0.14	2.36	1.24
4	0.10	0.18	0.14	1.08	1.93	1.50
4A	0.19	0.28	0.235	2.04	3.00	2.52
4B	0.12	0.29	0.205	1.29	3.12	2.20
5	0.05	0.05	0.05	0.55	0.55	0.55
6	0.14	0.24	0.19	1.50	2.57	2.04
7	0.10	0.01	0.055	1.08	0.14	0.61
8	0.21	0.20	0.205	2.25	2.14	2.20
9	0.04	0.20	0.12	0.45	2.14	1.29
9A	0.01	0.06	0.035	0.14	0.66	0.40
10	0.30	0.22	0.26	3.22	2.36	2.79
10A	0.20	0.18	0.19	2.14	1.93	2.04
11	0.12	0.02	0.07	1.29	0.24	0.76
12*	0.21	0.16	0.19	2.25	1.72	2.04

Note: * Denotes slabs with substantial rotations occurring after the peak capacity was reached.

LATERAL LOADS

One of the objectives for the experimental phase of this project was to measure the axial forces generated from the restrained lateral movement of the slabs. During the initial phase of loading, the geometry of deformation of the slabs caused in-plane forces to act outward at the support and resulted in compressive membrane behavior. As the slabs underwent very large deflections, the in-plane forces changed directions and resulted in tensile membrane behavior. Load washers were used to measure both the compressive and tensile in-plane forces which were generated as the slab deformed.

The load washers were positioned in specially designed assemblies located on the large shafts at the ends of the support racks. Each of the four support shafts were capable of utilizing the load cells; however, to minimize the number of data channels, load cells were not used at every support.

The design of the reaction structure permitted the thrusts to be measured at the mid-thickness of each slab. By varying the thickness of the plates between the slab and the support rack, the central axis of each different slab was made to correspond with the center of the support shafts. The load washers were positioned on studs located at the same level as the center of each shaft.

Fig. 3.5 illustrates the way in which the actual thrusts were measured. Application of the equation for horizontal equilibrium of the support rack shows that the total lateral force in the slab is equal to the summation of forces in the spring assemblies, F2, and the shaft assemblies, F1. Thrusts were calculated at the time each slab reached its peak flexural capacity. Those results are provided in Table 3.3.

Observations of the load washer records after the initial tests led to concerns about the magnitudes of thrusts being generated. Several attempts were made to improve the quality of the recorded thrust data including (1) the use of precision- machined washers adjacent to the load washers to improve the load transfer, (2) the use of lubricated, stainless-steel bearings to minimize the effects of friction,

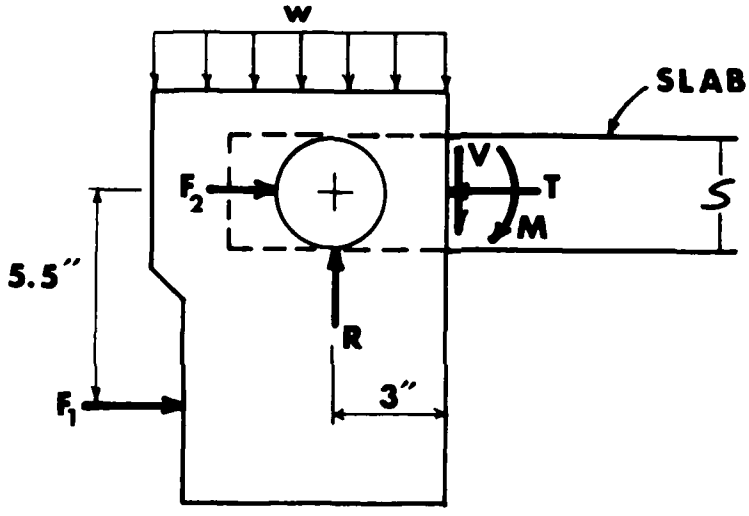

F_1 = SUM OF FORCES IN SPRING ASSEMBLIES

F_2 = SUM OF FORCES IN SHAFT ASSEMBLIES

FIG. 3.5.-Free-Body Diagram Used in Computing Support Thrusts and Moments

TABLE 3.3.-Load-Washer Data

	Left Support				Right Support				Average	
Slab	F1, kips	F2, kips	T, kips	M, in-k	F1, kips	F2, kips	T, kips	M, in-k	T, kips	M, in-k
1	30.9	7.2	38.1	120.0	20.6	21.8	42.4	63.3	40.3	91.7
2	16.7	4.1	20.8	58.6	11.7	3.1	14.8	31.1	17.8	44.9
3	15.8	0.8	16.6	40.9	7.3	1.6	8.9	-5.8	12.8	17.6
4	24.5	1.9	26.4	89.2	21.6	*	*	73.2	26.4	81.2
4A	19.8	0.8	20.6	64.7	15.7	*	*	42.2	20.6	53.5
4B	23.6	0.4	24.0	80.4	19.4	*	*	57.3	24.0	68.9
5	16.1	2.4	18.5	26.0	22.6	6.2	28.8	61.7	23.7	30.9
6	29.9	4.0	33.9	106.3	24.9	1.7	26.6	78.8	30.3	92.6
7	*	4.5	*	*	*	4.4	*	*	*	*
8	*	1.7	*	*	4.8	9.0	13.8	11.8	13.8	11.8
9	14.8	3.8	18.6	55.9	15.0	6.3	21.3	56.5	39.9	56.5
9A	6.7	3.0	9.7	10.7	9.9	5.8	15.7	19.5	12.7	19.5
10	4.4	1.5	5.9	6.2	5.1	1.1	6.2	8.2	6.1	8.2
10A	7.0	1.8	8.8	20.5	4.9	1.2	6.1	14.8	7.5	14.8
11	14.0	4.2	18.2	47.7	*	4.1	*	47.7	18.2	47.7
12	0.0	*	*	-14.0	0.9	*	*	-11.5	*	-11.5

Notes:
(1) * Denotes unavailable or erroneous data.
(2) Some of the averages are actually based on single records when second records are unavailable.

and (3) the preloading of the load washers by the tightening of adjustment screws in order to reduce losses in thrust from seating between the load cells and reaction structure. The latter change resulted in some irregularities in the format of data from test to test because each washer could actually measure both tensile and compressive in-plane loads.

SUPPORT MOMENTS

The design of the reaction structure was such that the various member end action components such as lateral thrusts, vertical reactions, rotations, and moments could essentially be isolated from each other and measured. In a previous section, support rotations were computed by considering the lateral displacement of a point on a support rack. The moments at the supports were found by monitoring the loads which passed through the spring assemblies located at approximately the same position on the rack. Utilizing the same concept as for rotations, i.e., knowing the center of rotation and geometry, the moment resistance provided by external sources at the supports could be determined.

The conversion of measured loads to member end actions is illustrated in Fig. 3.5 (p. 79). Moments at the end of each slab were measured by applying the equation of moment equilibrium to the support rack. Because the load in the shaft assemblies, F2, the vertical supporting force, R, and the thrust at mid-surface of the slab, T, each passed through the axis of the shaft, a summation of moments would only include the resultant load in the spring assemblies, F1, the shear force at the edge of the slab, V, and the pressure acting on the surface of the support rack. The pressure on the support rack added an eccentric force due to the assymetric design of the rack with respect to a vertical axis passing through the center of the support shaft. It proved

to add a significant component to the resisting moment for several of the slabs.

Load washers were placed in each of the spring assemblies along the support racks to determine the coupling forces for the support moments. For most tests, data from three load washers along each support rack were added to compute the total coupling force for each supported end of the slab. Difficulties in accurately balancing the initial loads and precisely controlling the deflections in the spring assemblies sometimes led to an unequal distribution of loads in each of the washers. Nevertheless, because of the extreme stiffness of the support racks, the distribution of moments along the widths of the slabs at the supports was considered to be uniform. In other words, each unit portion of the slab's width was considered to carry an equal part of the end moment.

Both qualitative and quantitative evaluations of the load-washer data were made. Quantitatively, support moments were computed at the time each slab reached its peak flexural capacity, or in the cases of slabs 10 and 10A, at the time they reached Johansen's load. A summary of the load-washer data and results of the moment calculations are illustrated in Table 3.3 (p. 80). A qualitative evaluation of the load-washer data throughout the total range of loading follows.

Since the support moments were linearly related to the coupling forces detected by the load washers, discussions of the moment resistance have been expressed in terms of the

actual loads which were measured. Those loads, as monitored by LW1-LW6, typically resulted in the idealized curve of Fig. 3.3(b) (p. 72). The general character of that curve was found to occur in most tests, particularly when the load-deflection curve of the slab was similar to the one illustrated in Fig 3.3(a) (p. 72).

As the applied pressure was initially increased, the support rotations occurred, the spring assemblies were seated, and some load was transmitted to the washers. When the disc springs closed completely, the coupling forces significantly increased until the peak flexural capacity was reached. From that point until the applied pressure was decreased to terminate the test, the coupling forces remained nearly constant. That action indicated that plastic hinges had been formed at the supports and plastic rotations occurred with a small change in support moments.

STRAIN GAGE DATA

Steel strain gages were placed on the principal reinforcement in every slab. Top and bottom bars located nearest the middle portion of each slab were instrumented with strain gages at midspan, quarterspan, and one support. Alternate strain gages were mounted on an adjacent pair of bars to provide backup instrumentation and, in some cases, to provide duplicate records for verification of the major strain-gage records.

Because the strain gages could not be located in advance exactly at the critical sections and because of the bond characteristics between the strain gage and adjacent materials, the quantitative aspects of the strain gage records are of little value. However, the general character of the strain plots can be of assistance in determining the overall behavior of the steel in the general vicinity of the critical sections. For example, evidence of tension or compression in the reinforcement can be observed from the data. Also, the records may reveal if the reinforcement yielded. However, records that do not indicate yielding of the steel may not accurately reflect the actual conditions at the critical sections.

Concrete strain gages were cemented to the exterior surfaces of several of the slabs. Although the gages were capable of being mounted internally, there was concern that the gages might induce spalling or otherwise influence the behavior of the slabs.

AD-A174 597 BEHAVIOR OF PARTIALLY RESTRAINED REINFORCED CONCRETE SLABS(U) ARMY ENGINEER WATERWAYS EXPERIMENT STATION VICKSBURG MS STRUCTURES LAB L K GUICE SEP 86 2/3

UNCLASSIFIED WES/TR/SL-86-32 F/G 13/3 NL

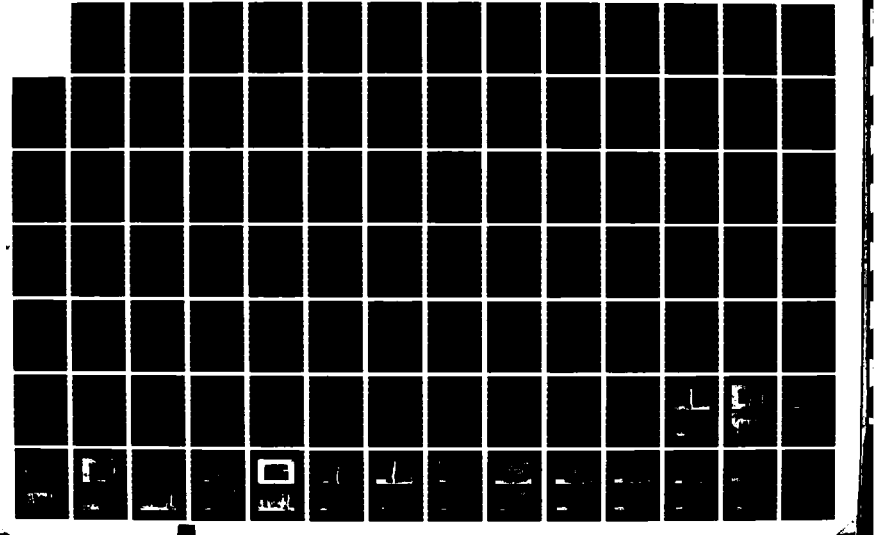

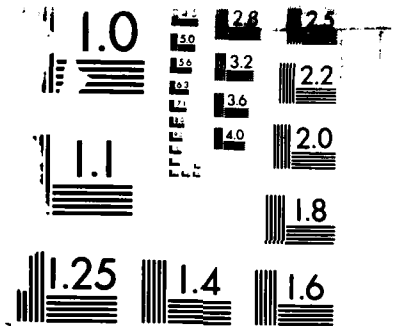

MICROCOPY RESOLUTION TEST CHART

Plots of all strain gage records can be found in Reference 10. To arrive at a meaningful way to summarize those data, Table 3.4 was created to illustrate the stage of loading at which each strain gage recorded first yield. In the cases where yielding did not occur, the final state of the reinforcement, i.e., tension or compression, was recorded. The symbols used in Table 3.4 correspond to the letters representing the different phases of loading illustrated in Fig. 3.3(a) (p.72). Strain gage positions are shown in Fig. 2.4 (p. 51).

TABLE 3.4.-Strain Gage Data

	Stage at which yielding of steel is first observed or final state of strain if yield does not occur, (+) Tension (-) Compression						Maximum Concrete Strain, in./in.	
Slab	ST1	ST2	ST3	SB1	SB2	SB3	CT1	CB3
1	BC+	-	C-	CD+	-	AB+	0.0005	0.009
2	BC+	D+	-	DE+	AB+	AB+		
3	BC+	DE+	CD+	D+	AB+	AB+	0.011	0.0002
4	BC+	+	BC+	DE+	CD+	AB+		
4A	C+	DE+	DE+	DE+	AB+	AB+		
4B	BC+	+	D+	+	AB+	AB+		
5	C+	DE+	AB+	BC+	E+	CD-	0.008	0.001
6	BC+	D+	BC-	+	DE+	AB+		
7	AB+	-	BC+	DE+	DE+	BC+	0.006	0.0006
8	CD+	+	DE+	DE+	AB+	AB+		0.0001
9	C+	DE+	DE+	DE+	DE+	BC+	0.004	0.0015
9A	C+	DE+	DE+	DE+	DE+	BC+	0.004	0.0009
10	DE+	DE+	DE+	AB-	AB+	AB+		
10A	-	+	+	DE+	DE+	AB+		
11	BC+	DE+	-	DE+	DE+	CD+		
12	DE+	DE+	DE+	DE+	DE+	C+	0.004	0.0004

Note: Each mnemonic represents a load stage as represented in Fig. 2.4 (p. 51). The sign indicates state of strain.

An investigation of the tabulated results yields valuable insight into the behavior of the slabs. In practically every case, yielding was first observed in the steel located at the bottom of the slab at midspan and was followed by yielding at the bottom at quarterspan and then at the top of the supports. Those results indicate significant flexural action in the slabs. It is also interesting to note that except at the bottom midspan and top support, yielding generally did not occur anywhere in the thin slabs until they reached the tensile membrane stage. This suggests very little flexural damage occurred in those slabs.

Also listed in Table 3.4 (p. 85) are the values of the maximum recorded concrete strains for the tests in which those results were available. Although larger strains were recorded in some cases, the values listed in Table 3.4 (p. 85) are considered to be the maximum reliable strains. With regard to those values, two things are worthy of note. First, very large strains were apparent in most of the tests at midspan indicating a probable enhancement in the ultimate strains due to the effects of confinement. Second, the maximum strains at the support were fairly small because the gages could not be mounted precisely at the critical sections.

CHAPTER IV

ANALYSIS

INTRODUCTION

One of the objectives of this program was to develop a better understanding of the behavioral characteristics of slabs with the given parameters. To meet that objective, analyses of the slabs were performed using existing theoretical relationships. A comparison of analytical and experimental load-deflection curves was used as the criterion for evaluating the effectiveness of the analytical procedures. The aspects of the slabs' response which were considered to be most important for analysis were the peak flexural capacity and the tensile membrane response.

Existing analytical techniques do not permit a full consideration of imperfect boundary conditions. Most slab theories consider only perfectly-fixed or simply-supported boundaries. In reality, relatively few slabs fit into those categories. How slabs respond with partial restraint, both lateral and rotational, is the major focus of this study.

The analytical efforts of this program were two-fold. First, analyses were conducted to determine if existing techniques for perfectly-restrained slabs can be used to provide bounds for the capacities of slabs with variable boundary conditions. Second, new methodologies for analyzing partially-restrained slabs were investigated.

CONVENTIONAL SLAB ANALYSES

Yield Line Theory and Analysis.-The flexural behavior of reinforced concrete slabs has received a great deal of attention by engineers for many years. Since conventional failure criteria were originally based on small deflections, only the initial flexural behavior was considered to be of importance by the early investigators. More recently, engineers have recognized that the predominant response of slabs under large loads is controlled by plastic behavior at various critical sections. Because of their relative simplicity and ease of application to more complex slab geometries, plasticity-based theories have received the greatest amount of attention in recent years.

Johansen's yield line plasticity theory [17] offers a means for determining the pure ultimate flexural capacity of slabs, i.e., the capacity neglecting in-plane forces in the slab. The yield line theory is based on the plastic moment capacities of a slab's critical cross-sections. When the moment capacities of enough sections have been exceeded to permit a mechanism to form, the slab is considered to have achieved its limiting capacity. The load which theoretically produces a mechanism is known as Johansen's load. Portions of the slab between yield lines are considered to behave elastically and have a negligible effect on the ultimate capacity. Provided a correct failure mechanism is assumed and neglecting thrusts, the yield line method will provide an

upper bound solution for the ultimate capacity of a slab.

Yield line analyses were conducted for the one-way slab strips which were tested in the experimental program. The geometric characteristics of the slab strips were such that the correct failure mechanism could be postulated with confidence. That mechanism was defined by plastic hinges formed at midspan and both supports. However, because various degrees of free rotation were permitted at supports, the formation of plastic hinges at those locations could not be assured. If hinges did not form at the supports during the initial stage of loading, then the slabs essentially would have behaved as simply-supported slabs. On the other hand, if free rotations were small enough to require plastic hinges to form at the supports, then the slabs would have been essentially fixed. Consequently, yield line values were computed for both simply-supported and fixed boundary conditions.

The ultimate flexural load for a slab may be derived by equating the work caused by external forces to the internal work performed along the hinge lines. The ultimate capacity for a uniformly-loaded, simply-supported, one-way slab may be expressed as follows

$$w = \frac{8M_n}{L^2 B} \qquad \ldots\ldots\ldots\ldots\ldots\ldots\ldots\ldots (4.1)$$

in which w = the maximum uniform load on the slab in psi; M_{nm} = the nominal moment of resistance along the plastic hinge

line at midspan in in-lb; L = the length of the slab in the principal direction in inches; and B = the width of the slab in inches. For a one-way slab with fixed boundary conditions, the sum of the nominal moments of resistance along the hinge lines at midspan and one support would replace the term M_{nm} in Eq. 4.1.

The nominal moment capacities for the critical cross-sections were calculated in accordance with the procedure contained in the 1983 American Concrete Institute Code (1). The analyses accounted for the contributions of the compression reinforcement to the total moment of resistance. Because the same areas of steel were used in the top and bottom of each slab, the nominal resisting moments at midspan and supports were identical. Specific quantities used in computing the nominal moments are presented in Table 4.1. Results of the yield line flexural analyses are provided in Table 4.2. Yield line capacities based on simply supported conditions are labeled W_{js} and on fixed conditions are labeled W_{jf}.

TABLE 4.1.-Values for Parameters Used in Analytical Computations

	Reinforcement		Slab		Materials	
Slab	Area, sq.in.	Ratio	Thickness, in.	Depth, in.	Steel Strength, psi	Concrete Strength, psi
1	0.240	0.0052	2.3125	1.9375	50000	4414
2	0.240	0.0052	2.3125	1.9375	50000	4269
3	0.343	0.0074	2.3125	1.9375	58470	4443
4	0.343	0.0074	2.3125	1.9375	58470	4258
4A	0.343	0.0074	2.3125	1.9375	58470	4165
4B	0.343	0.0074	2.3125	1.9375	58470	4201
5	0.490	0.0106	2.3125	1.9375	58470	4450
6	0.490	0.0106	2.3125	1.9375	58470	4279
7	0.175	0.0058	1.625	1.25	67330	5023
8	0.175	0.0058	1.625	1.25	67330	4968
9	0.343	0.0114	1.625	1.25	58470	5015
9A	0.343	0.0114	1.625	1.25	58470	5005
10	0.343	0.0114	1.625	1.25	58470	4965
10A	0.343	0.0114	1.625	1.25	58470	4963
11	0.441	0.0147	1.625	1.25	58470	5018
12	0.441	0.0147	1.625	1.25	58470	4973

Notes:
(1) All slabs had lengths = 24 in. and widths = 24 in.
(2) All slabs had depth to compression steel = 0.375 in.
(3) Steel areas and percentages were same for each face.
(4) The ultimate strain in concrete was assumed = 0.003.

TABLE 4.2-Results of Yield Line Analyses

Slab	Cross-Sectional Moment Capacity M_n, kip-in	Johansen's Load Simple Supports W_{js}, psi	Johansen's Load Fixed Supports W_{jf}, psi
1	24.1	14.0	28.0
2	24.0	13.9	27.8
3	37.2	21.6	43.2
4	37.0	21.4	42.8
4A	37.0	21.4	42.8
4B	37.0	21.4	42.8
5	51.0	29.5	59.0
6	50.8	29.4	58.8
7	16.0	9.2	18.4
8	16.0	9.2	18.4
9	24.0	13.9	27.8
9A	24.0	13.9	27.8
10	24.0	13.9	27.8
10A	24.0	13.9	27.8
11	29.3	17.0	34.0
12	29.3	16.9	33.8

Compressive Membrane Theory.-Recent tests [11] have confirmed that the yield line theory significantly underpredicts the ultimate capacity of slabs, particularly if the slabs are laterally restrained. The enhancement in strength over the yield line capacity is attributable to compressive membrane action. Compressive membrane thrusts resulting from the restricted movement of the slab's edges increase the moment capacities of the critical cross-sections and, consequently, enhance the total capacity of the slab.

Theories have been developed to predict the peak capacity of slabs with compressive membrane forces [5, 24,

28]. Most of the theories are quite similar, and are developed by considering the equilibrium and deformations of a slab strip similar to Fig. 4.1. The theory, as presented by Park and Gamble [27] and Keenan [19] and modified to conform with notation used in this work, follows.

This derivation is based on a rigid-plastic slab strip formed as the result of a three-hinge mechanism in a one-way slab. Consideration is given to axial deformations and lateral support movements. From Fig. 4.1 (a) and (b), the geometry of deformations of the flexurally-rigid slab strip yields the relationship

$$\cos\theta = \frac{(x+t)}{x + (h-c_s)\tan\theta - c_m \tan\theta - \varepsilon x} \quad \ldots\ldots (4.2a)$$

in which ε = the sum of elastic, creep and shrinkage strains, and t = lateral movement of one support. The other undefined terms are represented in Fig. 4.1.

Rewriting the equation using trigonometric identies

$$h - c_s - c_m = \frac{2x \sin^2(\theta/2) + \varepsilon x \cos\theta + t}{\sin\theta} \quad \ldots\ldots (4.2b)$$

For small angles, $\sin\theta = \delta/x$ and $\cos\theta = 1$. Therefore

$$c_s + c_m = h - \delta/2 - \frac{\varepsilon x^2}{\delta} - \frac{xt}{\delta} \quad \ldots\ldots\ldots\ldots (4.2c)$$

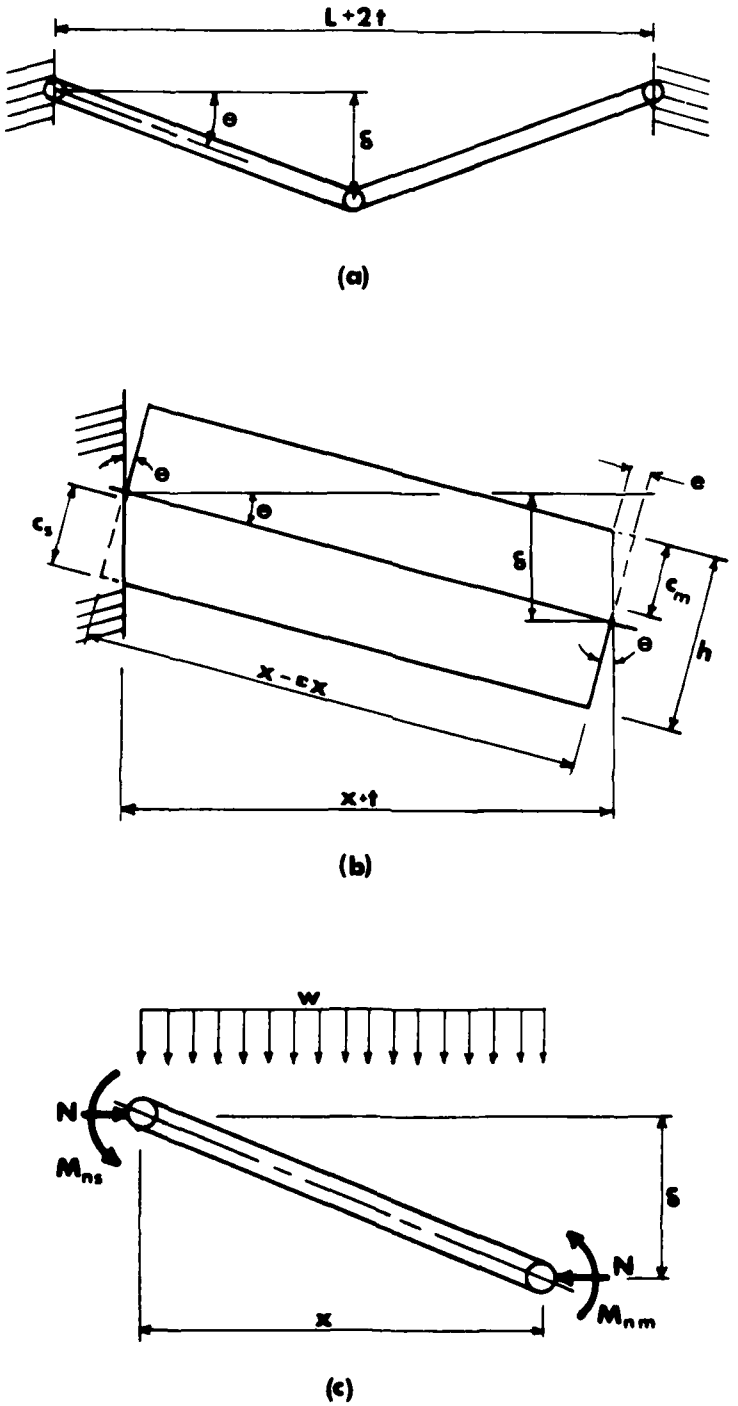

FIG. 4.1.-Geometry of Deformation for (a) Slab Strip, (b) Half-Slab Strip, and (c) Free-Body Diagram

In the previous expression there are essentially five unknowns, those being the depths of the neutral axis at midspan, c_m, the depth of the neutral axis at the support, c_s, the midspan deflection, δ, the axial strain, ε, and the lateral support movement, t. Four more equations or assumptions are required in order to find a unique solution to Eq. 4.2c.

One additional equation involving the same unknowns is derived by enforcing horizontal equilibrium requirements on the rigid strip in Fig. 4.2

$$C_{cs} + C_{ss} - T_s = C_{cm} + C_{sm} - T_m \quad \ldots\ldots\ldots\ldots \quad (4.3)$$

The forces in the concrete, C_{cs} and C_{cm}, in the compression steel, C_{ss} and C_{sm}, and in the tension steel, T_s and T_m, can be computed if given a strain distribution along each section. Using Bernoulli's principle to establish the variation of strains throughout each section results in the following expressions for strains in the tension and compression steels, respectively,

$$\varepsilon_s = \varepsilon_c(d-c)/c$$

$$\varepsilon'_s = \varepsilon_c(c-d')/c \quad \ldots\ldots\ldots\ldots\ldots\ldots \quad (4.4)$$

where ε_c = the strain in the outer fiber of the concrete, and c, d, and d' are the distances illustrated in Fig. 4.2 for

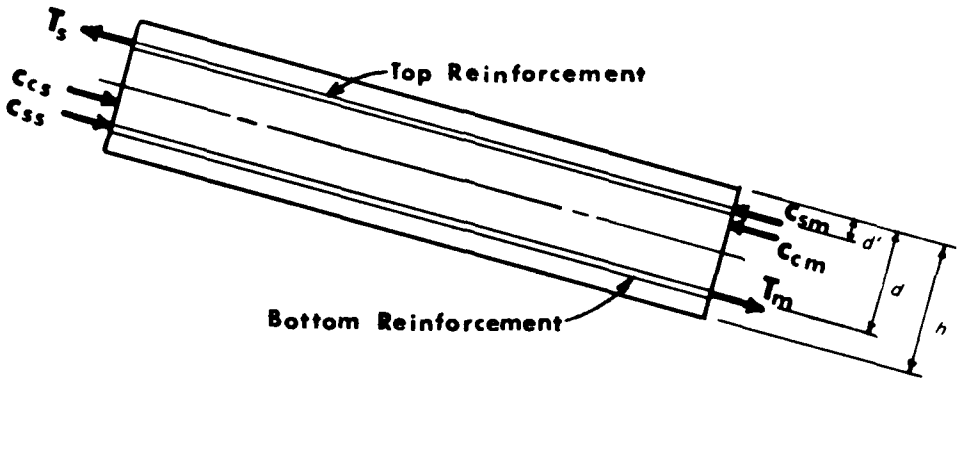

(a)

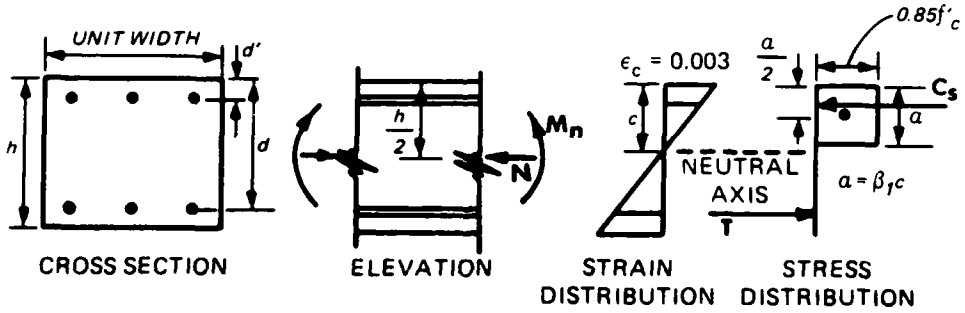

(b)

FIG. 4.2.-(a) Forces on Yield Sections of Slab Strip and (b) Details of Yield Sections

each section as appropriate. Equation 4.4 essentially adds two unknowns to the system of equations, those being the outer concrete strains at each section. The strain in the concrete at each section is typically assumed to be at its ultimate value at the time the slab is at its peak flexural capacity. However, this imposes some rather strict limitations in the applicability of this theory as is discussed in the following paragraphs.

With the strains known, each of the sectional forces can be readily computed and then substituted into Eq. 4.3. Consistent with the assumption that the concrete is at ultimate strain, Whitney's stress block relationship is used to determine the forces in the concrete at each section

$$C_{cs} = 0.85\, f'_c\, \beta_1\, c_s$$
$$C_{cm} = 0.85\, f'_c\, \beta_1\, c_m \qquad \ldots\ldots\ldots\ldots\ldots\ldots \quad (4.5)$$

The steel forces are expressed in terms of the average stresses over the respective steel areas. Stresses are derived from the strains given by Eq. 4.4 and the specified constitutive model. Although any steel model may be used, an elastic-perfectly plastic model is most common. The substitution of the expressions for steel and concrete forces into Eq. 4.3 yields a second equation for determining the load-deflection relationship of a slab.

A third equation can be derived from moment equilibrium of the rigid strip in Fig. 4.1(c) (p. 94)

$$M_{ns} + M_{nm} - N\delta = \frac{WL^2}{8} \quad \ldots\ldots\ldots\ldots\ldots\ldots \quad (4.6)$$

The moments and thrust required for Eq. 4.6 can be expressed in terms of the sectional forces shown in Fig. 4.2

$$N = C_c + C_s - T$$

$$M_n = C_c\left(\frac{h}{2} - \frac{\beta_1 c}{2}\right) + C_s\left(\frac{h}{2} - d'\right) + T\left(d - \frac{h}{2}\right) \quad \ldots\ldots \quad (4.7)$$

where the forces and distances are substituted for each section as appropriate. Substitution of Eq. 4.7 into Eq. 4.6 yields the third equation in terms of the unknowns c_s and c_m.

Eq. 4.2 accounts for the effects of axial shortening and support movements. As is the case for actual slabs, the equation is very sensitive to those secondary effects. The magnitude of thrust is reduced as supports are displaced and as elastic, creep, and shrinkage axial strains occur. Accompanying that relief in thrust is a reduction in the internal moment of resistance.

The final two equations are expressed in terms of the axial thrust. The strains due to axial deformations of the strip can be computed by summation of the strains due to elastic shortening and strains due to creep and shrinkage,

$$\varepsilon = \frac{N}{E_c A_c} + \varepsilon_p \quad \ldots\ldots\ldots\ldots\ldots\ldots\ldots \quad (4.8)$$

where E_c = modulus of elasticity of the concrete and A_c = gross cross-sectional area of the strip. Effects of the longitudinal reinforcement on the axial stiffness are neglected.

If lateral support movement is considered, and if it is due to elastic displacement of the support, then

$$t = \frac{N}{S} \qquad \text{. . . . . (4.9)}$$

where t = the lateral displacement of one support and S = the surrounding support stiffness.

With all terms defined, Eqs. 4.2-4.9 can be used to solve for the response of the slab. Equation 4.6 relates the deflection of the slab to the load imposed on it. The sectional forces and moments defined in Eq. 4.6 are computed from Eq. 4.7 and are based on an assumed strain distribution at each cross-section. Strains in the concrete are implicitly assumed to be independent of deformation or load since the concrete is always defined as being at its ultimate strain. The absence of a true strain-deformation relationship is the most significant drawback of this analytical procedure.

Although an assumption of ultimate concrete strains is valid near the peak capacity, such an assumption leads to significant errors when the slab is behaving elastically or partially elastic. Consequently, the previous theory is only valid when the deflection at which the peak capacity actually occurs is used. Park and Gamble get around this difficulty

by assuming a deflection at which the slab reaches its peak capacity, implying that at that time the concrete reaches its ultimate strain. Using the results of several tests, they conclude that a peak capacity deflection of one-half the slab thickness is adequate from the design standpoint since it normally underpredicts the ultimate load.

Rather than use an empirical approach, Keenan proposed a strain-deformation relationship which is valid for the strip geometry of Fig. 4.1,

$$\tan \theta = \frac{\delta}{x + t} = \frac{e}{c_m} \qquad \text{(4.10a)}$$

Assuming that the deformation, e, can be related to the ultimate strain in the concrete by the expression

$$e = \frac{x}{2}\epsilon_u \qquad \text{(4.10b)}$$

then Eqs. 4.10a and 4.10b can be rewritten to yield the midspan deflection in terms of the concrete strain or the midspan curvature

$$\delta = \frac{x\epsilon_u}{2c_m}(x + t) = \frac{x}{2}\phi_m(x + t) \qquad \text{(4.10c)}$$

where ϵ_u = ultimate strain in the concrete and ϕ_m = curvature at midspan. Equation 4.10c can be used to solve for the deflection at which the peak capacity is reached.

It should be noted that the above expression essentially lumps the total deformations at the support and midsection. It is implied that those deformations are due to curvatures. That is somewhat inconsistent with the assumption of a rigid strip which only undergoes rotations and axial deformations and by definition is not permitted to bend. However, Keenan demonstrated that the equation provides a reasonable estimate of the peak capacity deflection.

He did suggest that the deflection predicted by the equation should be limited to some upper value as the span-thickness ratio increases. In those cases where the slab was relatively thin, i.e., span-thickness ratio greater than about 18, Keenan indicated that failure would probably occur by geometric instability rather than material instability.

Equation 4.10c is very sensitive to the lateral movement of the supports, which is in turn dependent on the stiffness of the surrounds. Since there is very little information on the lateral stiffness of the supports for most experimental programs including the previous programs at WES, Eq. 4.10c has not been rigorously verified. However, analyses of rigidly restrained slabs which were tested at WES have revealed that an upper bound solution for the peak capacity can be obtained by using Eq. 4.10c and assuming an infinite lateral stiffness at the supports.

Compressive Membrane Analyses.-A computer code was developed incorporating an iterative solution scheme for Eqs. 4.2-4.10. To obtain an upper bound compressive membrane solution a very large support stiffness was used, effectively permitting no support movement. Only elastic shortening due to the large thrusts was considered in reducing the magnitudes of the computed thrusts and resisting moments.

Other solutions were determined for support stiffnesses which were assumed to be more representative of the experimental conditions. To obtain those stiffnesses, a portion of the shaft assembly (See Appendix II) was loaded in a uniaxial compression device. It was determined that the assembly had a lower stiffness during the initial stage of loading due to seating between the threaded bolt and cylinder. Consequently, in the tests where the shaft assemblies were preloaded, a slightly higher support stiffness would be expected. Results of the analyses for the different support stiffnesses are included in Table 4.3.

The code initially computed the deflection at which peak capacity would be reached according to Eq. 4.10c and then followed with a computation of the peak capacity using Eqs. 4.2-4.9. To check the validity of Eqs. 4.2-4.9 independent of Eq. 4.10c, the code was modified to give the ultimate capacity for different values of deflection ranging from approximately zero to some arbitrary point where tensile membrane forces would normally occur, e.g., a deflection approximately equal to the thickness of the slab. A line

passing through each computed point was constructed on the experimental load-deflection curves shown in Figs. 4.3-4.18. Each line is labeled as W_{um} indicating that it is the ultimate load as predicted by compressive mebrane theory. Also included on each of Figs. 4.3-4.18 is a horizontal line labeled as W_{ua} representing the peak capacities as predicted by Eqs. 4.2-4.10c using the stiffest support condition.

TABLE 4.3.-Results of Compressive Membrane Analyses

	Analytical						Experimental	
	Condition A		Condition B		Condition C			
Slab	W_{ua}, psi	δ/t	W_{ub}, psi	δ/t	W_{uc}, psi	δ/t	W_u, psi	δ/t
1	74.4	0.11	66.6	0.16	63.5	0.17	78	0.32
2	72.9	0.11	65.4	0.16	62.5	0.17	52	0.37
3	89.3	0.11	81.3	0.16	78.2	0.17	72	0.52
4	89.3	0.11	79.9	0.16	77.0	0.17	71	0.65
4A	86.2	0.11	79.1	0.16	76.3	0.17	69	0.58
4B	86.6	0.11	79.4	0.16	76.6	0.17	77	0.56
5	105.1	0.11	97.1	0.16	94.0	0.17	98	0.37
6	103.5	0.11	96.0	0.16	93.1	0.17	91	0.65
7	32.6	0.25	28.2	0.32	26.2	0.35	32	0.37
8	32.4	0.25	28.0	0.32	25.7	0.36	23	0.62
9	40.9	0.25	37.4	0.32	34.1	0.33	40	0.43
9A	40.9	0.25	37.4	0.32	34.1	0.33	41	0.31
10	40.7	0.25	37.2	0.32	34.1	0.33	--	----
10A	40.7	0.25	37.2	0.32	33.9	0.33	--	----
11	46.6	0.25	43.3	0.32	39.7	0.32	46	0.40
12	46.4	0.25	43.1	0.32	39.7	0.32	22	0.31

Notes:

(1) Condition A - Support stiffness = 1.0×10^{20} lb./in.
Condition B - Support stiffness = 5.4×10^{6} lb./in.
Condition C - Support stiffness = 3.0×10^{6} lb./in.

(2) W_{ua} = peak capacity for condition A
W_{ub} = peak capacity for condition B
W_{uc} = peak capacity for condition C

(3) δ/t = peak capacity deflection/thickness

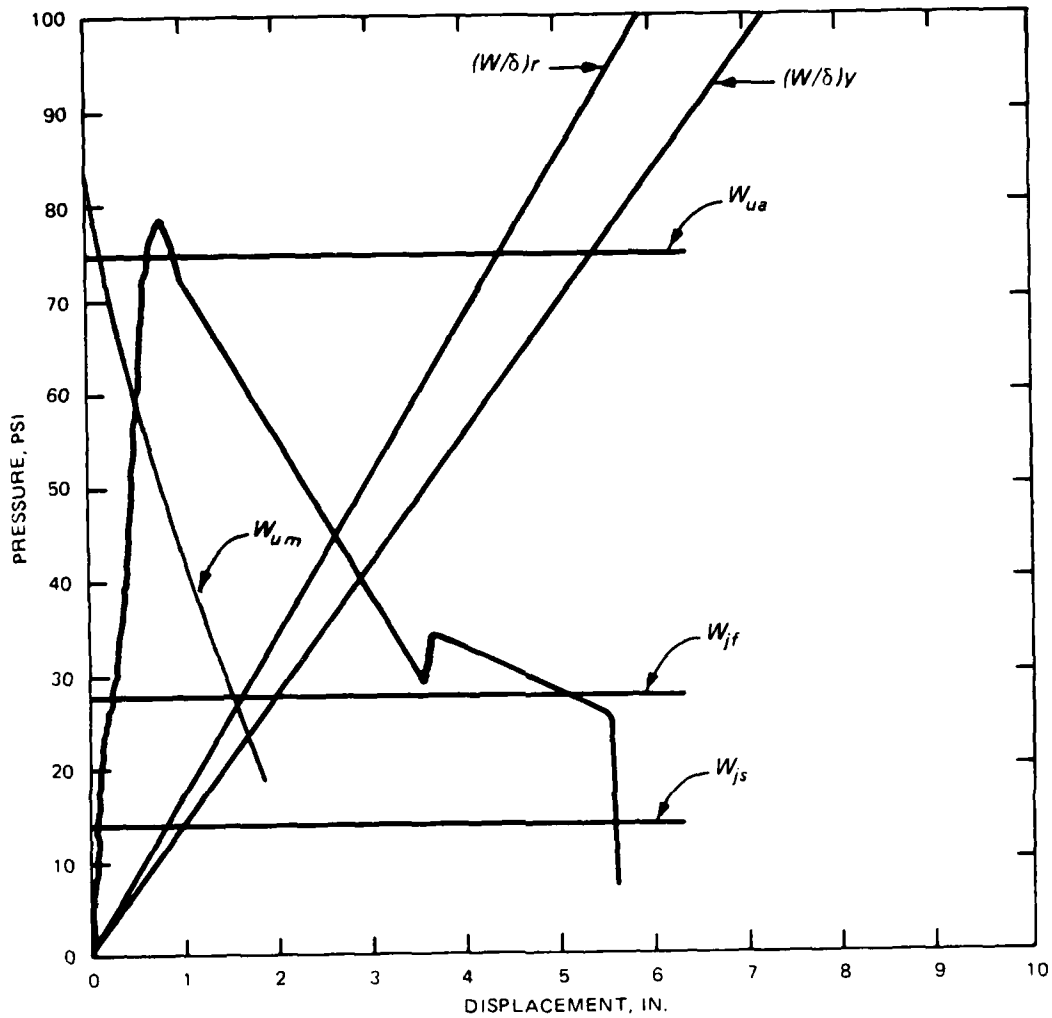

Notation:

W_{js}	=	Yield line load assuming simple supports
W_{jf}	=	Yield line load assuming fixed supports
W_{ua}	=	Compressive membrane capacity considering Eq. 4.10c for predicting peak deflection
W_{um}	=	Compressive membrane capacity evaluated at different peak capacity deflections
$(W/\delta)y$	=	Slope of tensile membrane curve using yield strength of steel
$(W/\delta)r$	=	Slope of tensile membrane curve using rupture strength of steel

FIG. 4.3.-Experimental and Analytical Comparisons for Slab 1

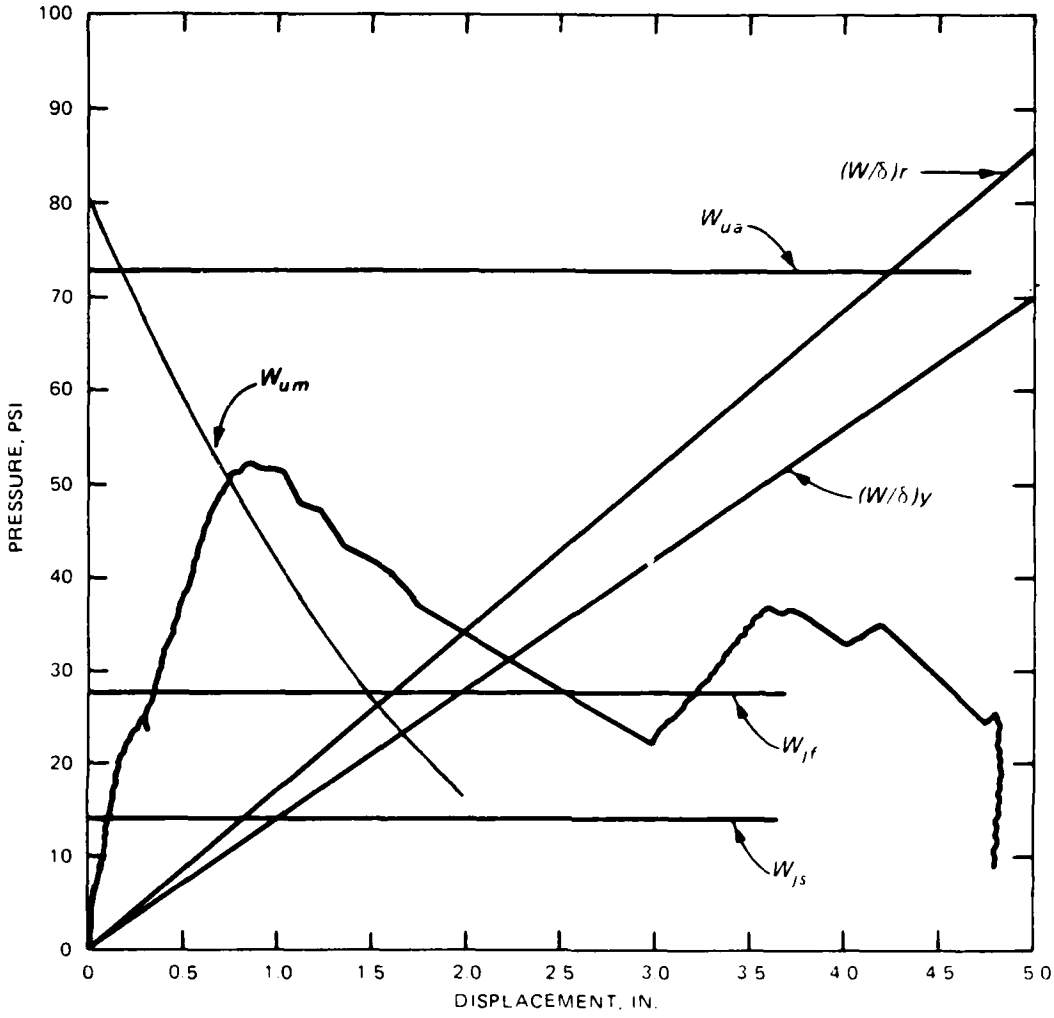

Notation:

W_{js}	=	Yield line load assuming simple supports
W_{jf}	=	Yield line load assuming fixed supports
W_{ua}	=	Compressive membrane capacity considering Eq. 4.10c for predicting peak deflection
W_{um}	=	Compressive membrane capacity evaluated at different peak capacity deflections
$(W/\delta)y$	=	Slope of tensile membrane curve using yield strength of steel
$(W/\delta)r$	=	Slope of tensile membrane curve using rupture strength of steel

FIG. 4.4.-Experimental and Analytical Comparisons for Slab 2

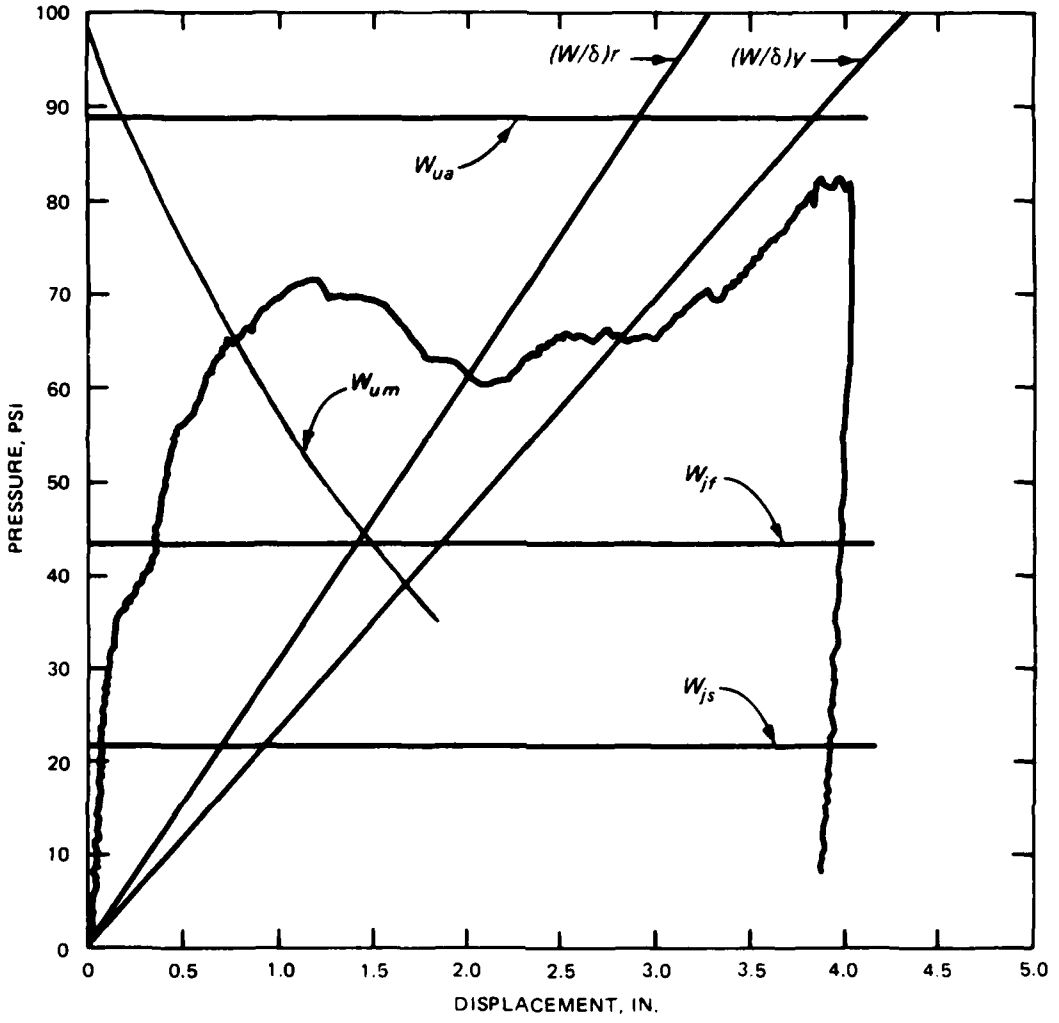

Notation:

W_{js}	=	Yield line load assuming simple supports
W_{jf}	=	Yield line load assuming fixed supports
W_{ua}	=	Compressive membrane capacity considering Eq. 4.10c for predicting peak deflection
W_{um}	=	Compressive membrane capacity evaluated at different peak capacity deflections
$(W/\delta)y$	=	Slope of tensile membrane curve using yield strength of steel
$(W/\delta)r$	=	Slope of tensile membrane curve using rupture strength of steel

FIG. 4.5.-Experimental and Analytical Comparisons for Slab 3

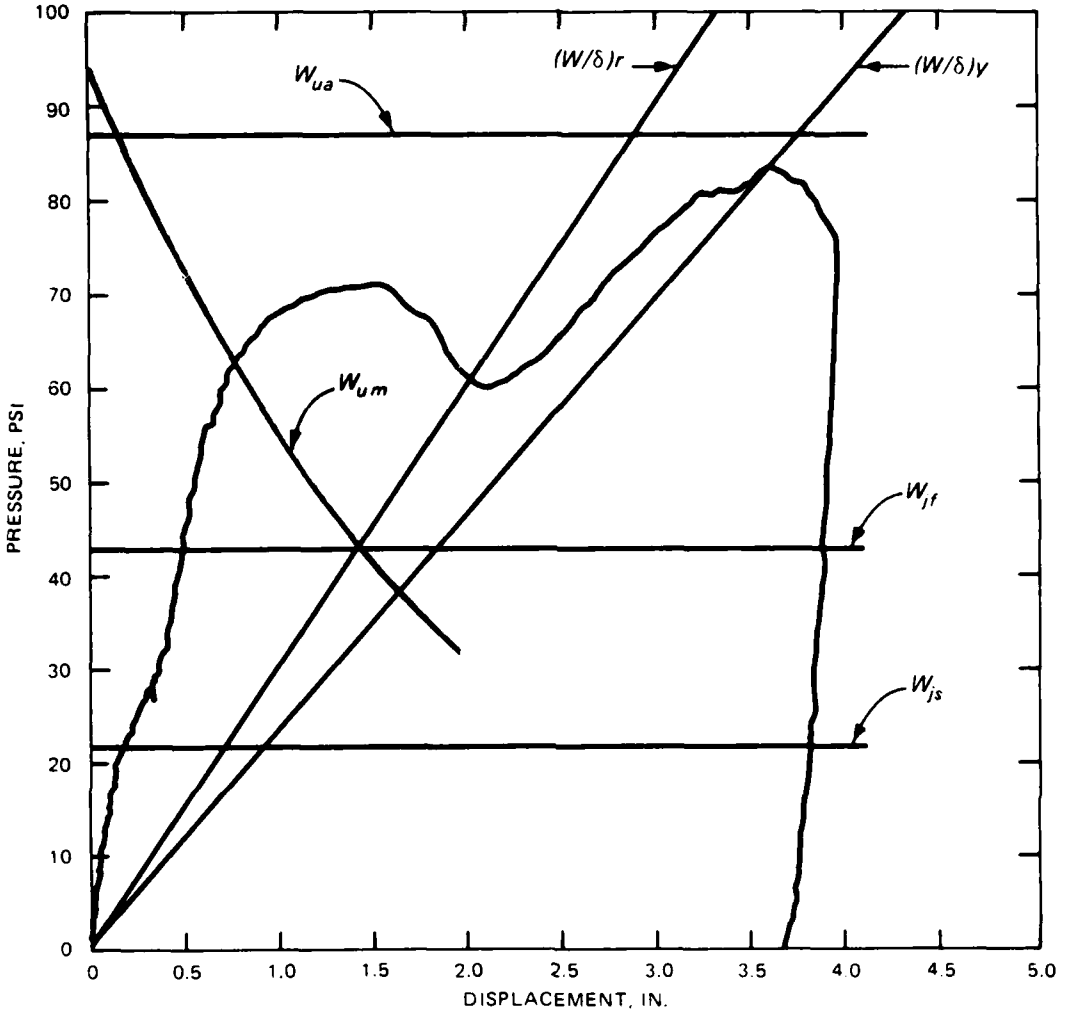

Notation:

W_{js}	=	Yield line load assuming simple supports
W_{jf}	=	Yield line load assuming fixed supports
W_{ua}	=	Compressive membrane capacity considering Eq. 4.10c for predicting peak deflection
W_{um}	=	Compressive membrane capacity evaluated at different peak capacity deflections
$(W/\delta)y$	=	Slope of tensile membrane curve using yield strength of steel
$(W/\delta)r$	=	Slope of tensile membrane curve using rupture strength of steel

FIG. 4.6.-Experimental and Analytical Comparisons for Slab 4

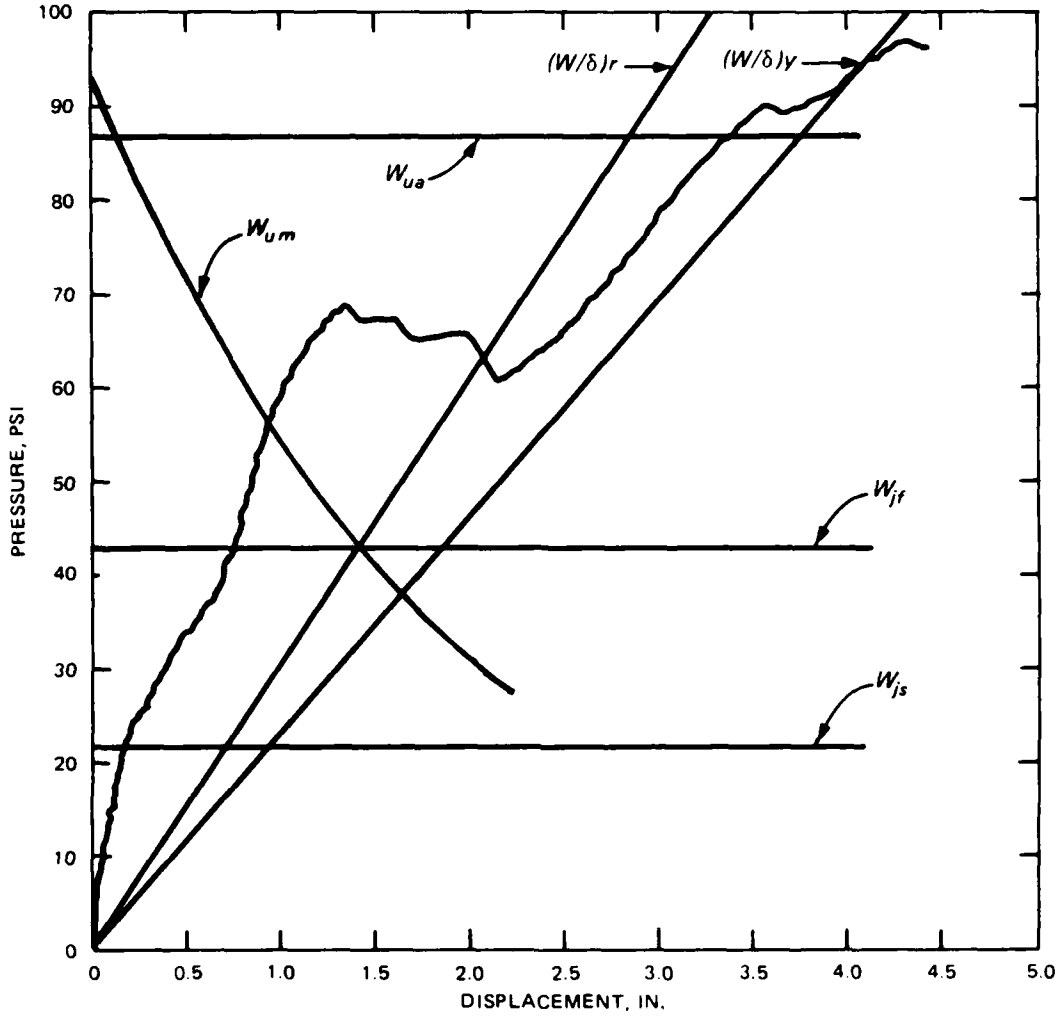

Notation:

W_{js}	=	Yield line load assuming simple supports
W_{jf}	=	Yield line load assuming fixed supports
W_{ua}	=	Compressive membrane capacity considering Eq. 4.10c for predicting peak deflection
W_{um}	=	Compressive membrane capacity evaluated at different peak capacity deflections
$(W/\delta)y$	=	Slope of tensile membrane curve using yield strength of steel
$(W/\delta)r$	=	Slope of tensile membrane curve using rupture strength of steel

FIG. 4.7.-Experimental and Analytical Comparisons for Slab 4A

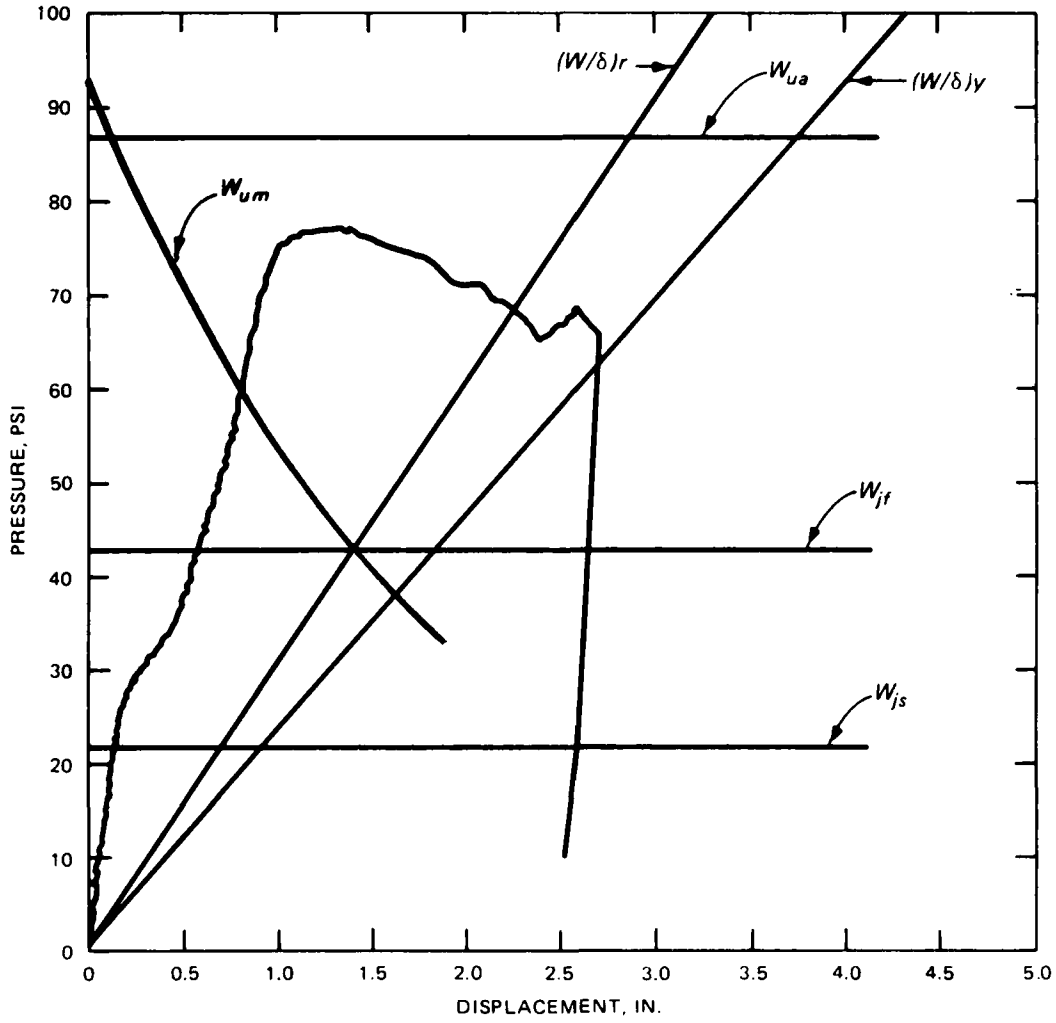

Notation:

W_{js}	=	Yield line load assuming simple supports
W_{jf}	=	Yield line load assuming fixed supports
W_{ua}	=	Compressive membrane capacity considering Eq. 4.10c for predicting peak deflection
W_{um}	=	Compressive membrane capacity evaluated at different peak capacity deflections
$(W/\delta)y$	=	Slope of tensile membrane curve using yield strength of steel
$(W/\delta)r$	=	Slope of tensile membrane curve using rupture strength of steel

FIG. 4.8.-Experimental and Analytical Comparisons for Slab 4B

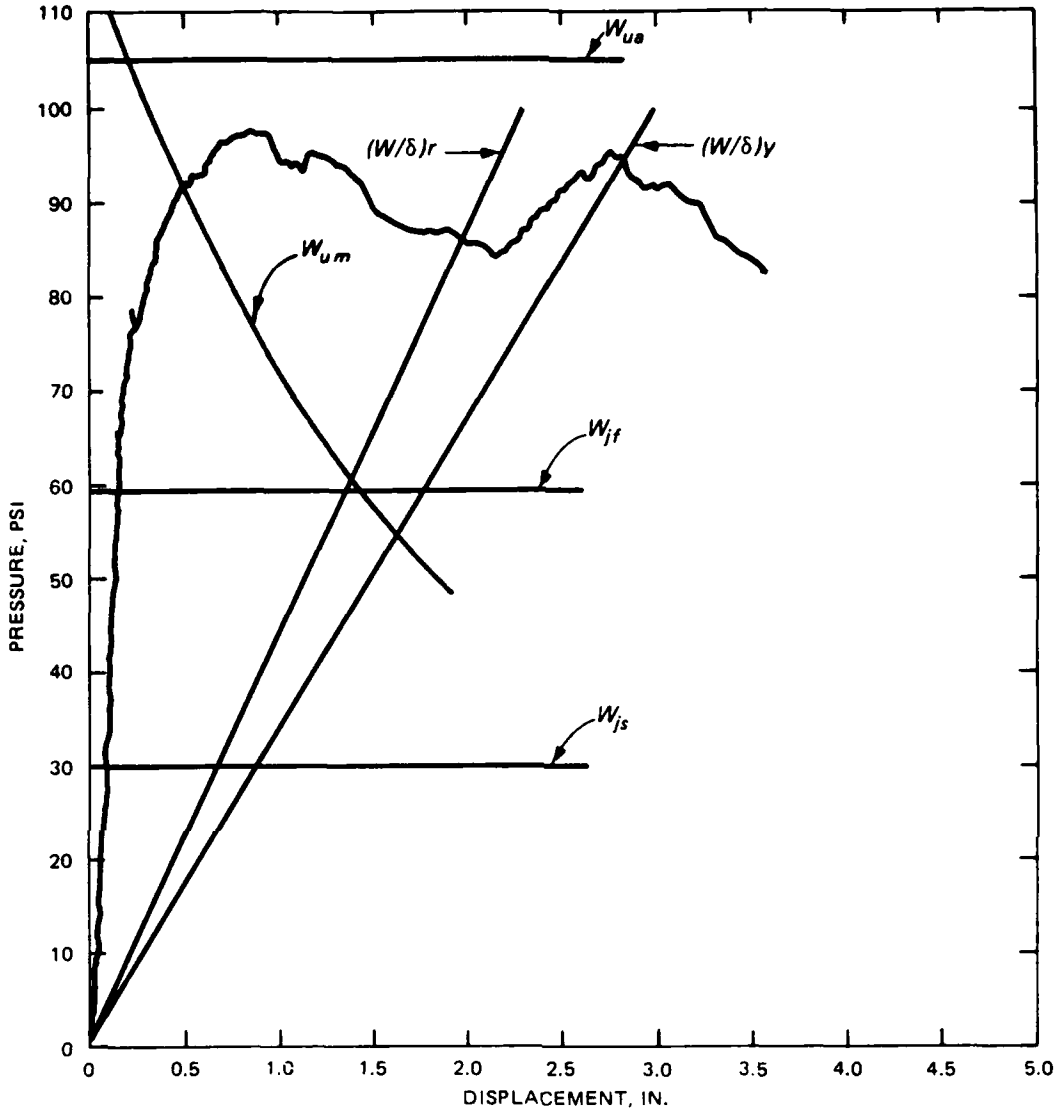

Notation:

W_{js}	=	Yield line load assuming simple supports
W_{jf}	=	Yield line load assuming fixed supports
W_{ua}	=	Compressive membrane capacity considering Eq. 4.10c for predicting peak deflection
W_{um}	=	Compressive membrane capacity evaluated at different peak capacity deflections
$(W/\delta)y$	=	Slope of tensile membrane curve using yield strength of steel
$(W/\delta)r$	=	Slope of tensile membrane curve using rupture strength of steel

FIG. 4.9.-Experimental and Analytical Comparisons for Slab 5

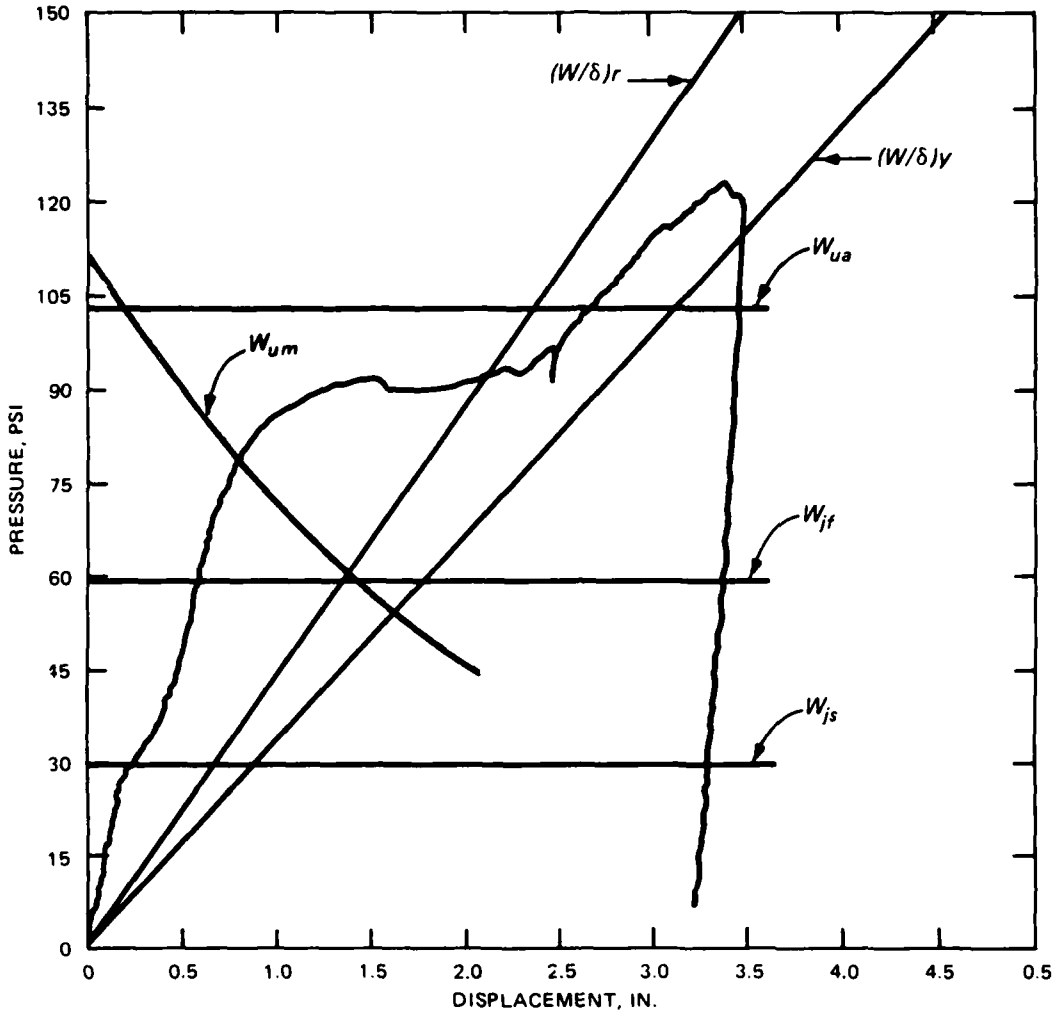

Notation:

W_{js}	=	Yield line load assuming simple supports
W_{jf}	=	Yield line load assuming fixed supports
W_{ua}	=	Compressive membrane capacity considering Eq. 4.10c for predicting peak deflection
W_{um}	=	Compressive membrane capacity evaluated at different peak capacity deflections
$(W/\delta)y$	=	Slope of tensile membrane curve using yield strength of steel
$(W/\delta)r$	=	Slope of tensile membrane curve using rupture strength of steel

FIG. 4.10.-Experimental and Analytical Comparisons for Slab 6

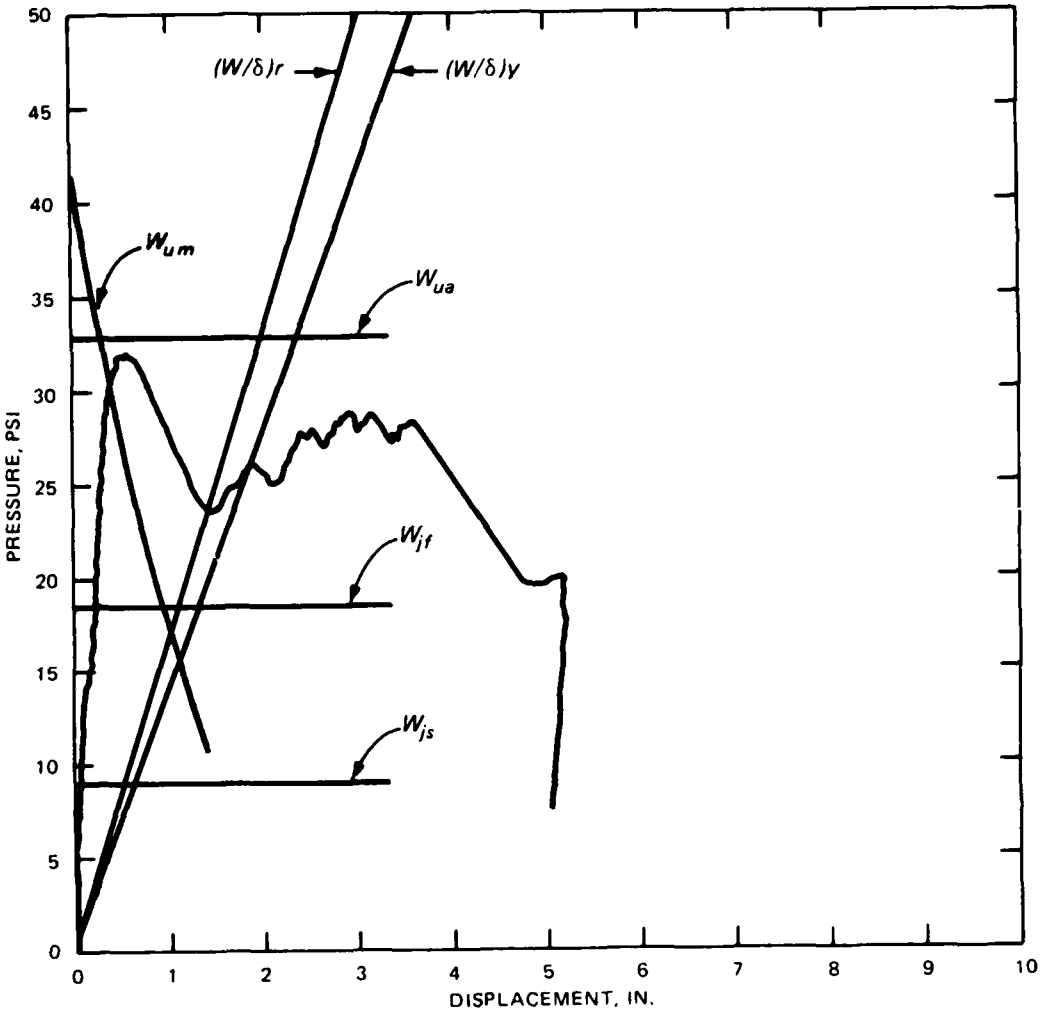

Notation:

W_{js}	=	Yield line load assuming simple supports
W_{jf}	=	Yield line load assuming fixed supports
W_{ua}	=	Compressive membrane capacity considering Eq. 4.10c for predicting peak deflection
W_{um}	=	Compressive membrane capacity evaluated at different peak capacity deflections
$(W/\delta)y$	=	Slope of tensile membrane curve using yield strength of steel
$(W/\delta)r$	=	Slope of tensile membrane curve using rupture strength of steel

FIG. 4.11.-Experimental and Analytical Comparisons for Slab 7

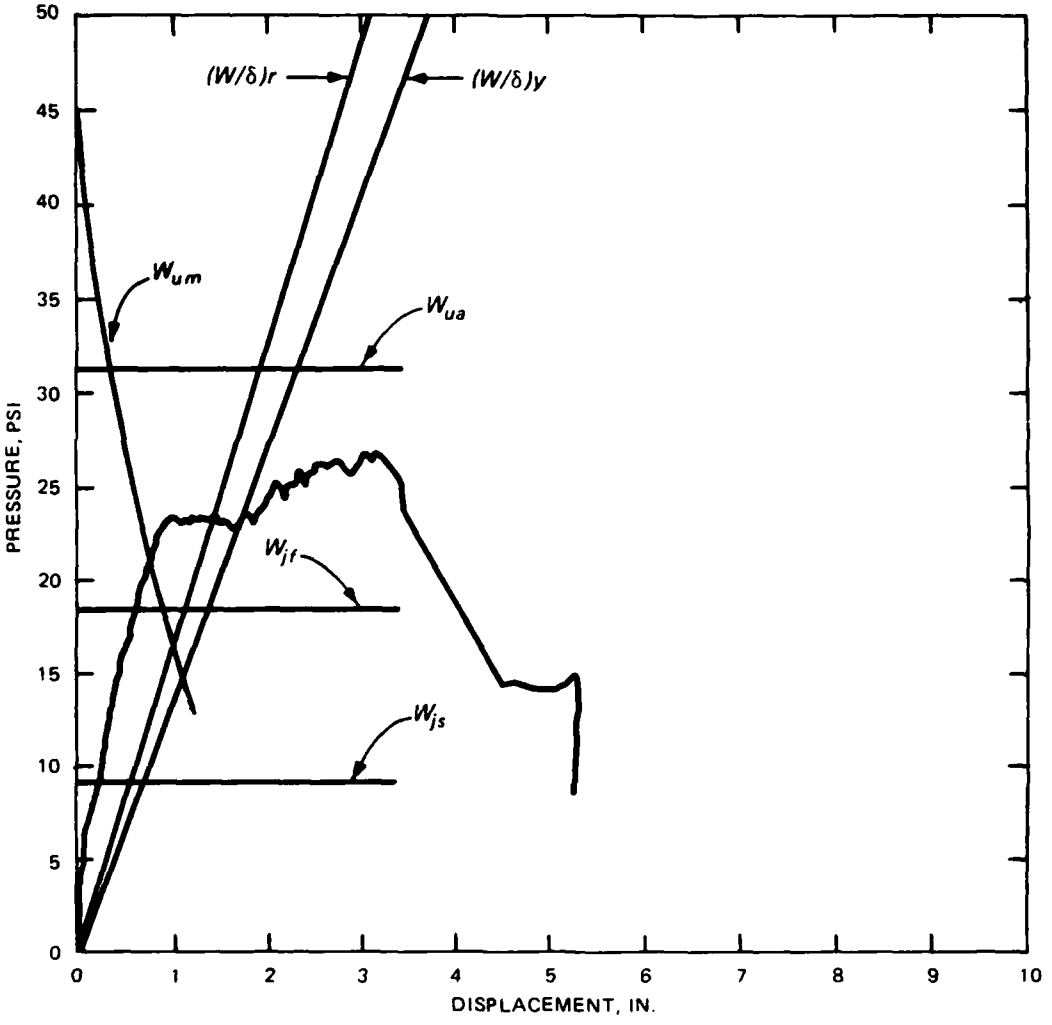

Notation:

W_{js}	=	Yield line load assuming simple supports
W_{jf}	=	Yield line load assuming fixed supports
W_{ua}	=	Compressive membrane capacity considering Eq. 4.10c for predicting peak deflection
W_{um}	=	Compressive membrane capacity evaluated at different peak capacity deflections
$(W/\delta)y$	=	Slope of tensile membrane curve using yield strength of steel
$(W/\delta)r$	=	Slope of tensile membrane curve using rupture strength of steel

FIG. 4.12.-Experimental and Analytical Comparisons for Slab 8

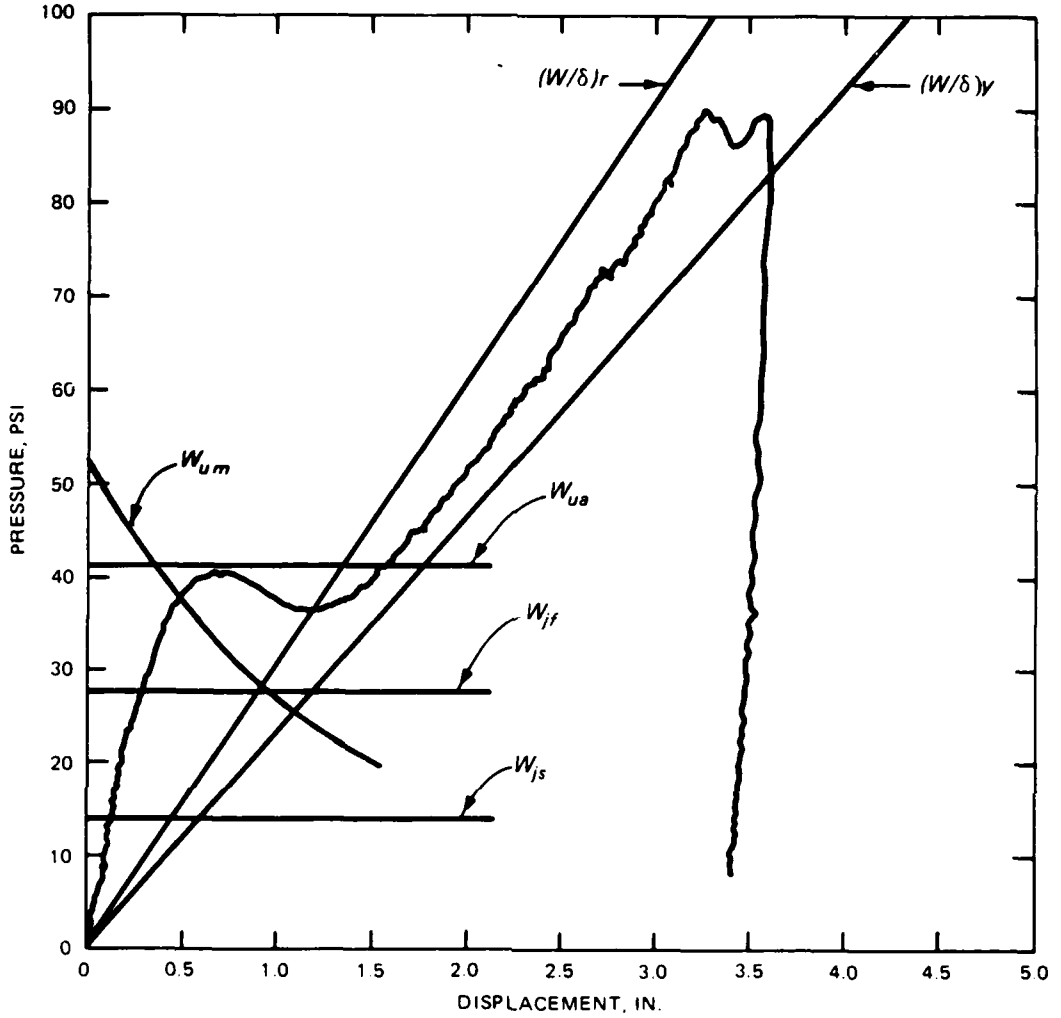

Notation:

W_{js}	=	Yield line load assuming simple supports
W_{jf}	=	Yield line load assuming fixed supports
W_{ua}	=	Compressive membrane capacity considering Eq. 4.10c for predicting peak deflection
W_{um}	=	Compressive membrane capacity evaluated at different peak capacity deflections
$(W/\delta)y$	=	Slope of tensile membrane curve using yield strength of steel
$(W/\delta)r$	=	Slope of tensile membrane curve using rupture strength of steel

FIG. 4.13.-Experimental and Analytical Comparisons for Slab 9

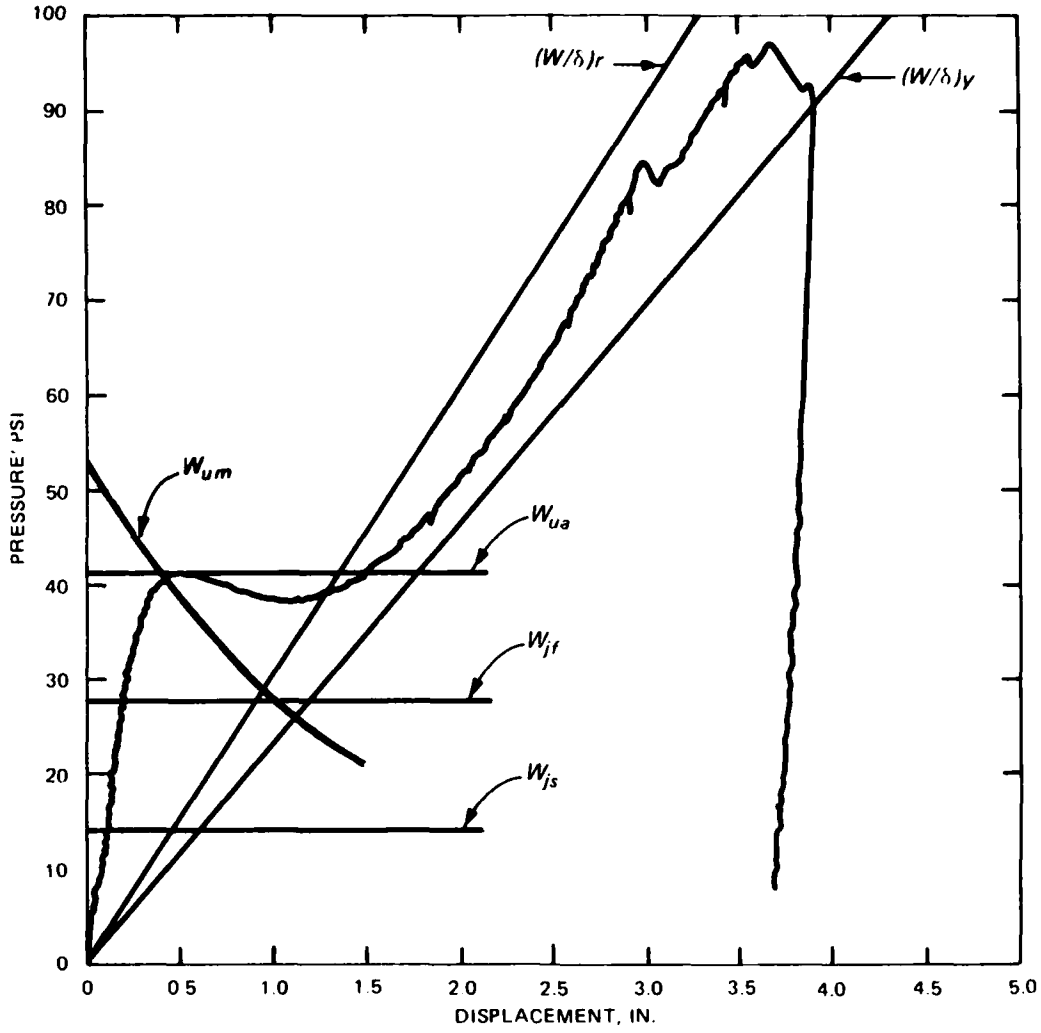

Notation:

W_{js}	=	Yield line load assuming simple supports
W_{jf}	=	Yield line load assuming fixed supports
W_{ua}	=	Compressive membrane capacity considering Eq. 4.10c for predicting peak deflection
W_{um}	=	Compressive membrane capacity evaluated at different peak capacity deflections
$(W/\delta)y$	=	Slope of tensile membrane curve using yield strength of steel
$(W/\delta)r$	=	Slope of tensile membrane curve using rupture strength of steel

FIG. 4.14.-Experimental and Analytical Comparisons for Slab 9A

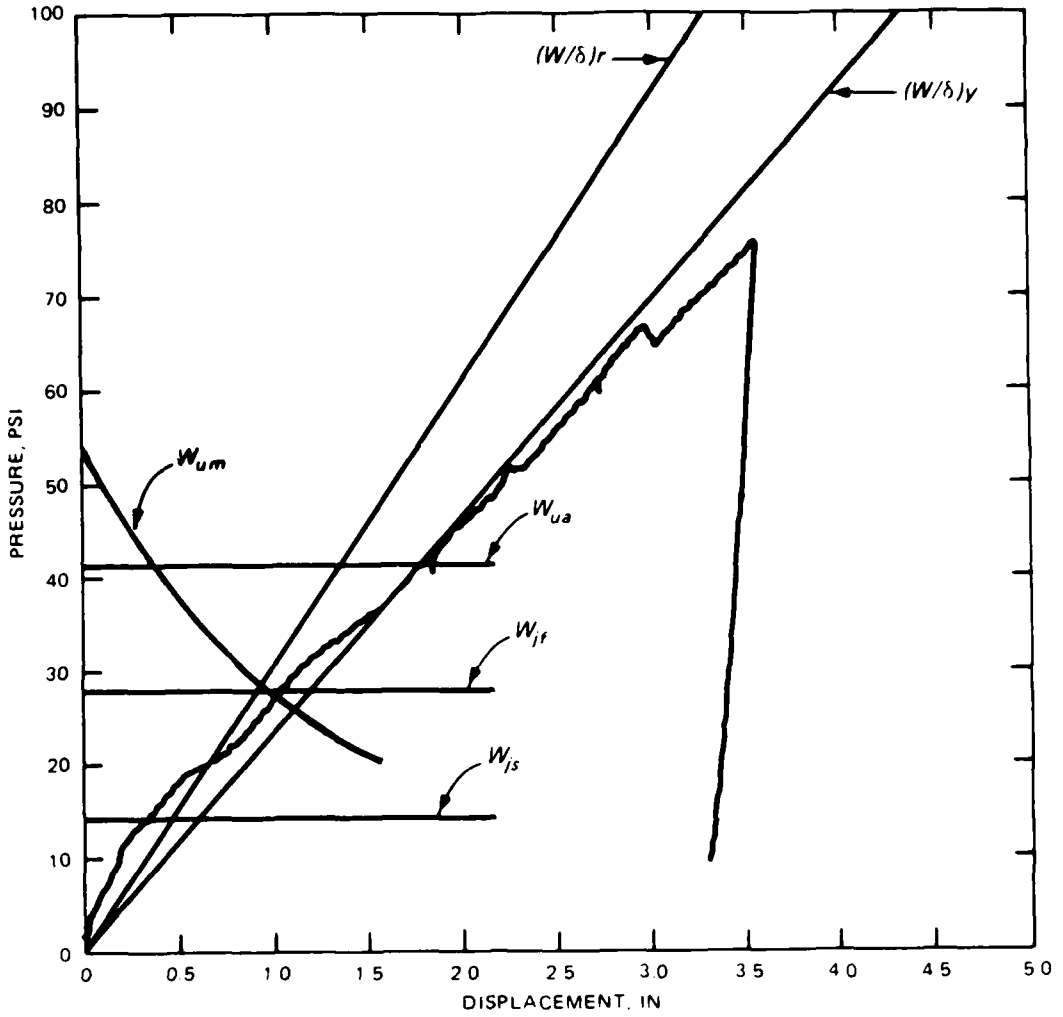

Notation:

W_{js}	=	Yield line load assuming simple supports
W_{jf}	=	Yield line load assuming fixed supports
W_{ua}	=	Compressive membrane capacity considering Eq. 4.10c for predicting peak deflection
W_{um}	=	Compressive membrane capacity evaluated at different peak capacity deflections
$(W/\delta)y$	=	Slope of tensile membrane curve using yield strength of steel
$(W/\delta)r$	=	Slope of tensile membrane curve using rupture strength of steel

FIG. 4.15.-Experimental and Analytical Comparisons for Slab 10

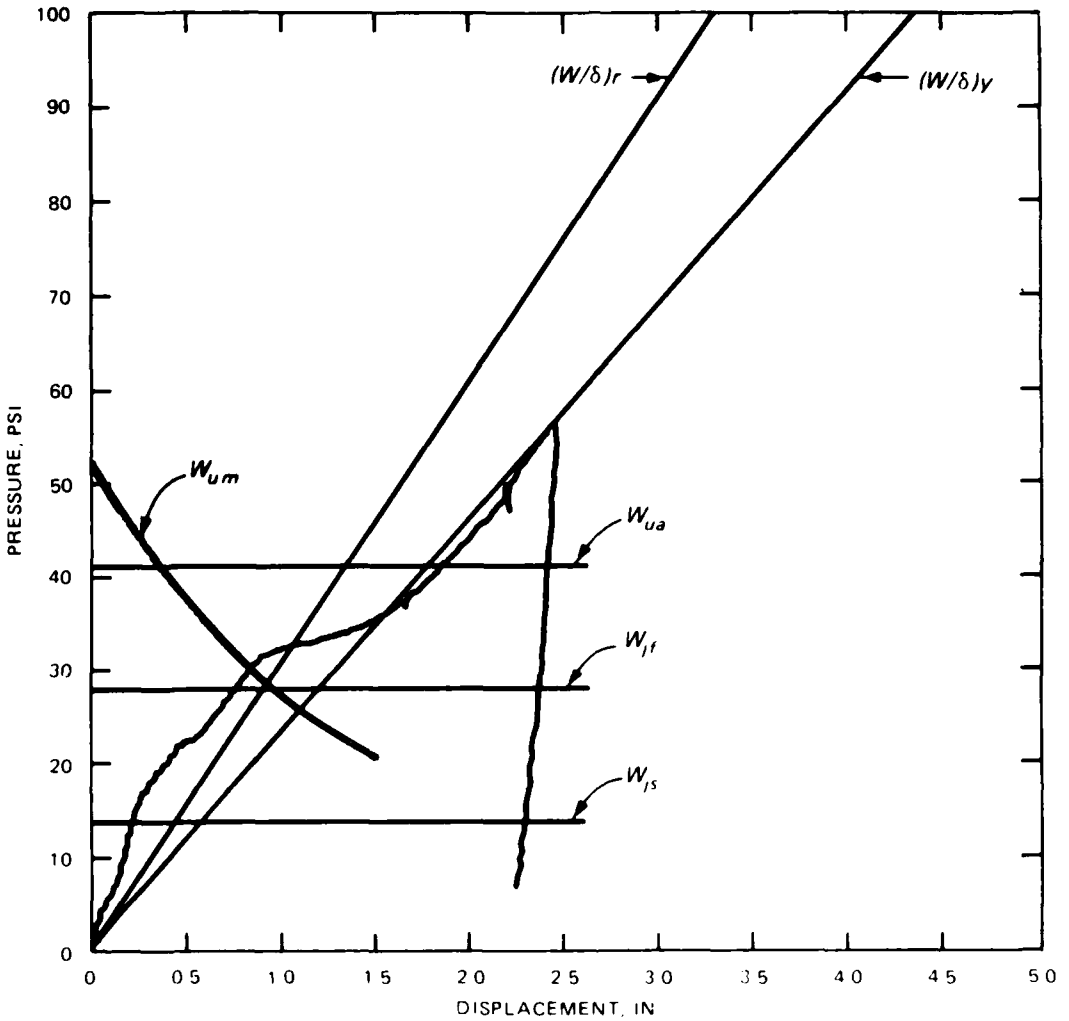

Notation:

W_{js}	=	Yield line load assuming simple supports
W_{jf}	=	Yield line load assuming fixed supports
W_{ua}	=	Compressive membrane capacity considering Eq. 4.10c for predicting peak deflection
W_{um}	=	Compressive membrane capacity evaluated at different peak capacity deflections
$(W/\delta)y$	=	Slope of tensile membrane curve using yield strength of steel
$(W/\delta)r$	=	Slope of tensile membrane curve using rupture strength of steel

FIG. 4.16.-Experimental and Analytical Comparisons for Slab 10A

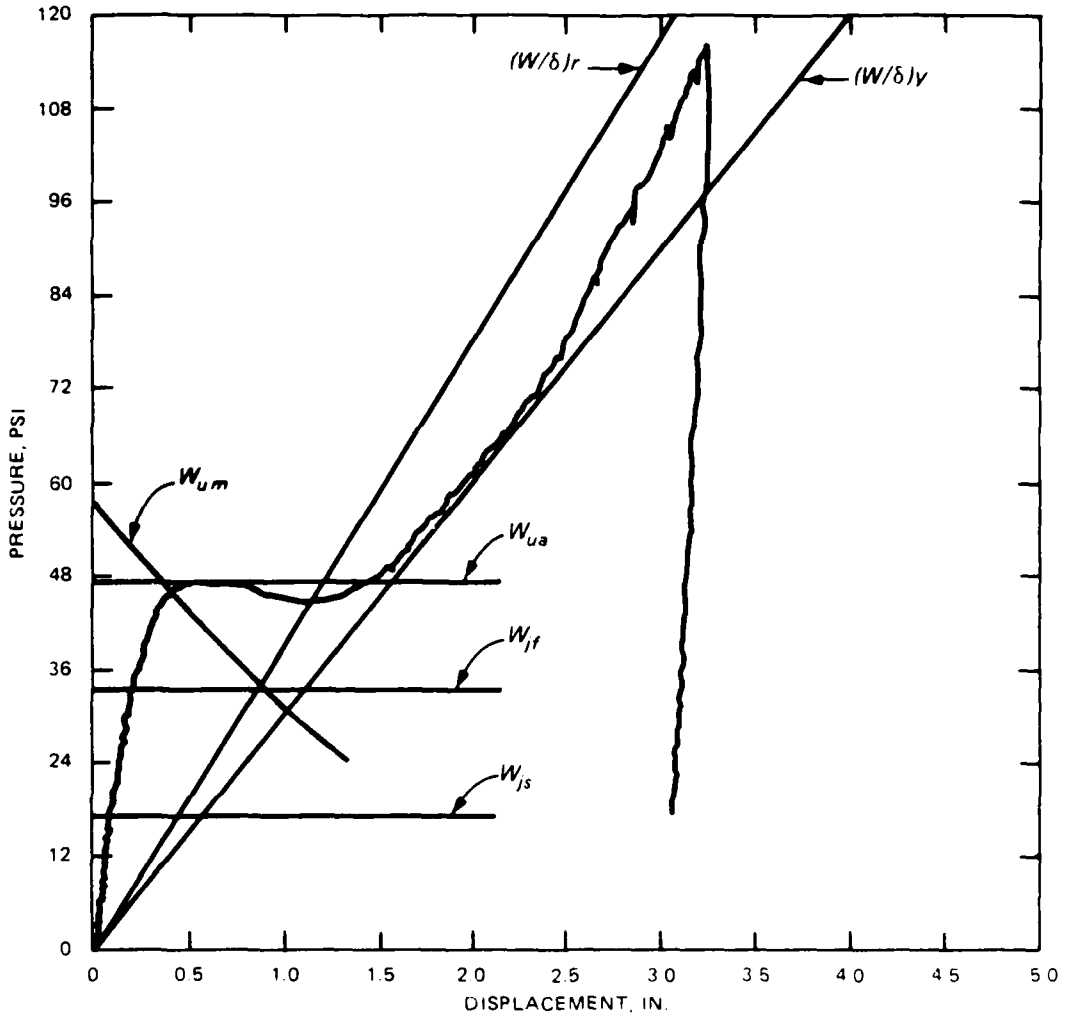

Notation:

W_{js}	=	Yield line load assuming simple supports
W_{jf}	=	Yield line load assuming fixed supports
W_{ua}	=	Compressive membrane capacity considering Eq. 4.10c for predicting peak deflection
W_{um}	=	Compressive membrane capacity evaluated at different peak capacity deflections
$(W/\delta)y$	=	Slope of tensile membrane curve using yield strength of steel
$(W/\delta)r$	=	Slope of tensile membrane curve using rupture strength of steel

FIG. 4.17.-Experimental and Analytical Comparisons for Slab 11

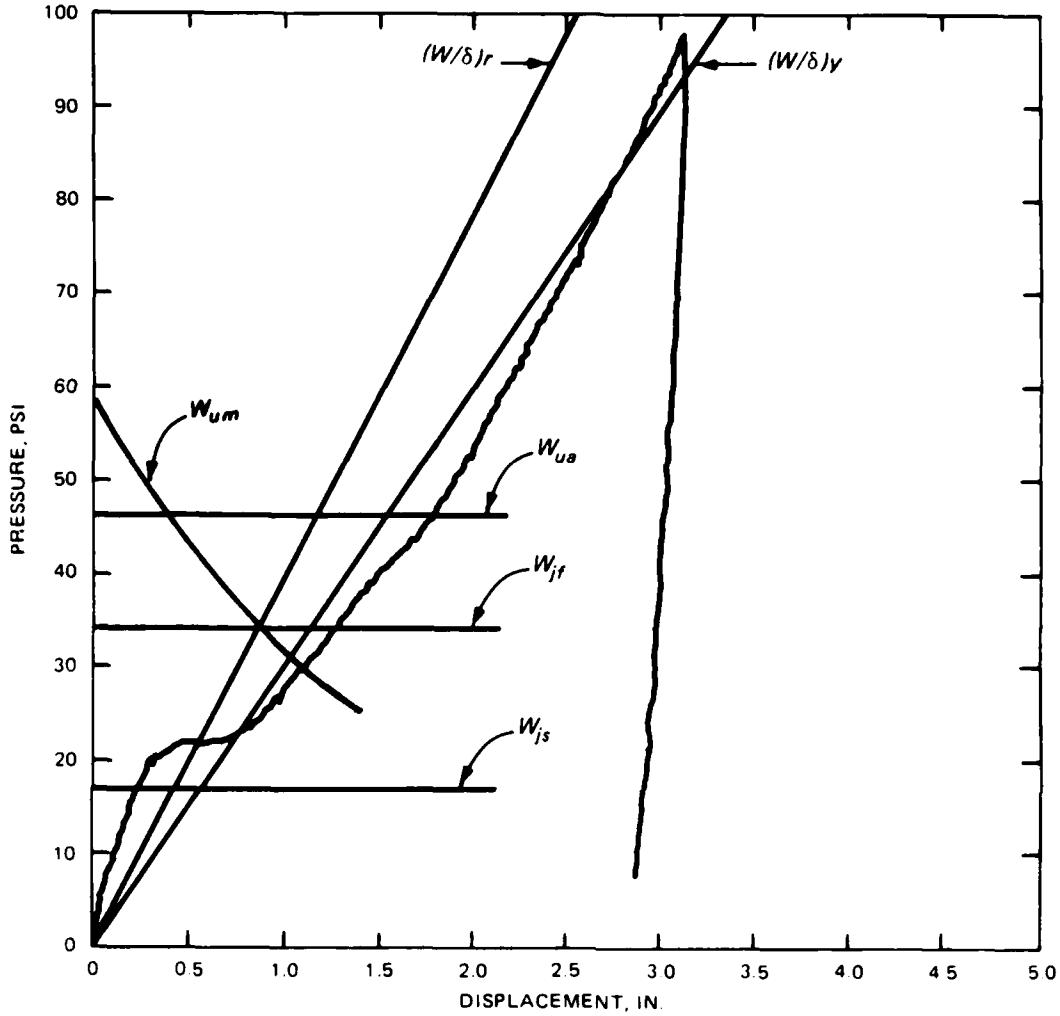

Notation:

W_{js}	=	Yield line load assuming simple supports
W_{jf}	=	Yield line load assuming fixed supports
W_{ua}	=	Compressive membrane capacity considering Eq. 4.10c for predicting peak deflection
W_{um}	=	Compressive membrane capacity evaluated at different peak capacity deflections
$(W/\delta)y$	=	Slope of tensile membrane curve using yield strength of steel
$(W/\delta)r$	=	Slope of tensile membrane curve using rupture strength of steel

FIG. 4.18.-Experimental and Analytical Comparisons for Slab 12

Tensile Membrane Theory.-Another phenomenon of slab behavior that has received considerable attention in recent years is tensile membrane action. Such action typically occurs after the slab has exceeded its compressive membrane capacity and has begun to undergo large deflections. If sufficient lateral restraint is provided, the tensile strength of the steel can supply a reserve capacity that will defer the progressive collapse of the slab. Tensile membrane action is usually accompanied with full-depth cracking, inward support movement, and large deflections. The largest deflection that a slab can withstand before there is a loss in tensile membrane capacity is referred to as the incipient collapse deflection.

Park and Gamble used standard plastic membrane theory to establish relationships between load and deflection for rectangular slabs. The theory assumes that tensile membrane forces are carried entirely by the steel. It does not account for combined bending and tensile membrane action, which would serve to enhance the capacity of the slab. For slabs with large aspect ratios, as idealized with one-way slab strips, the standard plastic tensile membrane theory formula is written

$$\frac{w}{\delta} = \frac{8\,T}{L^2} \qquad \ldots\ldots\ldots\ldots\ldots\ldots\ldots\ldots\ldots\ldots \quad (4.11)$$

where T = the total tensile force carried by the steel for a unit width.

Since at large deflections the strains in the reinforcement at the critical sections would be quite large, it is probable that some strain hardening would occur as tensile membrane action is induced. Strain hardening would definitely have occurred prior to the incipient collapse deflection. Therefore, Eq. 4.11 has been computed for the parameters of the experimental slabs and by using both the yield stress and ultimate stress of the steel in determining the tensile force, T. The computed results for the membrane slopes based on yield stresses , $(W/\delta)y$, and rupture stresses, $(W/\delta)r$, are presented in Table 4.4.

TABLE 4.4.-Results of Tensile Membrane Analyses

Slab	Yield Force Per Unit Width, pounds	Membrane Slope $(W/\delta)y$, psi/in	Ultimate Force Per Unit Width, pounds	Membrane Slope $(W/\delta)r$, psi/in
1	1000	13.9	1228	17.1
2	1000	13.9	1228	17.1
3	1671	23.2	2192	30.4
4	1671	23.2	2192	30.4
4A	1671	23.2	2192	30.4
4B	1671	23.2	2192	30.4
5	2388	33.2	3131	43.5
6	2388	33.2	3131	43.5
7	982	13.6	1134	15.7
8	982	13.6	1134	15.7
9	1671	23.2	2192	30.4
9A	1671	23.2	2192	30.4
10	1671	23.2	2192	30.4
10A	1671	23.2	2192	30.4
11	2149	29.8	2818	39.1
12	2149	29.8	2818	39.1

COMPARISON OF EXPERIMENTAL AND ANALYTICAL RESULTS

Lines representing Johansen's yield line load (Eq. 4.1), the compressive membrane capacity (Eq. 4.2-4.10), and the tensile membrane response (Eq. 4.11) have been constructed on the plots of the experimental load-deflection curves in Figs. 4.3-4.18 (pp. 104-119). Johansen's load for both fixed (W_{jf}) and simple (W_{js}) boundary conditions have been included. The tensile membrane slopes for both the yield strain, $(W/\delta)y$, and rupture strain, $(W/\delta)r$, have also been shown. In addition, a curve was plotted which represents the complete relationship between load and deflection (W_{um}) based on Eqs. 4.2-4.9, and not using Eq. 4.10c to establish the deflection at which the peak load occurs.

With the exception of Slab 1, the compressive membrane capacity predicted by Eqs. 4.2-4.9, in conjunction with the ultimate deflection predicted by Eq. 4.10c, provided an upper bound to the experimental flexural capacity. The analytical capacity was exceeded by less than 5% in Slab 1. With the exception of Slab 12, every slab which had a definitive flexural capacity was bounded from the low side by Johansen's load for fixed boundary conditions.

Another observation from the curves was that the change in load-deflection curvature which resulted from rotation of the support racks, generally occurred at a load between the two Johansen's loads for different boundary conditions. Although that phenomenon was primarily a function of the test

facility, it supported the concept that the slab followed the path of least resistance; it generally took less energy to exceed the yield section at midspan than to compress the springs providing resistance to rotation at the supports; it took less energy to compress the springs at the supports than to form a three-hinge mechanism in the slab.

Because most of the slabs exhibited an ultimate capacity beyond Johansen's load for fixed boundary conditions, it was apparent that thrusts acted to enhance the flexural capacities. The enhancement ratio, $(W_u - W_{jf})/W_{jf}$, ranged from a low of approximately 25% in Slab 8 to a high of about 180% in Slab 1. The slabs which showed no definitive peak capacity (Slabs 10 and 10A) were thin and had large free rotations at the supports. Those conditions probably resulted in a gradual loss of restraint with very little enhancement in the flexural capacity. The relatively small enhancements in flexural capacities for Slabs 8 and 12 could be attributed to a more sudden loss of restraint which occurred after significant thrusts had developed. Analysis of the load washer data substantiated the sudden reduction in thrust as the peak capacities were approached for those slabs.

The initial portions of the experimental load-deflection curves representing tensile membrane behavior were usually bounded or closely approached by the analytical curves computed from Eq. 4.11. As deflections became larger and reinforcement ruptured, the curves appropriately began to follow sloped lines representing membrane behavior for lower percentages of steel. The slabs which exhibited the poorest tensile membrane behavior (Slabs 1, 2, 7, and 8) were slabs which were constructed of a less ductile reinforcement. In each case, the reinforcement appeared to rupture before any significant tensile membrane action occurred. Because each of these slabs not only contained less ductile reinforcement but also contained the smallest steel percentage for each slab group, it could not be absolutely determined if steel percentage is an independent factor in ensuring tensile membrane action.

EVALUATION OF EFFECTS OF SUPPORT ROTATIONS

While the development of compressive membrane action has been attributed to lateral restraint, a review of all test data suggests that providing lateral restraint is only one condition required for ensuring an enhancement in capacity. A stricter interpretation of the data dictates that it is the restraint to both translation and rotation of the slabs' edges which really provides the enhancement in capacity. Lateral restraint acting at the midsurface of a slab would permit the edge to rotate and would apparently provide little or no enhancement. On the other hand, lateral restraint acting near the bottom (compression) surface restricts rotation and translation and, consequently, enhances the capacity of the slab. An investigation of the load-washer data recorded at midsurface of the slabs in this program confirms the ineffectiveness of restraint at that position.

Comparisons between the different slabs with the same geometric and material characteristics, but different boundary conditions, have led to some distinguishable patterns of behavior. A discussion of the effects of support rotation on each series of slabs follows. Beforehand, it should be noted that larger rotations in effect reduced the restraining forces in the slab.

Slabs 1 and 2 were from the thick slab group and contained the lowest percentage of reinforcement of all slabs. There was an inconsistency in the relative behavior

of Slabs 1 and 2 in that Slab 1 had a much higher peak capacity even though the support rotations were significantly greater than for Slab 2. An inspection of the load washer data led to a conclusion that there was a probable compression preloading of Slab 1 which resulted in an enhancement in the compressive membrane capacity. The preloading probably occurred during the setup of the test because the slab was fixed in the support racks while the large screws in the shaft assembly were tightened. Nevertheless, both slabs exhibited similar post-peak behavior in that there were very rapid decays, i.e., abrupt losses in capacity after the initial peaks. Excessive bar breakage prevented any significant tensile membrane action from occurring. The failure of each slab was characterized by well-defined yield lines, narrow crack bands, and practically total rupturing of the steel.

Although average support rotations varied between 1.24 to 2.52 degrees, there appeared to be no significant difference in the peak capacities of Slabs 3, 4, and 4A. However, an apparent initial compression in Slab 4B led to a slightly higher capacity. The peak capacities of Slabs 3, 4, and 4A were less than 5% different from the capacities of the similarly-constructed, rigidly-fixed slabs of Woodson [37]. The initial tensile membrane responses of all four slabs were almost identical. The points where plastic decay ended and tensile membrane action began were the same except for Slab 4B, which initiated the tensile behavior at a slightly higher

load. Slab 3 had the earliest deviation from the membrane slope, followed by Slabs 4 and 4A. Slab 3 also had more bars ruptured at the end of the test than either of the other two. All slabs exhibited significantly better tensile membrane behavior than Woodson's slabs.

Slabs 5 and 6 had the largest percentage of steel of the thick slab group. Even though Slab 5 had much smaller support rotations, the peak capacity was only about 7% greater than for Slab 6. Slab 6 exhibited practically no decay in the transition region of its load-deflection curve. The slopes of the tensile membrane responses were initially very close for Slabs 5 and 6. However, Slab 6 was able to achieve a much higher tensile capacity with significantly less steel breakage indicating that less damage probably occurred to Slab 6 in the early stages of loading.

Slabs 7 and 8 were from the thin slab group, and like Slabs 1 and 2, were constructed with low percentages of the nonductile heat-treated wire. The average support rotation was significantly less in Slab 7 and resulted in a significant compressive membrane enhancement. The apparent loss of restraint in Slab 8 seemed to have little effect on the tensile membrane behavior.

Four slabs, 9, 9A, 10, and 10A, each had approximately 1% of steel in a relatively thin cross-section. The overall behavior of Slabs 9 and 9A were remarkably similar even though the average support rotation was over 3 times greater

in Slab 9 (1.29 degrees) than in Slab 9A (0.4 degrees). Peak capacities were accurately predicted by the upper bound compressive membrane solution. The tensile membrane slopes and capacities as well as percentages of steel breakage and formation of crack patterns were almost identical in both slabs. On the other hand, Slabs 10 and 10A exhibited quite different behavior than Slabs 9 and 9A. No peak flexural capacities were apparent in these slabs, although Slab 10A exhibited some flexural response. Apparently, the loss of restraint due to support rotations which was sufficient to prohibit the development of compressive membrane forces occurred between the rotations of 1.29 degrees in Slab 9 and 2.04 degrees in Slab 10A. The tensile membrane slopes were significantly less in Slabs 10 and 10A, and appeared to follow the slope of the lower bound tensile membrane curves. Reinforcement ruptured at the supports in the two slabs with the smallest rotations. No reinforcement ruptured in the slab with the greatest rotations.

Slabs 11 and 12 were the slabs with the largest steel ratio and largest span-thickness ratio. As in most of the previous series of slabs, a reduction in the compressive membrane capacity occurred in the slab with the largest support rotations. Also apparent was a significant difference in the tensile membrane slopes. Slab 11 apparently had a higher tensile slope as a result of the initial flexural response. There was no steel breakage in either slab, but the effects of strain hardening in the

reinforcement were apparent in the latter parts of the curves.

Slabs 3, 4, 4A, 4B, 9, 9A, 10, and 10A all had the same gross area of steel. However, the last four slabs had thin cross-sections which resulted in a higher percentage of steel. In general, the thick slab series exhibited a much better flexural behavior with peak capacities of around 70 psi. The highest flexural capacity of the thin slab series was approximately 41 psi. Most of the slabs tended to follow similar tensile membrane slopes, although tensile responses were initiated at much smaller deflections for the thin slabs.

Slabs 3 and 9 had the same areas of steel, approximately the same support rotations, and each slab exhibited significant flexural action. However, the tensile membrane capacity was somewhat higher in the thin slab. On the other hand, Slabs 4A and 10 also had the same areas of steel and about the same rotational freedoms, but the tensile response was lower in the thin slab. The fact that the thicker slab responded in combined flexure and tension accounted for the difference in behavior.

PROPOSED SLAB ANALYTICAL PROCEDURE

Background.-As stated previously, the major shortcoming of the previous compressive membrane theory is that a true strain-deformation relationship is not included. For any given deflection, the concrete is assumed to be crushed and strains are chosen throughout each cross-section accordingly. Although this assumption is usually valid near the peak flexural capacity of the slab, it leads to significant errors when deflections are relatively small. Strains which are assumed to remain constant over a large range of deflections do not accurately portray the real behavior of slabs.

A second problem associated with the previous theory is that it neglects large deflections and has no provision for prediction of geometric instability. As Keenan pointed out, slabs which are relatively thin have a tendency to fail in a geometrically unstable mode rather than failing by material instability, i.e., crushing of the concrete. The ability to account for large deflection behavior and to predict unstable action is important in an analytical procedure.

Finally, the previous theory only permits a consideration of lateral support movement and does not include other types of boundary constraints. A procedure is needed which accounts for each of these conditions.

Concept and Implementation.-A methodology is proposed for consideration in the development of theories for

predicting the total load-deflection behavior of restrained reinforced concrete slabs. An energy approach is used as a basis for formulation of the theory. Large deformations, small elastic strains, and full lateral restraint are considered in the initial formulation. However, large strains, plasticity, and variable boundary conditions can be relatively easily incorporated. The theory is also consistent with works published by other analysts [12] and can be easily extended to finite element formulations.

An initially inclined slab element, as illustrated in Fig. 4.19 (a), is considered to represent the effective portion of the slab in resisting loads. Initially, when the action of the slab is dominated by arching action, the element has a stiffness primarily controlled by the stiffness of the portion of the slab which is in compression. The element has an angle of inclination which corresponds to the height of the arch formed by the internal action of the thrusts. When the thrusts reverse, and tensile forces predominate, the stiffness of the slab is controlled by the tensile stiffness of the steel. Because of symmetry, only half of the slab strip is modeled. For simplification of the concept, a straight truss representation is used.

The assumed boundary conditions must be compatible with the permissible displacement field of the element. If a linear displacement field is assumed, as is the case here, then only restraint to lateral and vertical displacements at the supports can be specified.

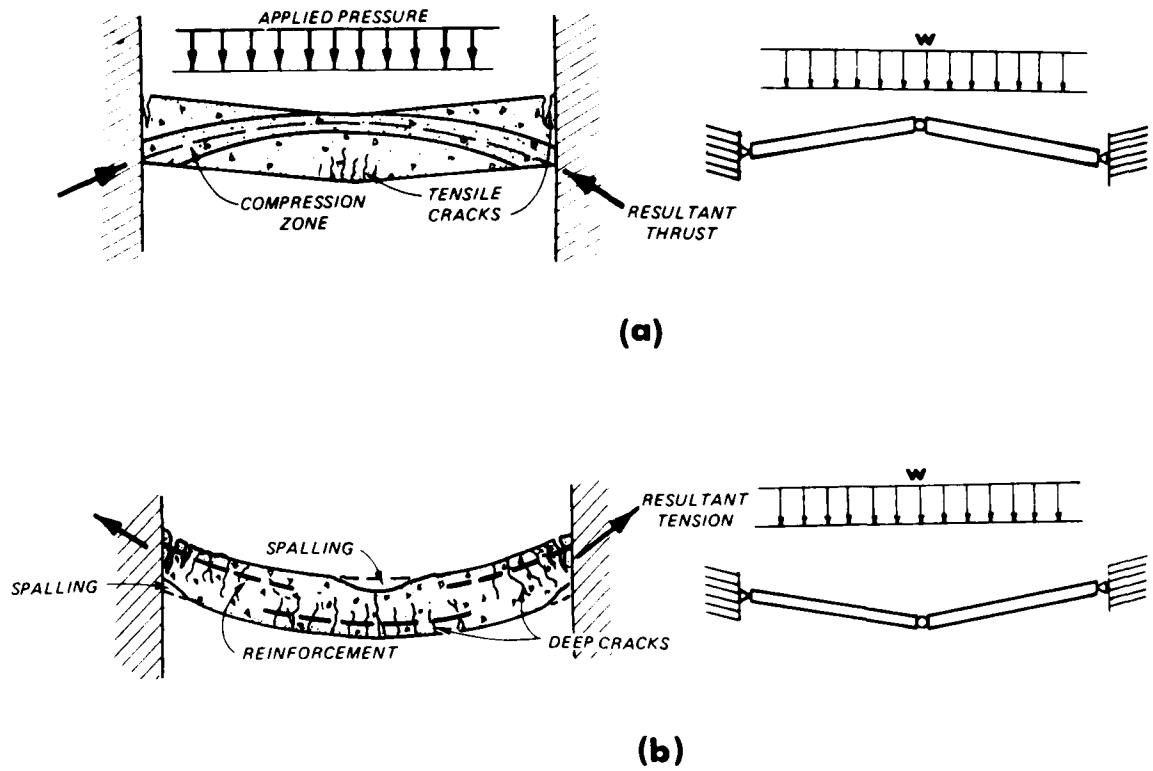

FIG. 4.19.-Physical and Analytical Models of
(a) Compressive Membrane Action and
(b) Tensile Membrane Action

Fig. 4.20 (b) illustrates the geometry and displacements for the proposed theoretical model. Displacements are assumed to occur along the length and transverse to the axis of the undeformed element. Each displacement field is represented in terms of nodal degrees of freedom (dof) at one end of the element. A linear displacement field is chosen for each displacement component

$$u(x) = \frac{x}{L} u_1$$

$$v(x) = \frac{x}{L} v_1 \qquad \ldots\ldots\ldots\ldots\ldots\ldots \quad (4.12)$$

A transformation of displacements from the local, undeformed coordinate system to the global coordinate system yields the following relationships

$$u_1 = \cos \theta_i \, q_1 + \sin \theta_i \, q_2$$

$$\ldots\ldots\ldots\ldots \quad (4.13)$$

$$v_1 = -\sin \theta_i q_1 + \cos \theta_i q_2$$

From LaGrange's strain-deformation relationships

$$\varepsilon_x = \frac{\partial u}{\partial x} + 1/2\left(\left(\frac{\partial u}{\partial x}\right)^2 + \left(\frac{\partial v}{\partial x}\right)^2\right) \qquad \ldots\ldots\ldots\ldots \quad (4.14)$$

If the extensional deformations are considered to be relatively small but rotations significant, the strain-deformation relationship is simplified to

$$\varepsilon_x = \frac{\partial u}{\partial x} + 1/2\left(\frac{\partial v}{\partial x}\right)^2 \qquad \ldots\ldots\ldots\ldots\ldots\ldots \quad (4.15)$$

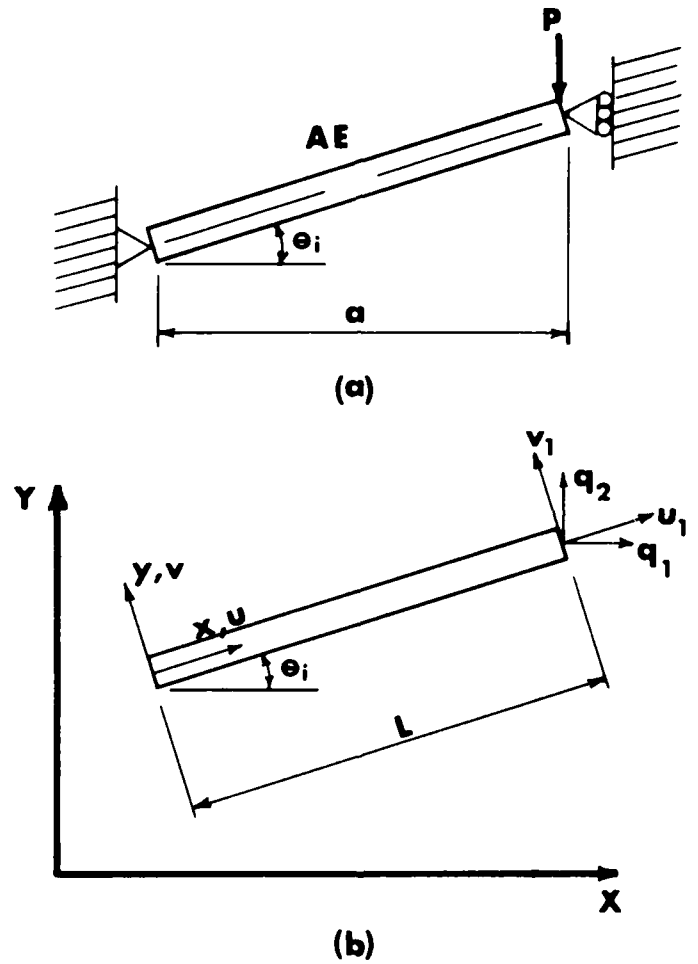

FIG. 4.20.-Notation for (a) Geometry and (b) Reference Coordinate Axes of Proposed Model

If significant curvatures exist along the member then the strains should be expressed as a function of the position along the cross-section, y,

$$\varepsilon_x = \frac{\partial u}{\partial x} + 1/2\left(\frac{\partial v}{\partial x}\right)^2 + y\frac{\partial^2 v}{\partial x^2}$$

or

$$\varepsilon_x = e + 1/2\ \theta^2 + y\phi \quad \ldots\ldots\ldots\ldots\ldots\ldots\ldots\ldots \quad (4.16)$$

where $e = \frac{\partial u}{\partial x}$, $\theta = \frac{\partial v}{\partial x}$, and $\phi = \frac{\partial^2 v}{\partial x^2}$.

However, for a first order displacement field, elastic curvatures do not exist since the second derivative of the displacement function is zero. For a second order displacement field, the curvature is constant along the length of the member.

To enforce equilibrium requirements, the principle of minimum potential energy is employed. First, the internal potential energy due to internal stresses and strains is written

$$U = \int_V \int_\varepsilon \sigma d\varepsilon dV$$

For a linear elastic material, then

$$U = 1/2\int_V \sigma\varepsilon dV = 1/2\int_V E\varepsilon^2 dV \quad \ldots\ldots\ldots\ldots\ldots\ldots\ldots \quad (4.17)$$

The external potential energy due to applied surface forces, p, is

$$V = -\int_S pqds \quad \ldots\ldots\ldots\ldots\ldots\ldots\ldots\ldots\ldots\ldots \quad (4.18)$$

When the total potential, $U_t = U + V$, is a minimum, the element has reached a state of equilibrium. Hence,

$$\frac{\partial U_t}{\partial q} = 0 \quad \ldots\ldots\ldots\ldots\ldots\ldots\ldots\ldots\ldots\ldots \quad (4.19)$$

essentially satisfies the equilibrium requirements.

Since a linear displacement field is assumed, and restraint to lateral movement is enforced, the major contribution to the internal strain energy is provided by axial deformations. An assumption of linear elastic axial strains is considered for the theoretical model.

Substituting the strain-deformation relationships of Eq. 4.16 into the expression for internal potential in Eq. 4.17

$$U = 1/2 \int_L \int_A E(e + 1/2\theta^2)^2 \, dA \, dx$$

and integrating over the length and cross-sectional area

$$U = 1/2 \, AEL(e^2 + e\theta^2 + 1/4\theta^4) \quad \ldots\ldots\ldots\ldots \quad (4.20)$$

where,

$$e = \frac{\partial u}{\partial x} = \frac{u_1}{L} = \frac{1}{L}(q_1 \cos \theta_i + q_2 \sin \theta_i)$$

$$\theta = \frac{\partial v}{\partial x} = \frac{v_1}{L} = \frac{1}{L}(-q_1 \sin \theta_i + q_2 \cos \theta_i) \quad \ldots\ldots \quad (4.21)$$

If the constraint of no lateral support movement is imposed, i.e., $q_1 = 0$, Eq. 4.20 simplifies to

$$U = 1/2\frac{AE}{L}(\sin^2 \theta_i \, q_2^2 + \frac{1}{L}(\sin \theta_i \cos^2 \theta_i \, q_2^3) + \frac{1}{4L^2}(\cos^4 \theta_i \, q_2^4)) \quad \ldots\ldots \quad (4.22)$$

Now, differentiating the strain energy with respect to the displacement, q_2, we can determine the internal force in the element

$$Q = \frac{\partial U}{\partial q_2} = Q_L + Q_{NL}$$

where

$$Q_L = \frac{AE}{L}(\sin^2 \theta_i \; q_2)$$

$$Q_{NL} = AE(3/2 \sin\theta_i \cos^2 \theta_i (\frac{q_2}{L})^2 + 1/2 \cos^4 \theta_i (\frac{q_2}{L})^3) \quad (4.23)$$

The first term represents the linear portion of the resisting forces and the last two terms represent the contribution from geometric nonlinearities. The corresponding stiffnesses are determined by differentiating once again

$$K_L = \frac{\partial Q_L}{\partial q_2} = \frac{\partial^2 U_L}{\partial q_2^2} = \frac{AE}{L} \sin^2 \theta_i$$

$$K_{NL} = \frac{\partial Q_{NL}}{\partial q_2} = \frac{3AE}{L^2}(\sin \theta_i \cos^2 \theta_i \; q_2 + \frac{1}{2L} \cos^4 \theta_i \; q_2^2) \quad (4.24)$$

In order to establish the equation of equilibrium, the external potential energy terms must be formulated. Using a consistent formulation, and assuming a uniform surface pressure and no lateral support movement

$$V = -\int_s pqds = -Bw\int_A \frac{x}{a} q_2 dx \quad (4.25)$$

and integrating

$$V = -1/2aBwq_2 \equiv -Pq_2 \quad (4.26)$$

where P = 1/2 a B w, a = 1/2 the slab length, B = the width of the slab, and w = uniform load. This is equivalent to lumping half of the segment load at the midspan node.

Now, combining all energy terms and applying the Principle of Minimum Potential Energy

$$\frac{\partial (U+V)}{\partial q_2} = 0 = Q_L + Q_{NL} - P \quad \ldots\ldots\ldots\ldots\ldots\ldots \quad (4.27)$$

Equation 4.27 is equivalent to the equation of equilibrium for the segment if considering nonlinear geometry terms. The linear equation may be obtained by simply omitting the Q_{NL} term

$$\frac{AE}{L} \sin^2 \theta_i \, q_2 - 1/2aBwq_2 = 0$$

and

$$P = \frac{AE}{L} \sin^2 \theta_i \quad \ldots\ldots\ldots\ldots\ldots\ldots\ldots\ldots \quad (4.28)$$

Solution.-The nonlinear equation (Eq. 4.27) was solved using the Newton-Raphson method. A fixed-end slab from one of the previous test programs at WES [11] and Slab 9A from this test program were used as a basis for evaluating the analytical procedure. The particular slab which was analyzed from the previous test program had material and geometric characteristics similar to Slabs 3 and 4 in this program.

The stiffness of the slab was assumed to be primarily controlled by the stiffness of the concrete, and its modulus was appropriately included in the analysis. All terms associated with the geometry, such as the length and cross-

sectional area, were taken from the actual geometry of the slab. The original angle of inclination of the equivalent model was assumed to be 2/3 of the slab thickness divided by 1/2 the total slab length. It was based on the fact that as the slab undergoes initial deformation, the centroid of the compression zone is located at approximately 1/6 of the slab's thickness from the outer compressive fiber of the cross-section. Therefore, the vertical distance between centroids of the compression zones at midspan and support is 2/3 of the slab's thickness.

The solution scheme employed for Eq. 4.27 varied during different stages of the response. Initially, in the compressive membrane region, loads were incremented and deflections were found by Newton-Raphson iteration. In the transition region, it was necessary to increment deflections and solve for the corresponding load. When the capacity predicted by Eq. 4.27 was found to be smaller than the tensile membrane capacity, the latter equation was used.

As expected, the results showed that the predicted deflections were significantly smaller than the deflections which actually occurred. In other words, the analytical model was much stiffer than the experimental model. This discrepency was primarily attributed to the fact that the theory, by assuming a linear displacement field, neglected any bending actions and omitted the internal strain energy due to changes in curvature. Also, because tension actually

existed in certain zones of the slab, the total slab thickness should not have been used in computing the axial stiffness term. Finally, omission of plastic strain energy terms led to some significant errors near the peak capacity.

To remedy the first problem, a higher order displacement field which accounts for bending of the element could be assumed and the appropriate energy terms then formulated. An alternative solution is to modify the energy contribution due to the external loads. This procedure is equivalent to using a lumped rather than a consistent approach in developing the loads. Both approaches were investigated, with the latter giving the most satisfactory results for the particular slabs which were analyzed. Results are illustrated in Fig. 4.21.

A reduction in axial stiffness can be accomplished by reducing the gross cross-sectional area of the slab. However, since the actual distribution of strains along each section is not determined by the theory, the portion of the slab in axial compression must be assumed. The stiffness would normally be influenced by a number of factors including the relative slab thickness, the percentage of steel, the material properties, and the actual support conditions. A parameter study would be required to determine the particular influence of each factor. The results illustrated in Fig. 4.21(a) were based on a sectional area of the slab equal to about 25% of the gross area and equal to about 50% of the gross area for Fig.4.21(b). These were based on best fits to the data.

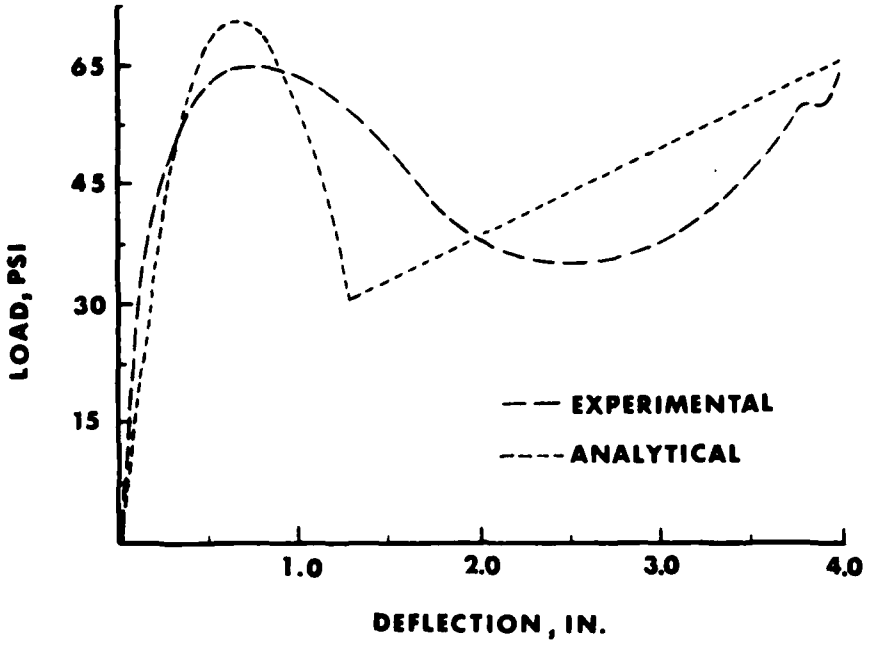

(a) Slab W283 from Reference 10 With Span-thickness Ratio of 10.4 and Reinforcement Ratio of 0.74%

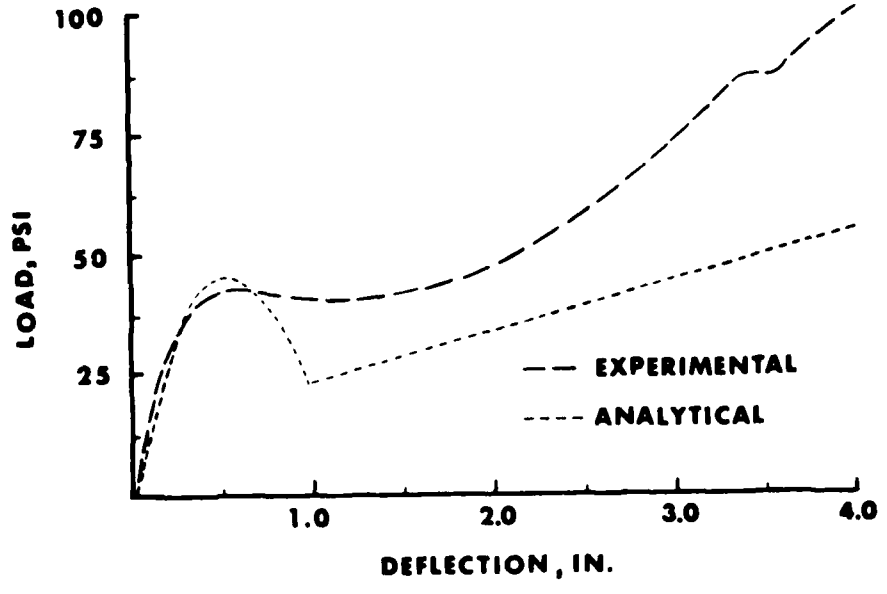

(b) Slab 9A With Span-Thickness Ratio of 14.8 and Reinforcement Ratio of 1.14%

FIG. 4.21.-Comparison of Analytical and Experimental Results for Proposed Model

Discussion.-It is evident that the theory yields results which somewhat parallels the actual behavior of a restrained slab. For the slabs under investigation, the predicted peak capacity deflections were extremely close to the respective experimental deflections. Although the predicted peak capacity was somewhat larger than its experimental counterpart, a consideration of plasticity in the derivation should make the difference in analytical and experimental capacities smaller.

The most significant aspect of this approach is that unlike previous theories, it offers a means for incorporating geometric instability into the analysis. In fact, for the particular slab under consideration, the transition portion of the load-deflection curve was totally attributed to geometric instability and did not account for any material instability, i.e., crushing of the concrete. This suggests that the decay in load-carrying capacity of slabs is at least in part due to nonlinear geometrical behavior. Such behavior is even more apparent in slabs which are partially restrained.

Although several approximations were incorporated into the procedure, it does provide a methodology for considering the different phenomena which affect the complex internal behavior of slabs. Also, such things as variable boundary conditions can be readily included with the addition of springs in the analytical model. The appropriate energy terms can be derived and incorporated into Eq. 4.27.

CHAPTER V

CONCLUSIONS AND RECOMMENDATIONS

SUMMARY

From observations of the physical specimens, examinations of experimental data, and comparisons with analytical results, a better understanding of slab behavior has been achieved. Of primary interest in this test program was the determination of the effects of partial rotational restraint on slabs with different geometric characteristics. The slab parameters which were considered were the span/thickness ratio and the reinforcement ratio.

At least two slabs for each of six slab configurations were constructed and tested. Each slab was permitted different degrees of rotational freedom. A specially designed reaction structure permitted measurements of the various member end actions, including thrusts and rotations. The following conclusions are based on the results of the sixteen slabs from this test program, and where appropriate, from the tests of the rigidly restrained slabs by Woodson [37].

CONCLUSIONS

1. Compressive membrane theory using an assumed infinite lateral stiffness, overpredicted the flexural capacity of slabs with partial rotational restraint when no external in-plane loads were present. For slabs which underwent relatively small rotations, the same theory combined with a realistic value for lateral stiffness, predicted the peak capacity within approximately 10%, and was a significantly better predictor for peak capacity than yield-line theory. Therefore, thrusts did act to enhance the flexural capacities of slabs with small rotational freedoms as long as the lateral stiffness was sufficient to develop in-plane forces.

2. The deflections at which the peak capacities were achieved were significantly different for slabs with varied rotational freedoms. However, as long as the rotational freedoms were small, the peak capacities were relatively unaffected and were not substantially different from the peak capacities of rigidly restrained slabs.

3. For larger rotational freedoms, the peak capacities occurred at large deflections, were significantly lower than the capacities which were predicted by compressive membrane theory, and in some cases, the slabs had no definitive flexural capacity at all. The distinct difference in behavior is attributed to a form of geometric instability. In this context, the term instability means that the slab was

not able to achieve its compressive membrane capacity because of large, early deflections. In other words, because the rotations were large, the slab snapped through to the tensile membrane stage before significant thrusts were developed.

4. Smaller rotational freedoms were necessary to induce that type of instability (loss of restraint under relatively small loads) in the thin slabs. The range of average support rotational freedoms at which the instabilities were induced was approximately 2.0 to 2.5 degrees. All three series of the thin slab group had developed instabilities at rotations of less than 2.2 degrees, and in two cases, at rotations of less than 2.04 degrees. On the other hand, Slab 9 appeared to be stable, i.e., exhibited significant compressive membrane behavior, at a rotation of 1.29 degrees. Even though Slab 6 experienced an instability at approximately 2.04 degrees, none of the other thick slabs demonstrated similar responses. Slab 4A did show appreciable signs of unstable action at a rotation of 2.52 degrees. Overall, the effects of instability were more apparent for the thin slabs.

5. There are insufficient data to draw conclusions on the effects of steel percentage on the flexural stability of partially restrained slabs.

6. There was significantly more tensile membrane response in the thin slab group than in the thick slab group. Under similar ranges of loading, the thin slabs carried a

larger percentage of the load by tensile membrane action. The tensile response was apparent in that the crack patterns for the thin slabs were much broader and the cracks were significantly narrower. The yielding of the reinforcement appeared to be less confined to the central yield zone and more evenly distributed throughout the whole slab.

7. The tensile membrane theory (Eq. 4.11) based on both yield strains and rupture strains, usually bounded the tensile response of the slabs prior to rupturing of the reinforcement. After some of the reinforcement ruptured, the load-deflection curve followed a reduced tensile slope.

8. For the thick slab group, higher tensile capacities were achieved as the rotational freedoms increased. The probable explanation for this behavior was that with small rotational freedoms, more strain energy was required at the critical sections in the flexural stage, causing more of the reinforcement to rupture in earlier portions of the tensile membrane stage.

9. For given deflections, the tensile capacities of the thin slabs were generally higher as rotational freedoms decreased. With smaller rotational freedoms, the slabs carried the load by combined flexure and tension, which resulted in a higher capacity than could be achieved in pure tension. Also, plastic rotations acted to increase the strains in the reinforcement such that strain-hardening contributed to the tensile capacities.

10. When instability was not a factor, the thin slabs came closer to approaching the maximum analytical compressive membrane capacity. Even though the actual support stiffnesses were approximately the same for all slabs, the relative lateral stiffness of the supports was greater for the thin slabs, making the peak capacity approach that for infinitely stiff surrounds.

11. Most slabs initiated the tensile membrane response at a deflection which fell between the slab's effective depth and thickness.

12. Only considering slabs which were reinforced with the ductile no. 2 bars, the average incipient collapse deflection occurred at approximately 1/8 of the span for the thick slab group and somewhat greater than that for the thin slab group. Since no reinforcement was apparently ruptured in three of the thin slabs, the average incipient collapse deflection was not computed. However, an examination of the data indicated that the deflection at which reinforcement first ruptured was somewhat greater for the thin slabs than for the thick slabs.

RECOMMENDATIONS FOR DESIGN

The following design recommendations have been based on the results of this test program. Since designs are frequently based on different criteria, the recommendations have been stated in terms of the particular performance affected.

1. Regardless of rotational freedoms, adequate lateral stiffness must be provided to develop both compressive and tensile membrane enhancements. However, some rotational restraint is necessary to achieve significant compressive membrane capacity. That restraint may be provided in the form of a monolithic slab-wall connection or by the application of a lateral restraining force in the lower portion of a slab's edges. In the latter case, the eccentricity of the restraining force serves to provide rotational resistance.

2. Increasing the area of steel and slab thickness each acts separately to enhance the compressive membrane capacity and energy absorption capacity of the slab, as long as rotational freedoms do not induce a loss in the restraining force.

3. Small rotational freedoms do not significantly affect the compressive membrane capacity, but do enhance the tensile membrane capacity and incipient collapse deflection. For design purposes, the largest possible rotational freedom which permits an enhanced peak capacity without inducing a

premature loss in restraint should result in the most favorable overall response. That rotational freedom appears to be between 2.0 to 2.5 degrees for the thicker slabs and from 1.5 to 2.0 degrees for the thin slabs.

4. If allowed small rotations, thicker slabs provide a substantial increase in flexural capacity and a decrease in tensile capacity with respect to thin slabs with the same total steel area. As a result of the larger area under the initial portion of the load-deflection curves, the energy absorption capacity of the thicker slabs is greater.

5. Regardless of the rotational freedom, thin slabs carry a much larger percentage of the load by tensile membrane action. The failure of a thin slab is characterized by a broad band of relatively small cracks. In terms of the resistance, thin slabs are much more likely to "catch" the load after the initial compressive membrane peak.

6. Sufficient reinforcement ductility must be provided to develop any tensile membrane resistance. In general, grade 60 or lower reinforcement should provide adequate ductility.

RECOMMENDATIONS FOR FURTHER STUDY

Additional tests should be conducted to more precisely evaluate the effects of various types of boundary conditions and to determine the permissible rotational freedoms for each of the design parameters. Such tests would also serve to verify the previous experimental results.

Further study should be made into the proposed analytical procedure. The application of higher order displacement fields, plasticity, and variable boundary conditions should be considered. The generalization of the theory for adaptation in a finite element analysis is also desirable.

REFERENCES

1. Black, M. S., "Ultimate Strength Study of Two-Way Concrete Slabs," Journal of the Structural Division, ASCE, Vol. 101, No. ST1, Jan., 1975, pp. 311-324.

2. Braestrup, M. W., "Dome Effect in RC Slabs: Rigid-Plastic Analysis," Journal of the Structural Division, ASCE, Vol. 106, No. ST6, June, 1980, pp. 1237-1253.

3. Braestrup, M. W., and Morley, C. T., "Dome Effect in RC Slabs: Elastic-Plastic Analysis," Journal of the Structural Division, ASCE, Vol. 106, No. ST6, June, 1980, pp. 1255-1262.

4. Brotchie, J. F., and Holley, M. J., "Membrane Action in Slabs," Cracking, Deflection, and Ultimate Load of Concrete Slab Systems, ACI Special Publication SP-30, American Concrete Institute, Detroit, Michigan, 1971, pp. 345-375.

5. Brotchie, J. F., Jacobson, A., and Okubo, S., "Effect of Membrane Action on Slab Behavior," Research Report R65-25, Department of Civil Engineering, Massachusetts Institute of Technology, Cambridge, Mass., Aug., 1965.

6. Building Code Requirements for Reinforced Concrete, ACI Committee 318, American Concrete Institute, Detroit, Michigan, 1983.

7. Christiansen, K. P., "The Effect of Membrane Stresses on the Ultimate Strength of the Interior Panel in a Reinforced Concrete Slab," The Structural Engineer, London, England, Vol. 41, Aug., 1963, pp. 261-265.

8. Datta, T. K., and Ramesh, C. K., "Some Experimental Studies on a Reinforced Concrete Slab-Beam System," Magazine of Concrete Research, London, England, Vol. 27, No. 91, June, 1975, pp. 111-120.

9. Desayi, P., and Kulkarni, A. B., "Load-Deflection Behavior of Restrained Reinforced Concrete Slabs," Journal of the Structural Division, ASCE, Vol. 103, No. ST2, Feb., 1977, pp. 405-419.

10. Guice, L. K., "Effects of Edge Restraint on Slab Behavior," Technical Report SL-86-2, U. S. Army Engineer Waterways Experiment Station, Vicksburg, MS, February, 1986.

11. Guice, L. K., and Slawson, T. R., "Static and Dynamic Slab Tests Conducted at WES: FY 78-84," Technical Report SL-86-1, U. S. Army Engineer Waterways Experiment Station, Vicksburg, MS.

12. Haisler, W. E., Jr., "Development and Evaluation of Solution Procedures for Nonlinear Structural Analysis," thesis presented to Texas A&M University, at College Station, Texas, in 1970, in partial fulfillment of the requirements for the degree of Doctor of Philosophy.

13. Hawkins, N. M.,and Mitchell, D., "Progressive Collapse of Flat Plate Structures," American Concrete Institute Journal, Title No. 76-34, July, 1979, pp. 775-807.

14. Herzog, M., "The Membrane Effect in Reinforced Concrete Slabs According to Tests," Beton and Stahlbetonbau, Vol. 11, 1976, pp. 270-275, in German.

15. Hung, T. Y., and Nawy, E. G., "Limit Strength and Serviceability Factors in Uniformly Loaded, Isotropically Reinforced Two-Way Slabs," Cracking, Deflection, and Ultimate Load of Concrete Slab Systems, ACI Special Publication SP-30, American Concrete Institute, Detroit, Michigan, 1971, pp. 301-323.

16. Jacobson, A., "Membrane-Flexural Failure Modes of Restrained Slabs," Journal of the Structural Division, ASCE, Vol. 93, No. ST5, Oct., 1967, pp. 85-111.

17. Johansen, K. W., Brudlinieteorier, Copenhagen, 1943; English translation, "Yield-Line Theory," Cement and Concrete Association, London, 1962.

18. Keenan, W. A., "Strength and Behavior of Laced Reinforced Concrete Slabs Under Static and Dynamic Load," Technical Report R620, U.S. Naval Civil Engineering Laboratory, Port Hueneme, California, April 1969.

19. Keenan, W. A., "Strength and Behavior of Restrained Reinforced Concrete Slabs Under Static and Dynamic Loadings," Technical Report R621, U.S. Naval Civil Engineering Laboratory, Port Hueneme, California, April 1969.

20. Morley, C. T., "Yield Line Theory for Reinforced Concrete Slabs at Moderately Large Deflexions," Magazine of Concrete Research, London, England, Vol. 19, 1967, pp. 211-222.

21. Nawy, E. G., and Blair, K., "Further Studies on Flexural Crack-Control in Structural Slab Systems," Cracking, Deflection, and Ultimate Load of Concrete Slab Systems, ACI Special Publication SP-30, American Concrete Institute, Detroit, Michigan, 1971, pp. 1-41.

22. Ockleston, A. J., "Arching Action in Reinforced Concrete Slabs," The Structural Engineer, London, England, Vol. 36, No. 6, June, 1958, pp. 197-201.

23. Park, R., "Tensile Membrane Behavior of Uniformly Loaded Rectangular Reinforced Concrete Slabs with Fully Restrained Edges," Magazine of Concrete Research, London, England, Vol. 16, No. 46, March, 1964, pp. 39-44.

24. Park, R., "Ultimate Strength of Rectangular Concrete Slabs Under Short-Term Uniform Loading with Edges Restrained Against Lateral Movement," Proceedings of the Institution of Civil Engineers, London, England, Vol. 28, June, 1964, pp. 125-150.

25. Park, R., "The Ultimate Strength and Long-Term Behaviour of Uniformly Loaded Two-Way Concrete Slabs with Partial Lateral Restraint at All Edges," Magazine of Concrete Research, London, England, Vol. 16, No. 48, Sept., 1964, pp. 139-152.

26. Park, R., "The Lateral Stiffness and Strength Required to Ensure Membrane Action at the Ultimate Load of a Reinforced Concrete Slab and Beam Floor," Magazine of Concrete Research, London, England, Vol. 17, No. 50, March, 1965, pp. 29-38.

27. Park, R., and Gamble, W. L., Reinforced Concrete Slabs, John Wiley and Sons, New York, 1980.

28. Powell, D. S., "The Ultimate Strength of Concrete Panels Subjected to Uniformly-Distributed Loads," thesis presented to Cambridge University, in Cambridge, England, in 1956, in partial fulfillment of the requirements for the degree of Doctor of Philosophy.

29. Ramesh and Datta, T. K., "Ultimate Strength of Reinforced Concrete Slab-Beam Systems: A New Approach," Indian Concrete Journal, Bombay, India, Vol. 47, 1973, pp. 301-308.

30. Regon, P. E., "Catenary Action in Damaged Concrete Structures," Industrialization in Concrete Building Construction, ACI Special Publication SP-48, American Concrete Institute, Detroit, Michigan, 1975, pp.191-224.

31. Roberts, E. H., "Load-Carrying Capacity of Slab Strips Restrained Against Longitudinal Expansion," Concrete, Vol. 3, No. 9, Sept., 1969, pp. 369-378.

32. Sawczuk, A., "Membrane Action in Flexure of Rectangular Plates with Restrained Edges," ACI Special Publication SP-12, American Concrete Institute, Detroit, Mich., 1965, pp. 347-358.

33. Sawczuk, A., and Winnicki, L., "Plastic Behavior of Simply-Supported Reinforced Concrete Plates at Moderately Large Deflections," International Journal of Solids and Structures, Vol. 1, 1965, pp. 97-111.

34. Takehira, T., Derecho, A.T., and Iqbal, M., "Design Criteria for Deflection Capacity of Conventionally Reinforced Concrete Slabs, State-of-the-Art Report," Report CR 80.026, prepared for Naval Civil Engineering Laboratory, Port Hueneme, CA, Portland Cement Association, Skokie, Illinois, 1979-1980.

35. Taylor, R., Maher, D.R.H., and Hayes,B., "Effect of the Arrangement of Reinforcement on the Behaviour of Concrete Slabs," Magazine of Concrete Research, London, England, Vol. 18, No. 55, June, 1966.

36. Wood, R. H., Plastic and Elastic Design of Slabs and Plates, Thames and Hudson, London, England, 1961.

37. Woodson, S. C., "Effects of Shear Stirrup Details on Ultimate Capacity and Tensile Membrane Behavior of Reinforced Concrete Slabs," Technical Report SL-85-4, U. S. Army Engineer Waterways Experiment Station, September, 1985.

38. Woodson, S. C., and Garner, S. B., "Effects of Reinforcement Configuration on Reserve Capacity of Concrete Slabs," Technical Report SL-85-5, U. S. Army Engineer Waterways Experiment Station, August, 1985.

APPENDIX I

REACTION STRUCTURE DETAILS

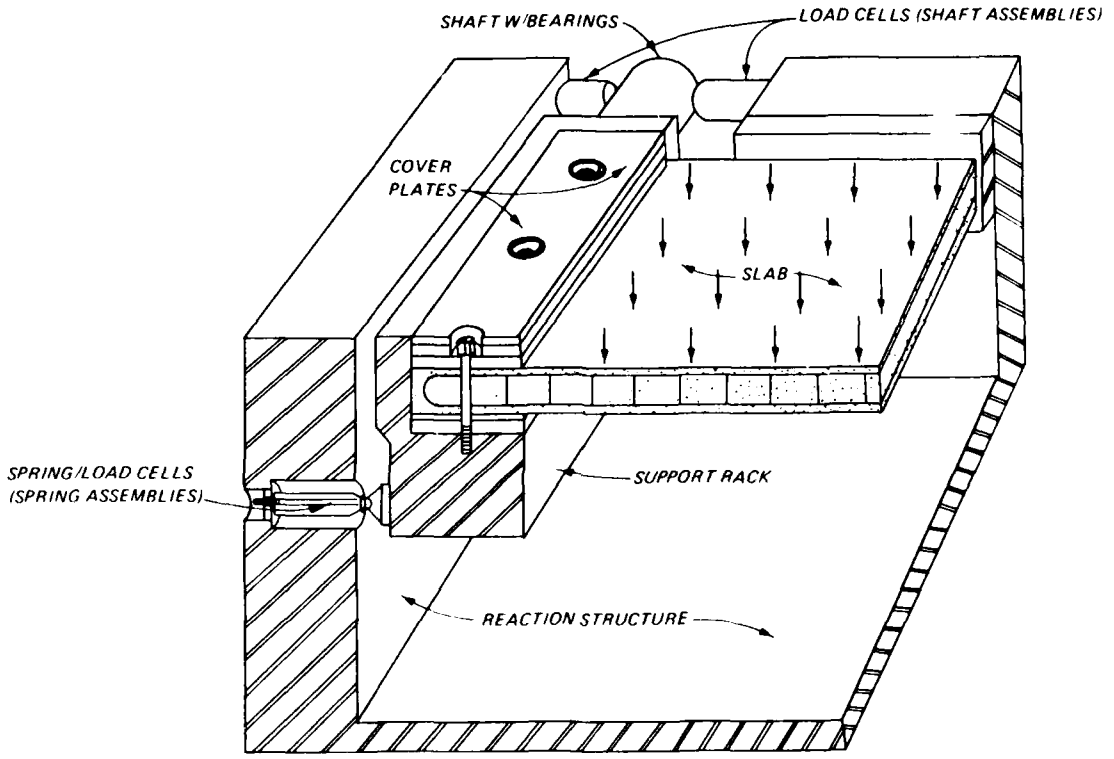

FIG. I.1.-Quarter-Section View of Reaction Structure With Slab in Place

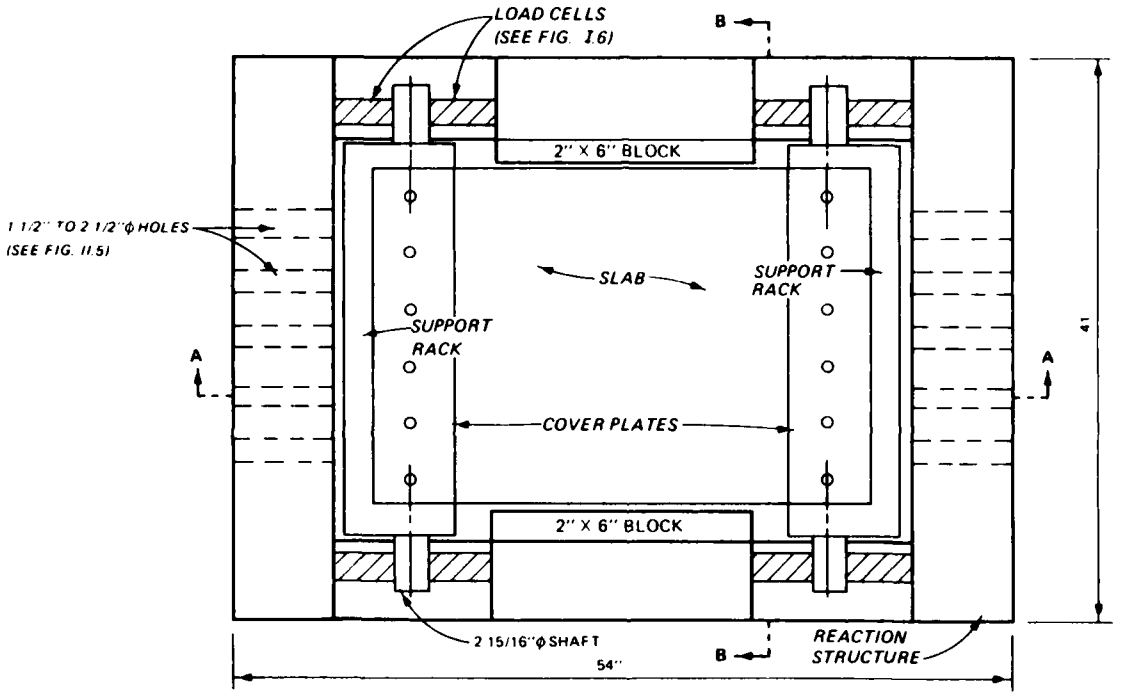

FIG. I.2.-Plan View of Reaction Structure and Assemblies

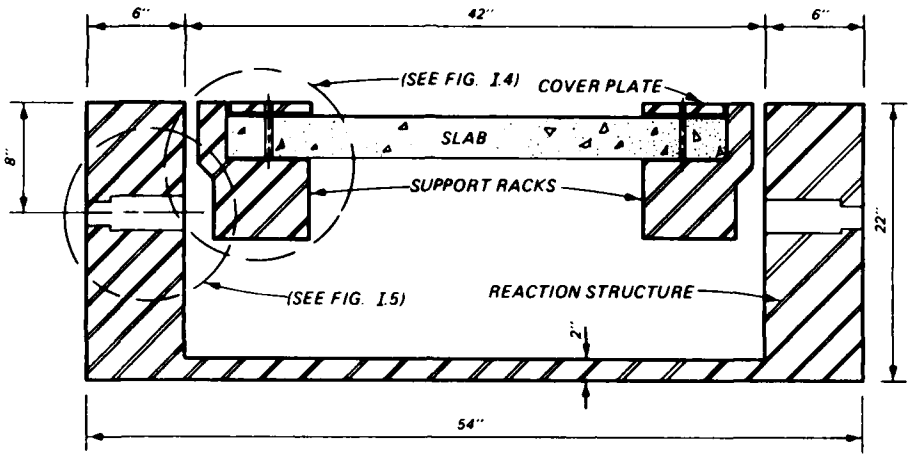

SECTION A-A

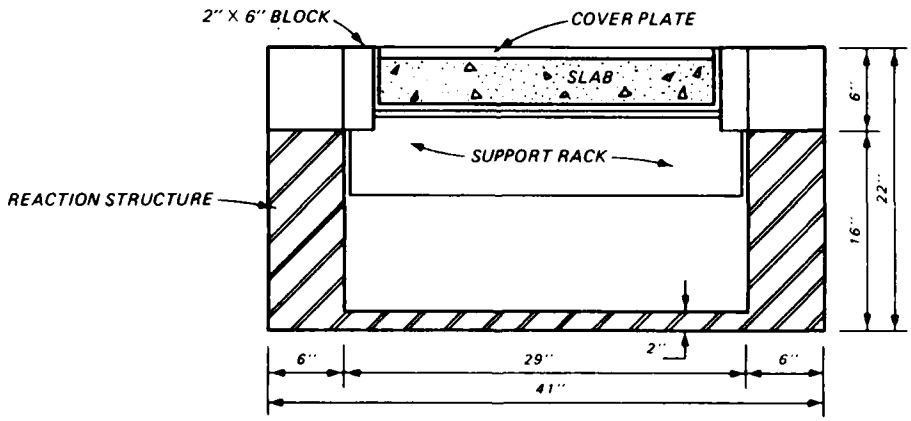

SECTION B-B

FIG. I.3.-Sections Through Reaction Structure

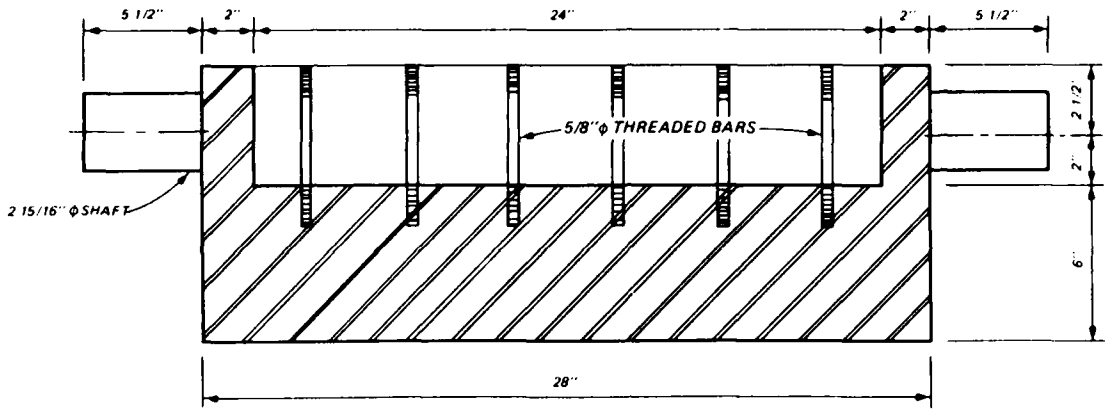

SECTION

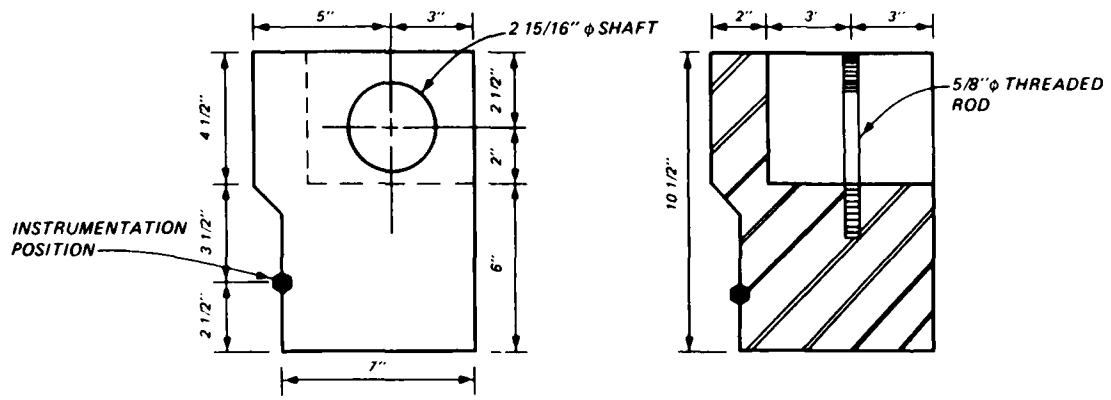

END VIEW

SECTION

FIG. I.4.-Support Rack Details

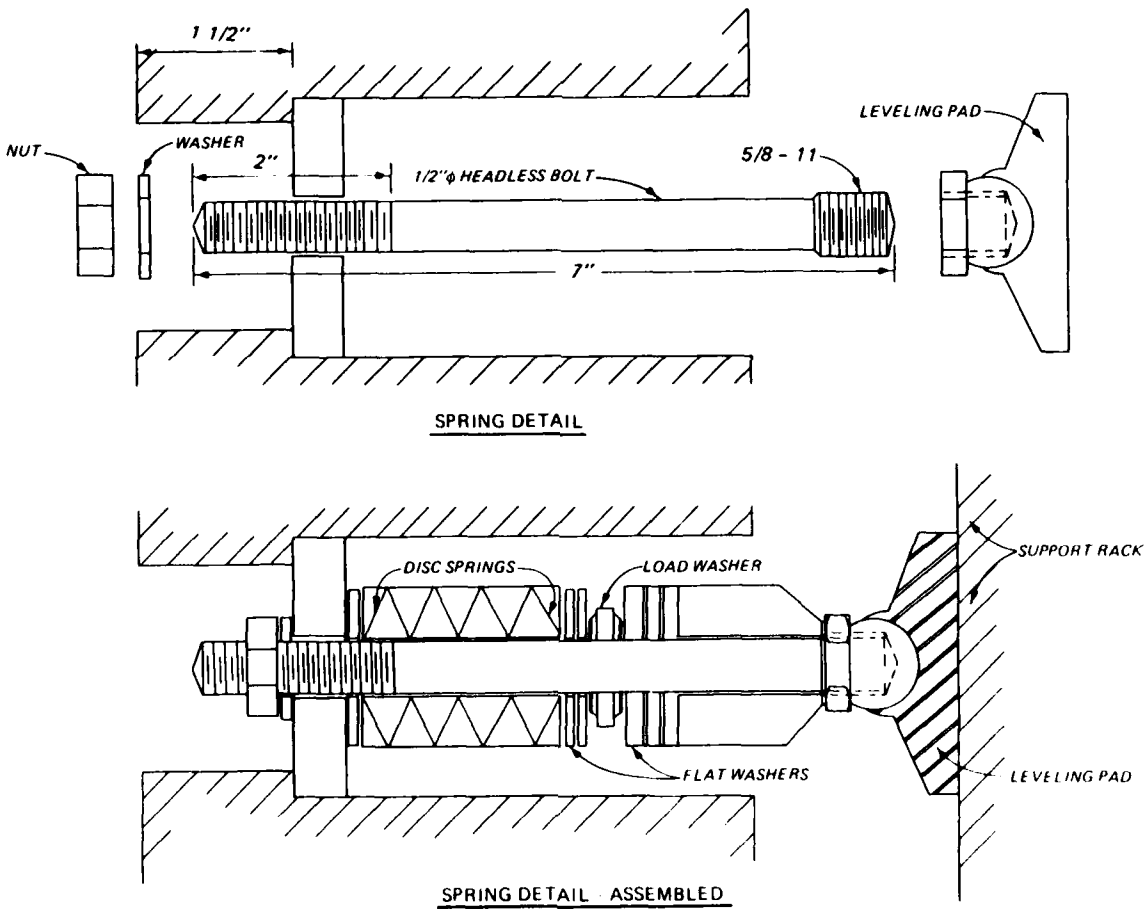

FIG. I.5.-Spring Assembly Details

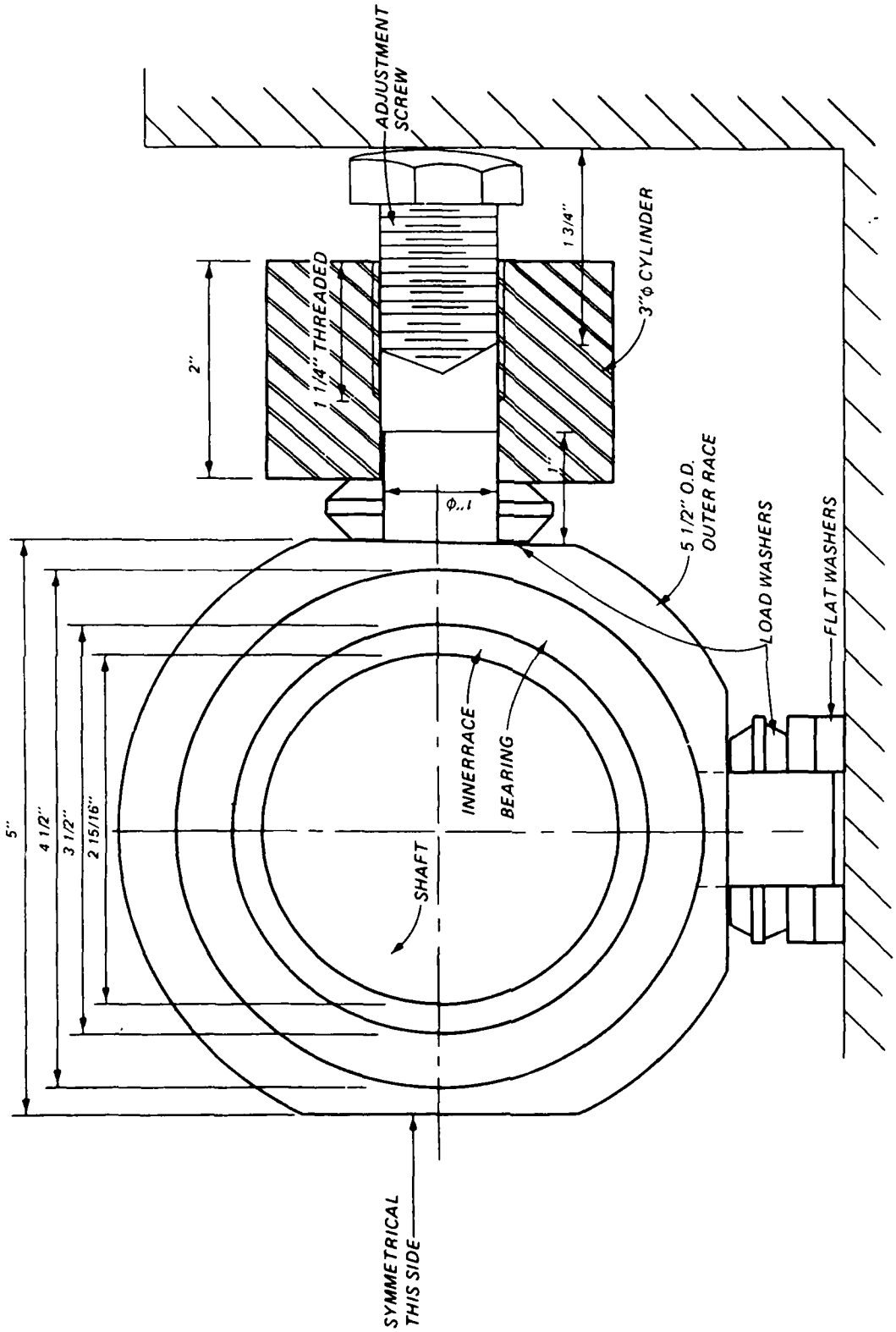

FIG. I.6.-Shaft Assembly Details

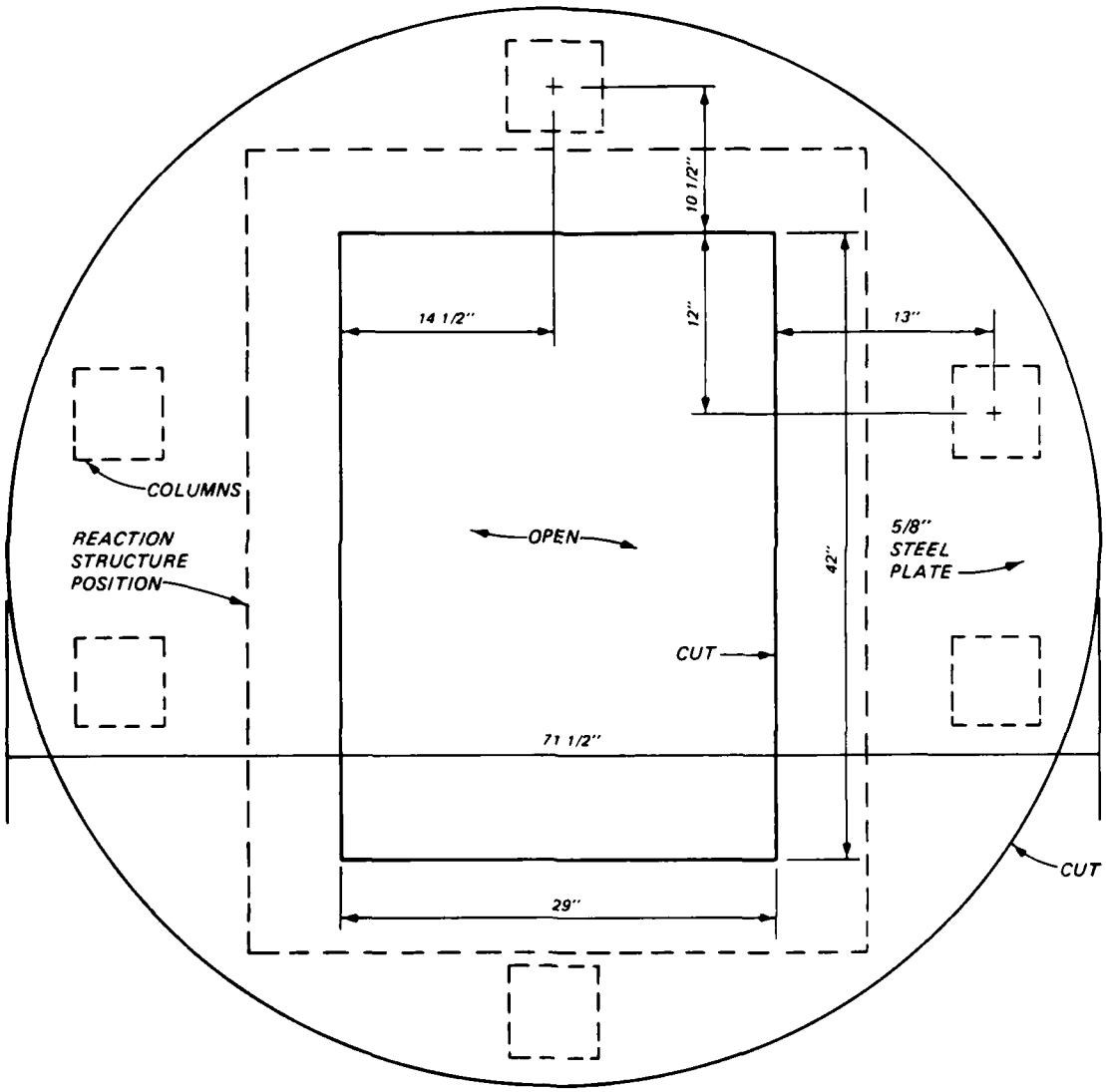

FIG. I.7.-Details for Protective Table

APPENDIX II

PHOTOGRAPHS

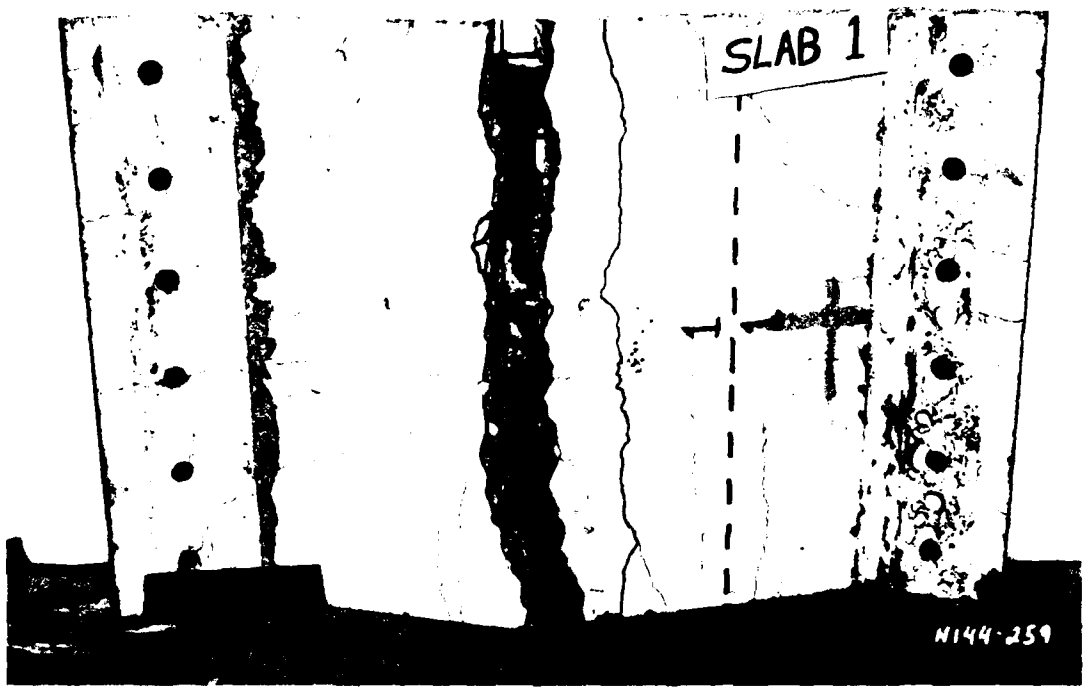

FIG. II.1.-Posttest Bottom View of Slab 1

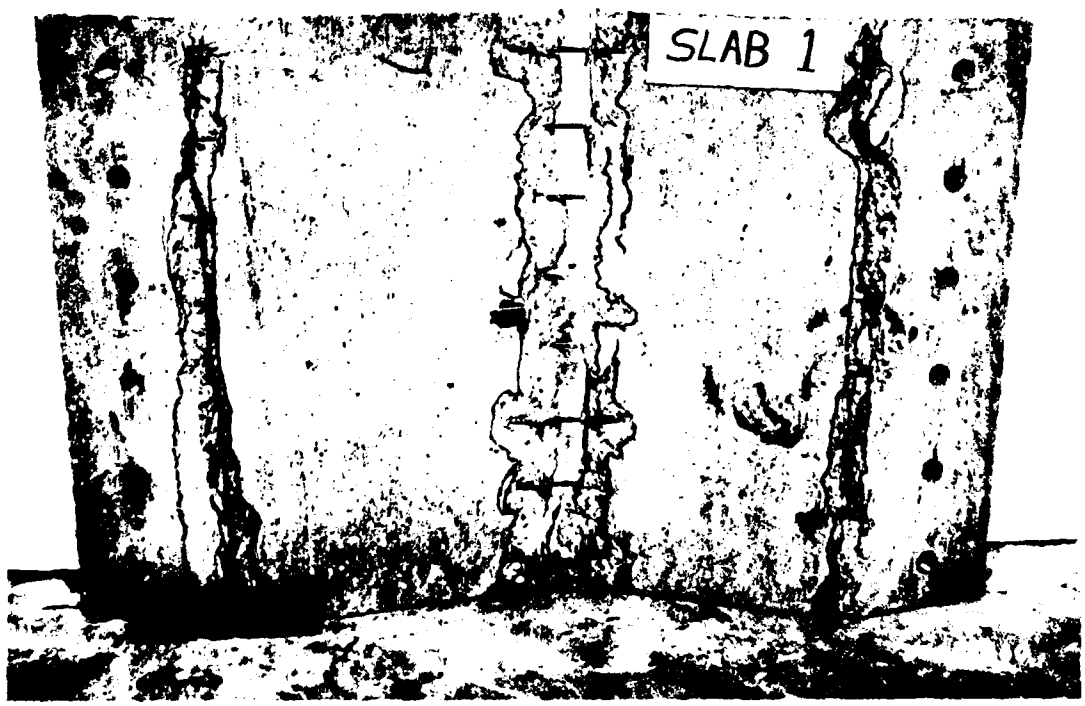

FIG. II.2.-Posttest Top View of Slab 1

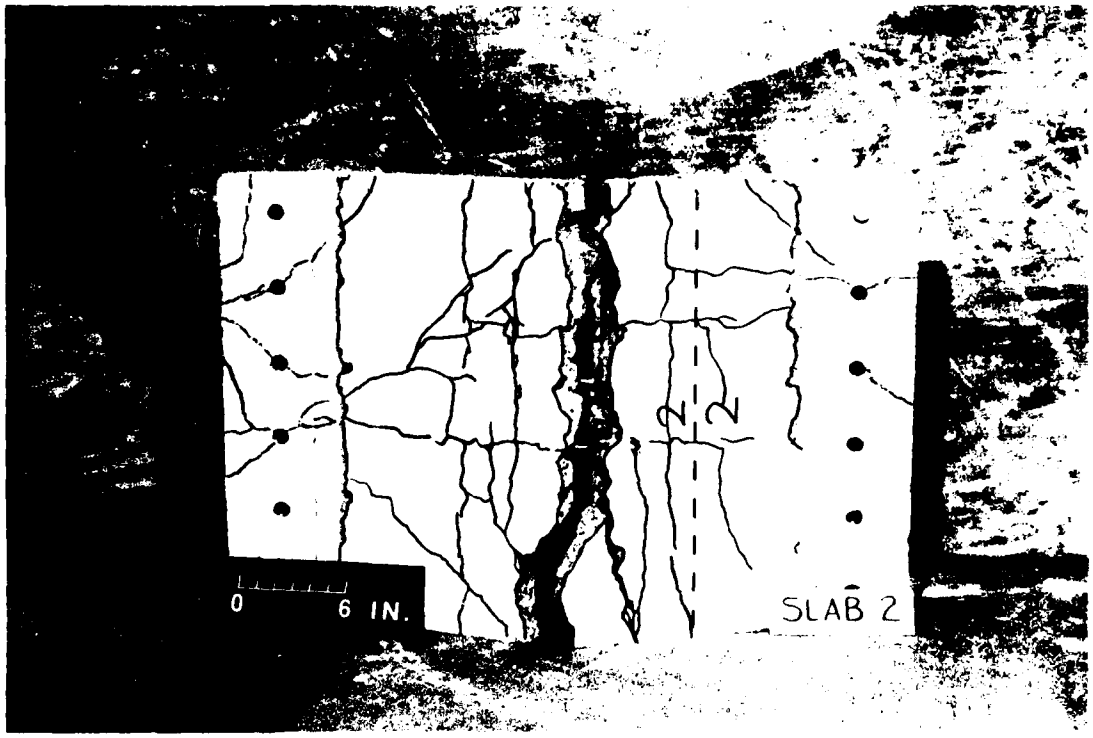

FIG. II.3.-Posttest Bottom View of Slab 2

FIG. II.4.-Posttest Top View of Slab 2

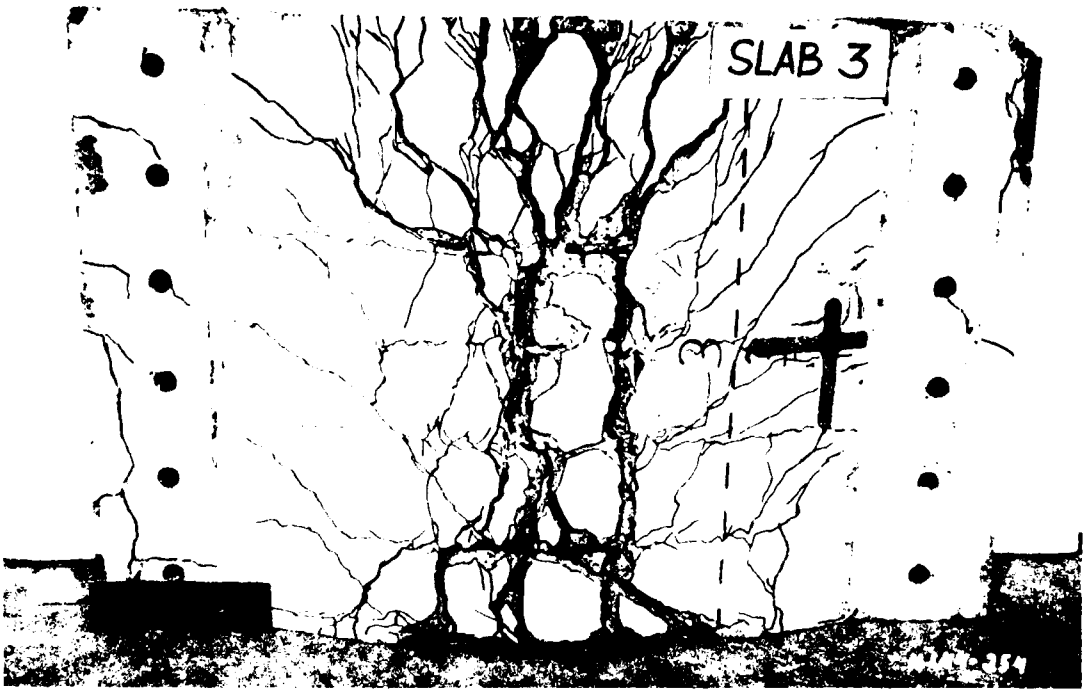

FIG. II.5.-Posttest Bottom View of Slab 3

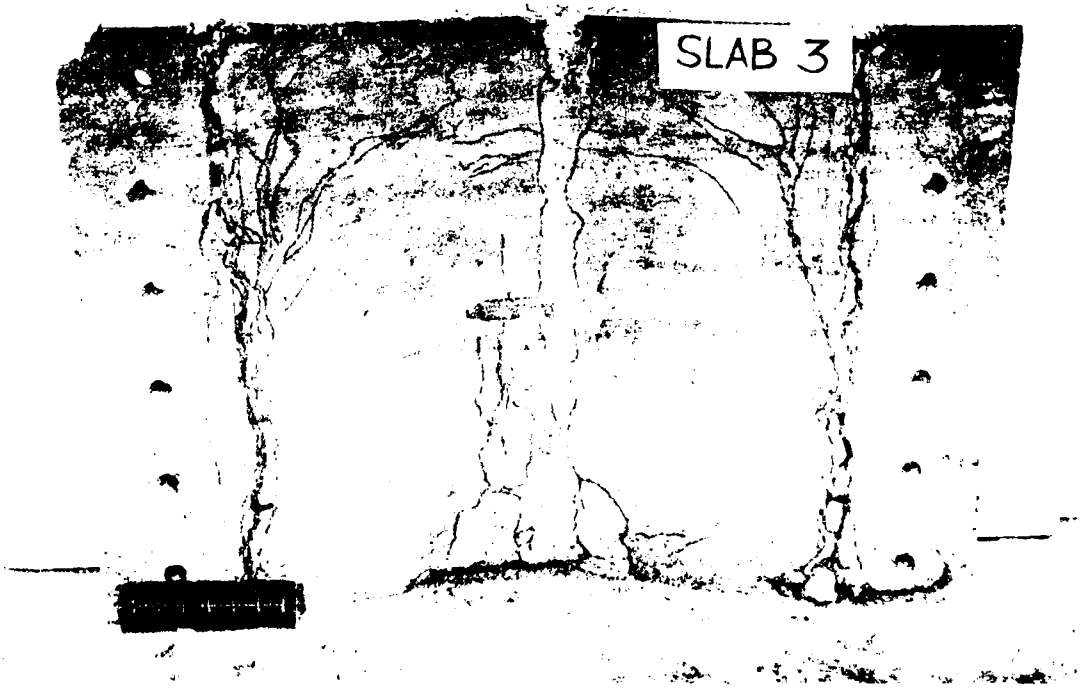

FIG. II.6.-Posttest Top View of Slab 3

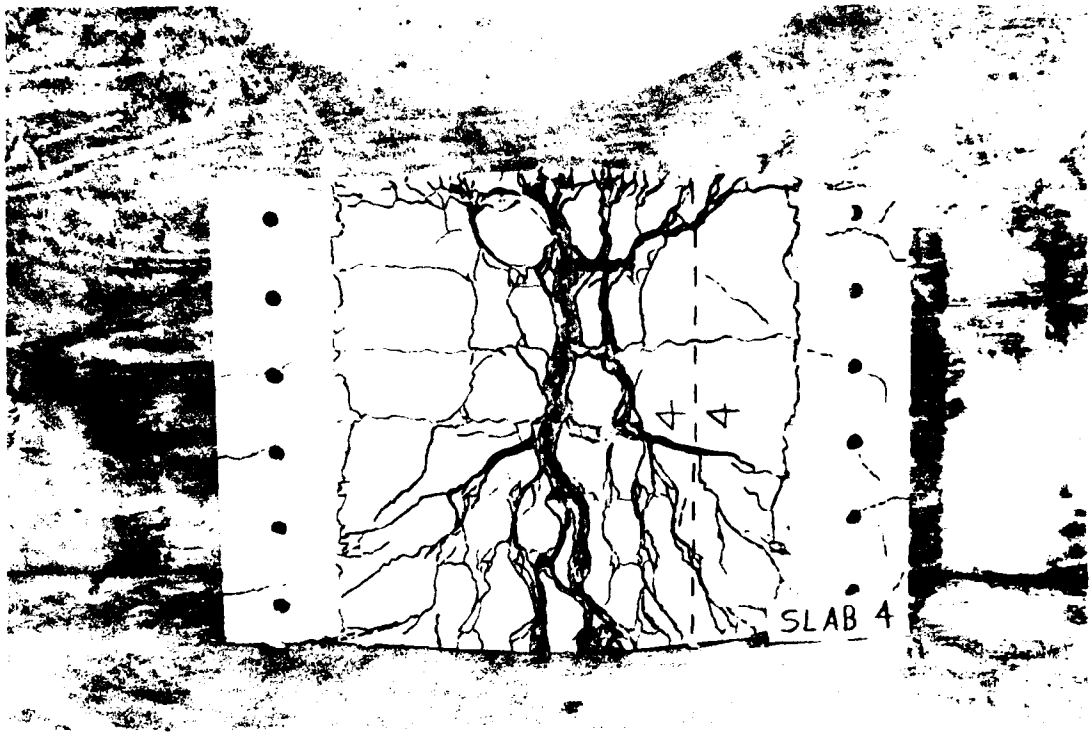

FIG. II.7.-Posttest Bottom View of Slab 4

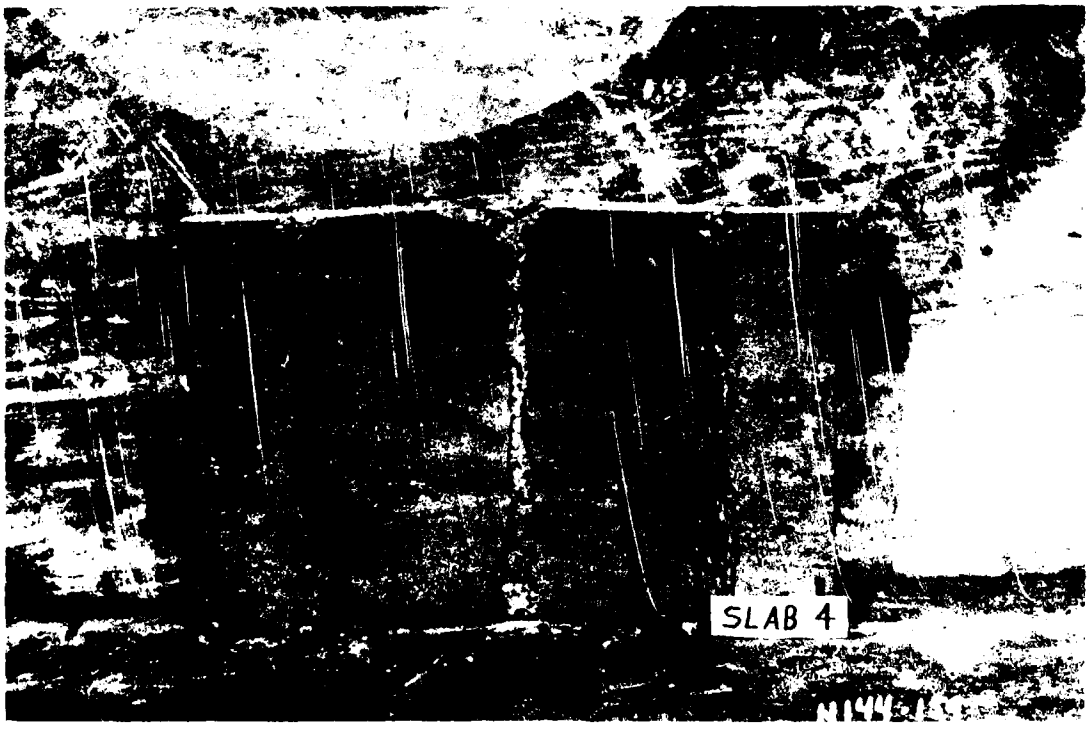

FIG. II.8.-Posttest Top View of Slab 4

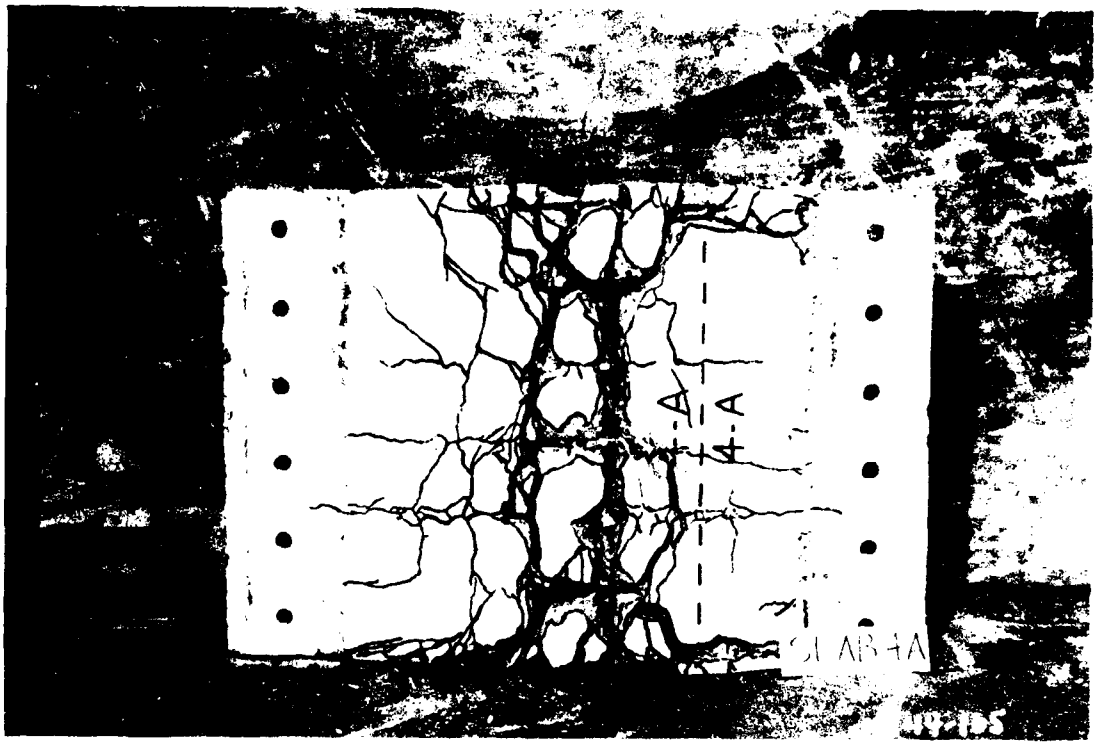

FIG. II.9.-Posttest Bottom View of Slab 4A

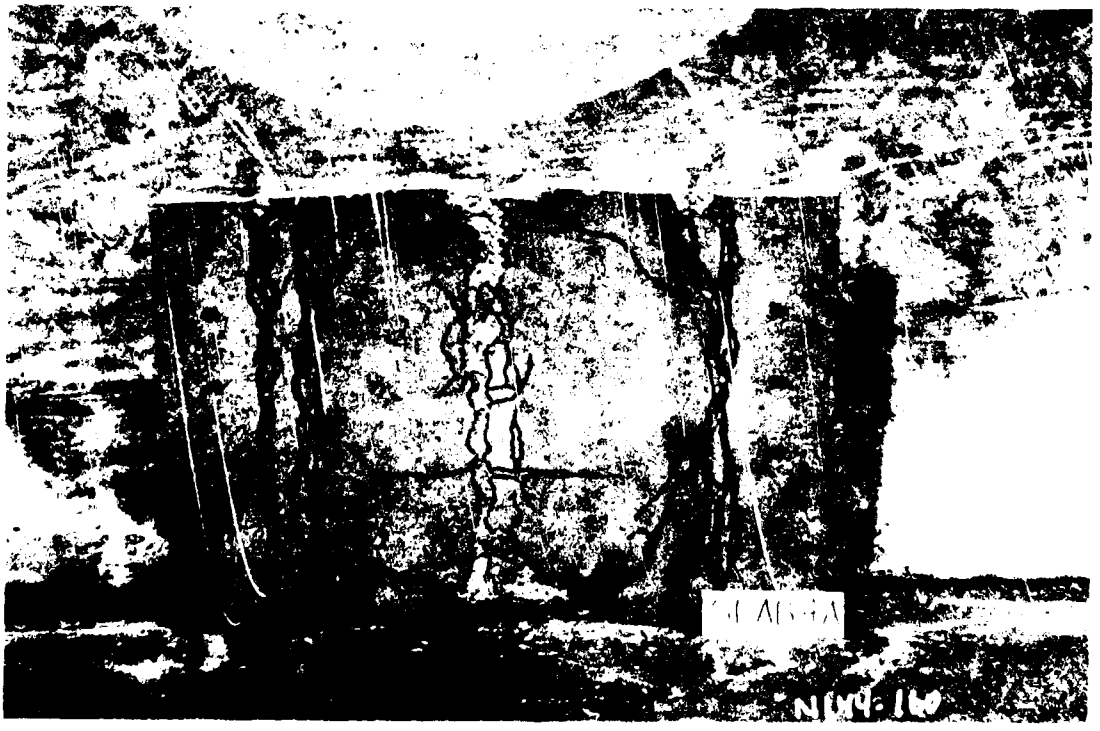

FIG. II.10.-Posttest Top View of Slab 4A

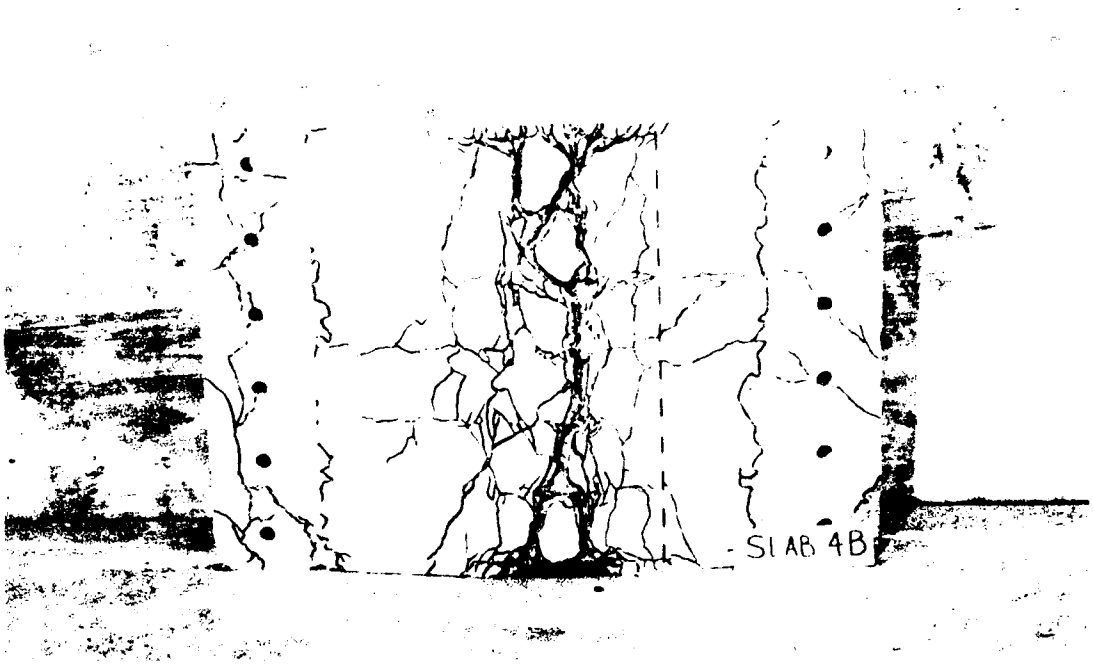

FIG. II.11.-Posttest Bottom View of Slab 4B

FIG. II.12.-Posttest Top View of Slab 4B

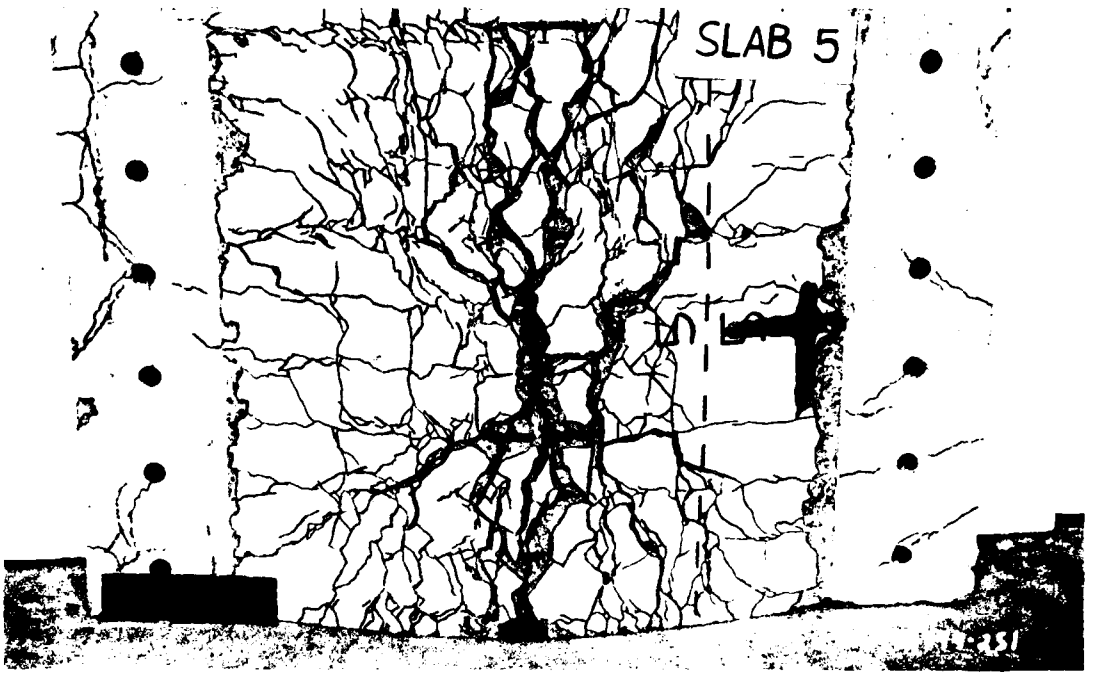

FIG. II.13.-Posttest Bottom View of Slab 5

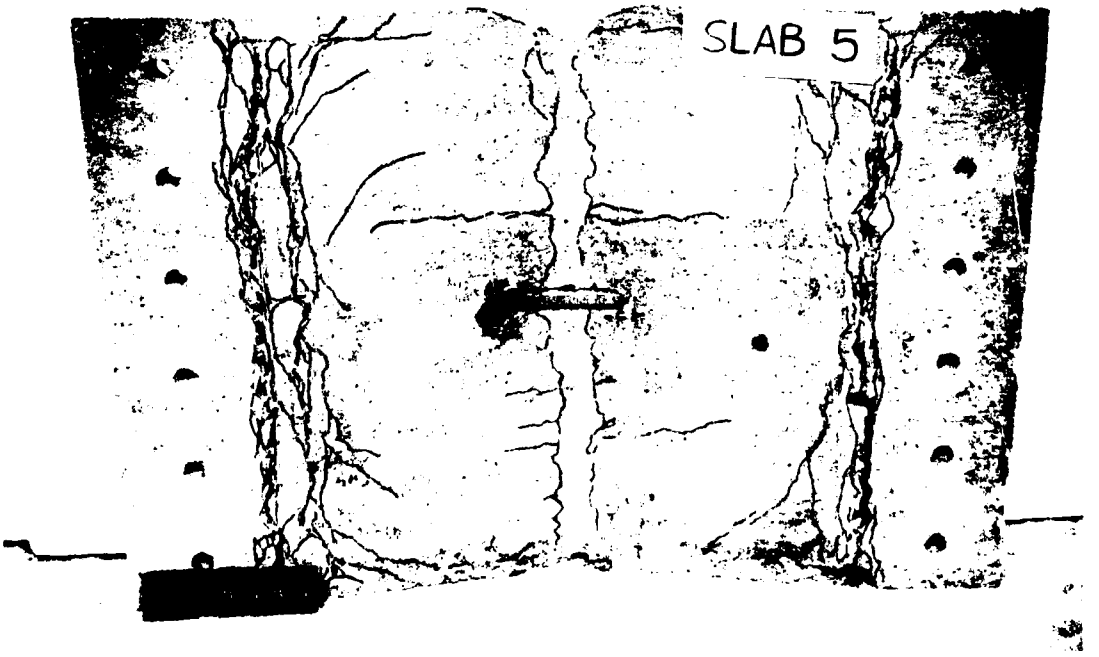

FIG. II.14.-Posttest Top View of Slab 5

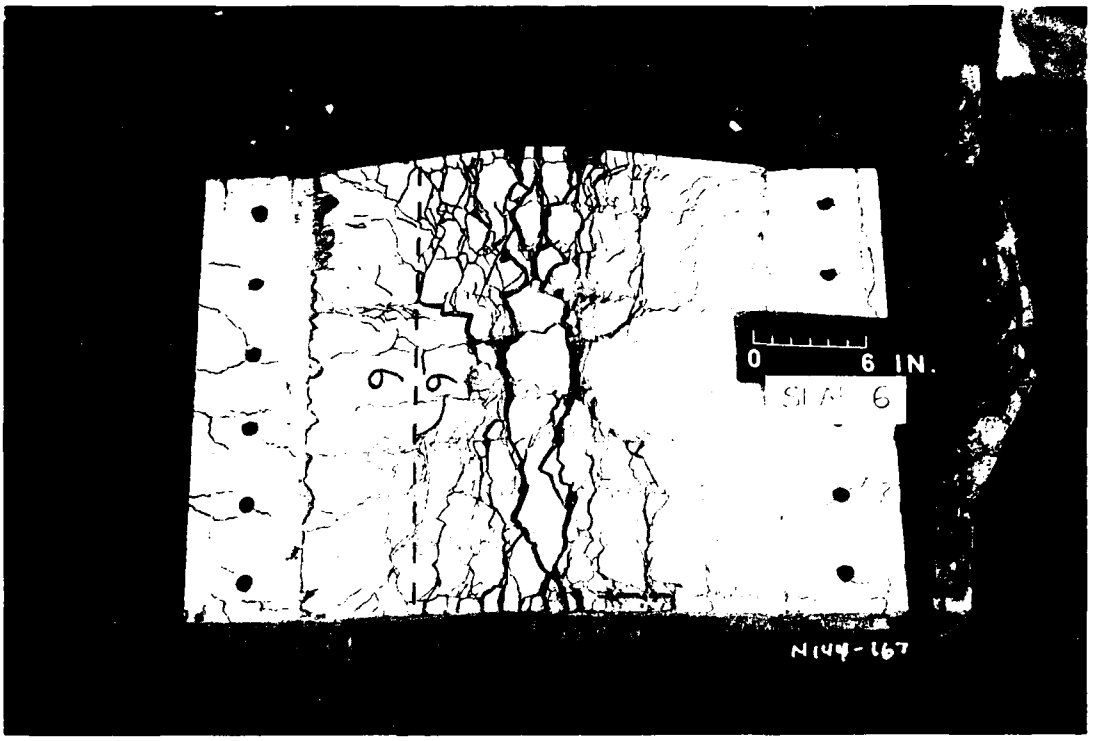

FIG. II.15.-Posttest Bottom View of Slab 6

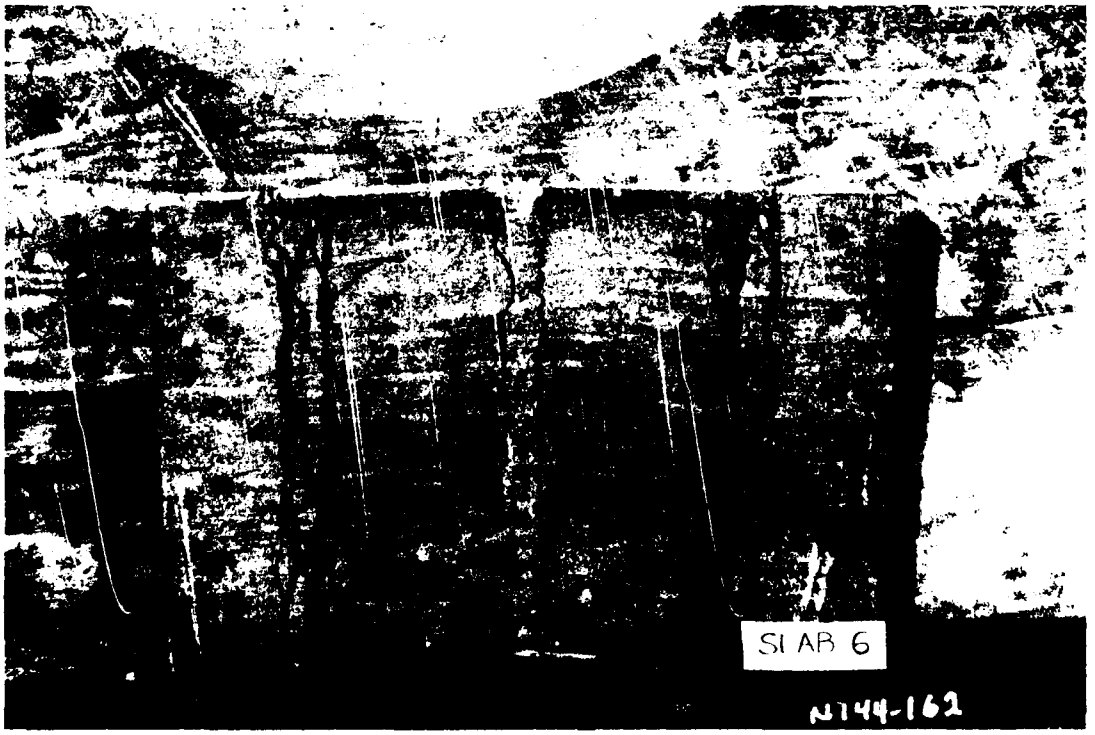

FIG. II.16.-Posttest Top View of Slab 6

FIG. II.17.-Posttest Bottom View of Slab 7

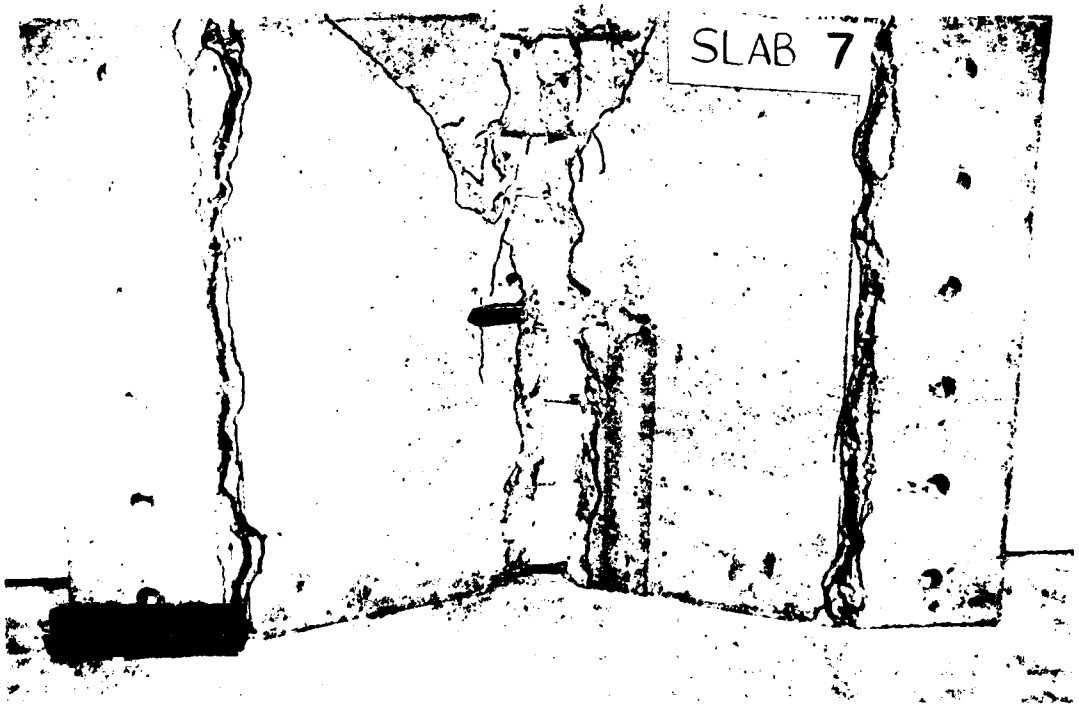

FIG. II.18.-Posttest Top View of Slab 7

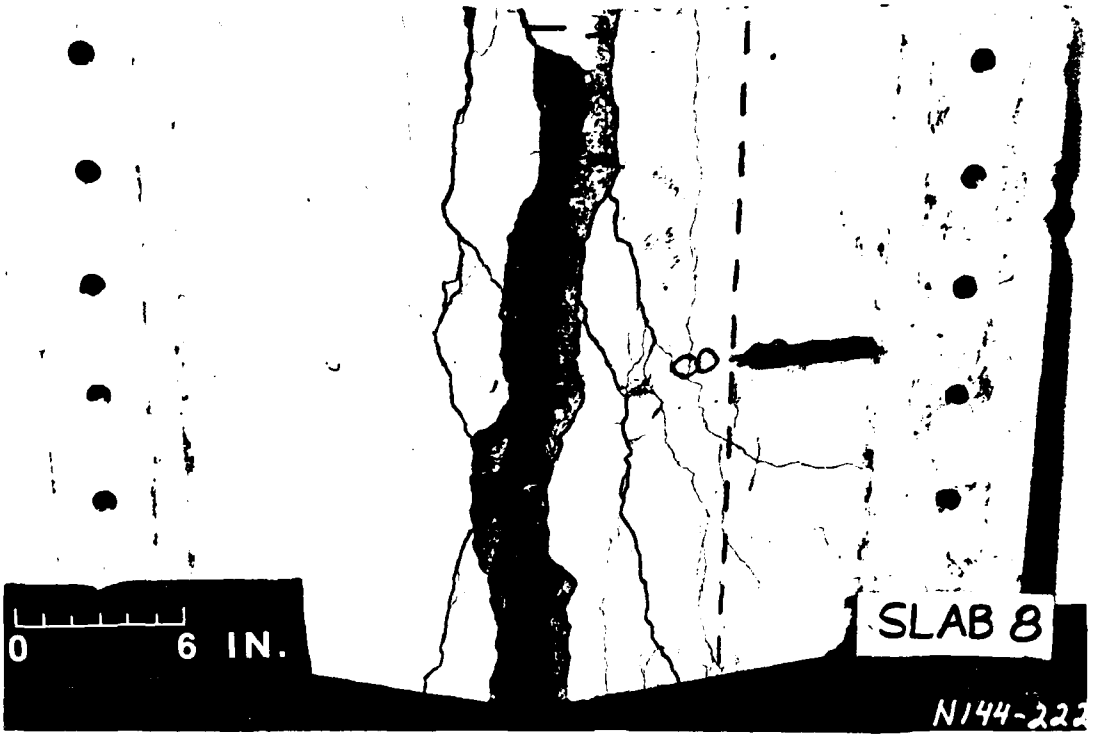

FIG. II.19.-Posttest Bottom View of Slab 8

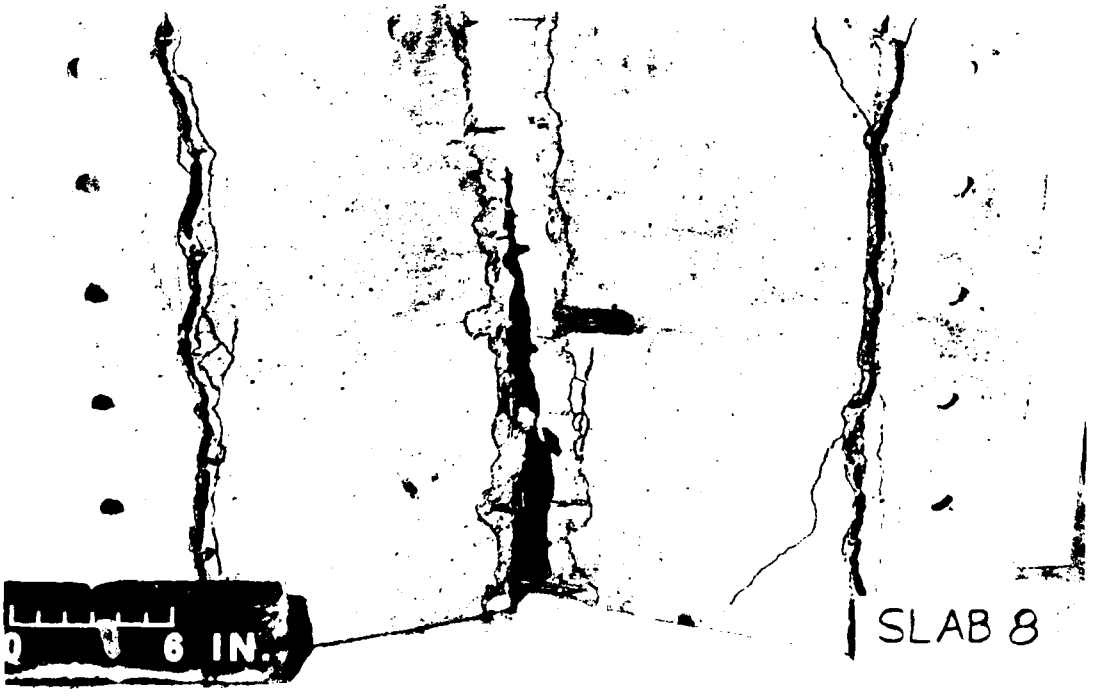

FIG. II.20.-Posttest Top View of Slab 8

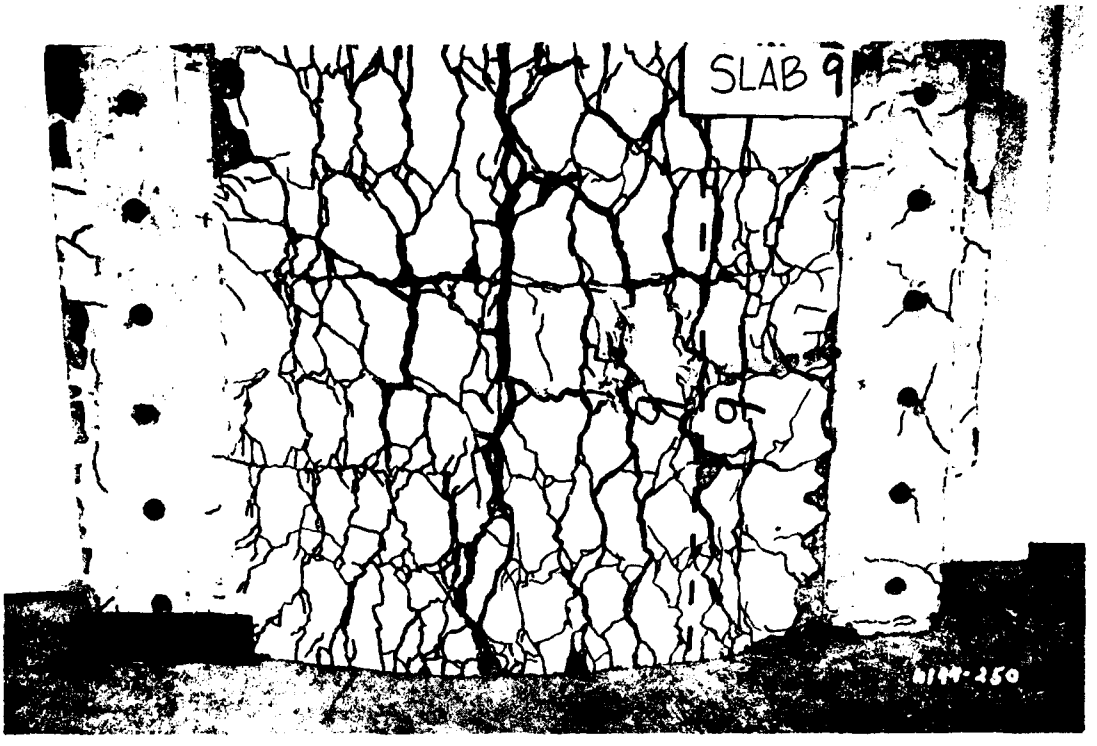

FIG. II.21.-Posttest Bottom View of Slab 9

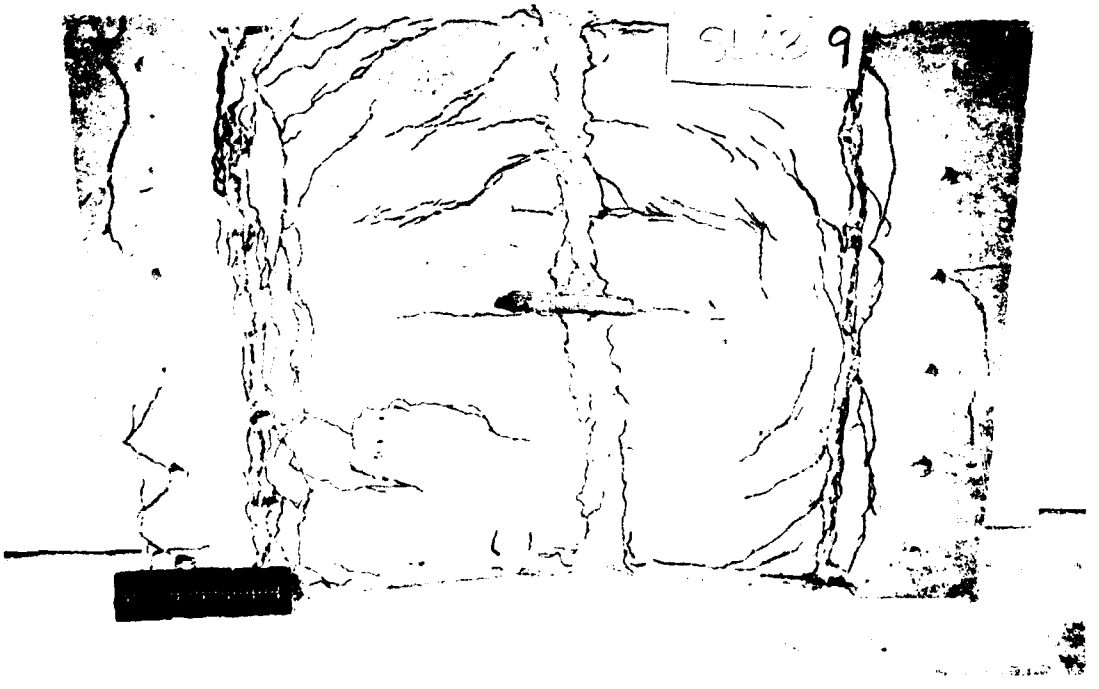

FIG. II.22.-Posttest Top View of Slab 9

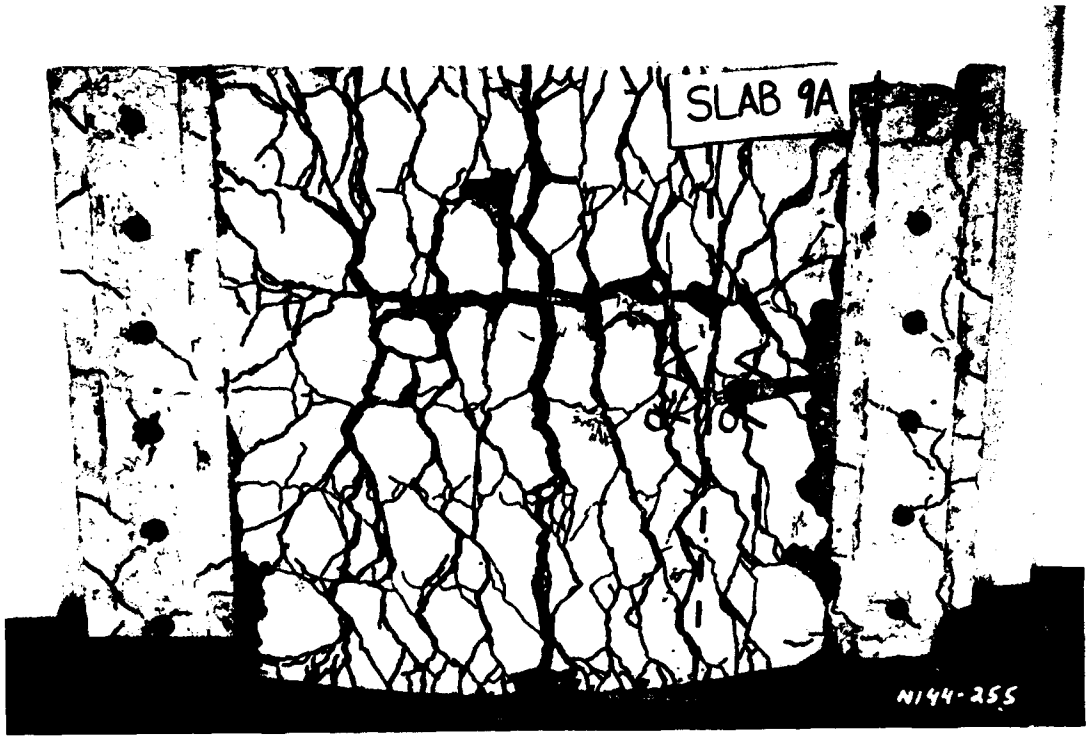

FIG. II.23.-Posttest Bottom View of Slab 9A

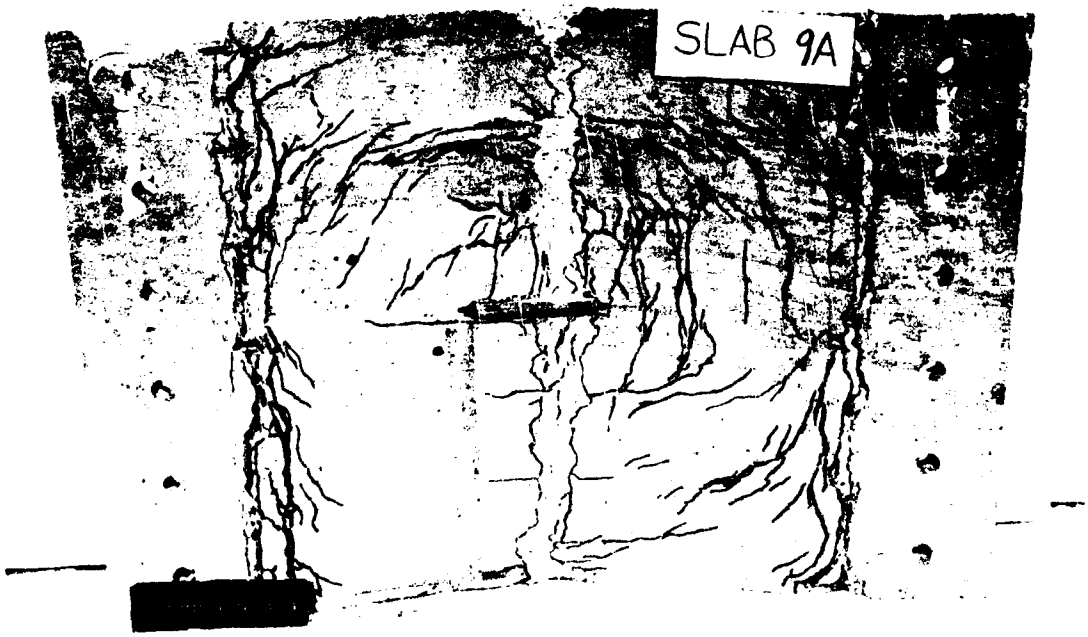

FIG. II.24.-Posttest Top View of Slab 9A

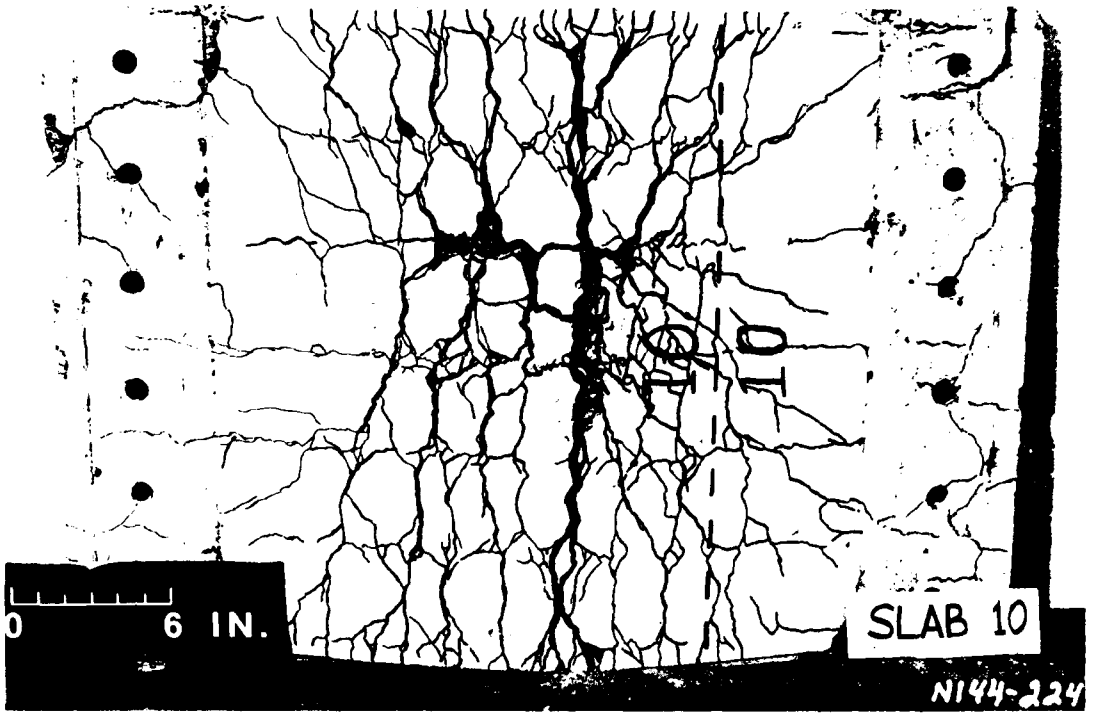

FIG. II.25.-Posttest Bottom View of Slab 10

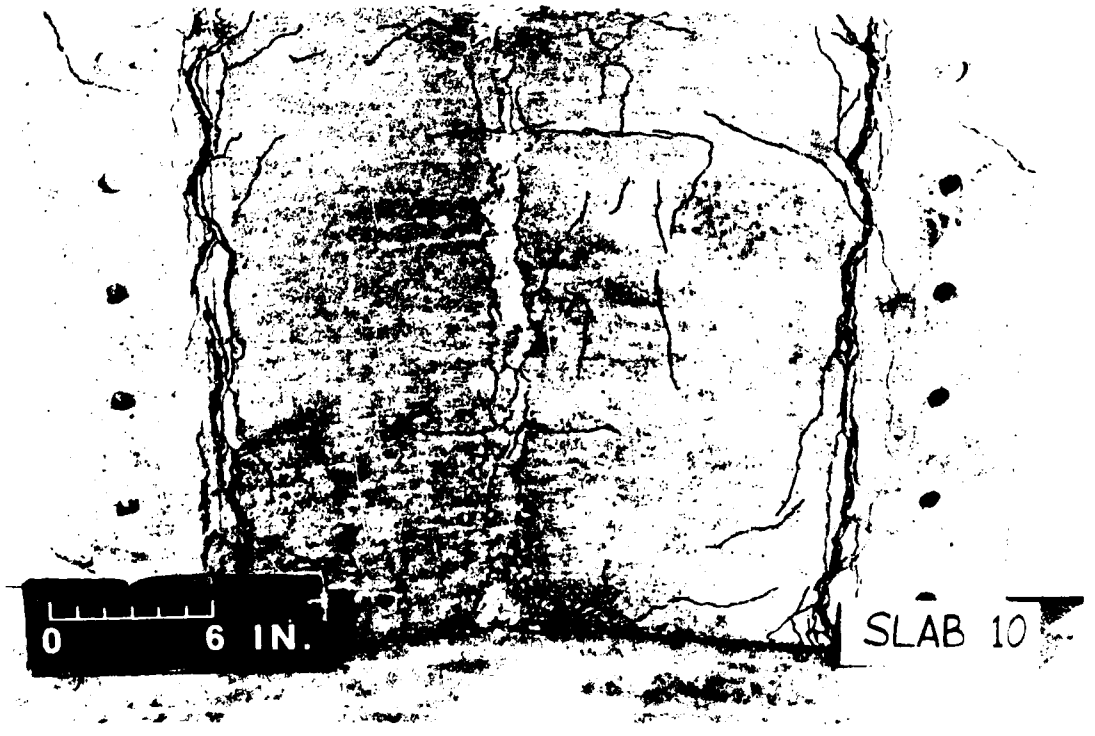

FIG. II.26.-Posttest Top View of Slab 10

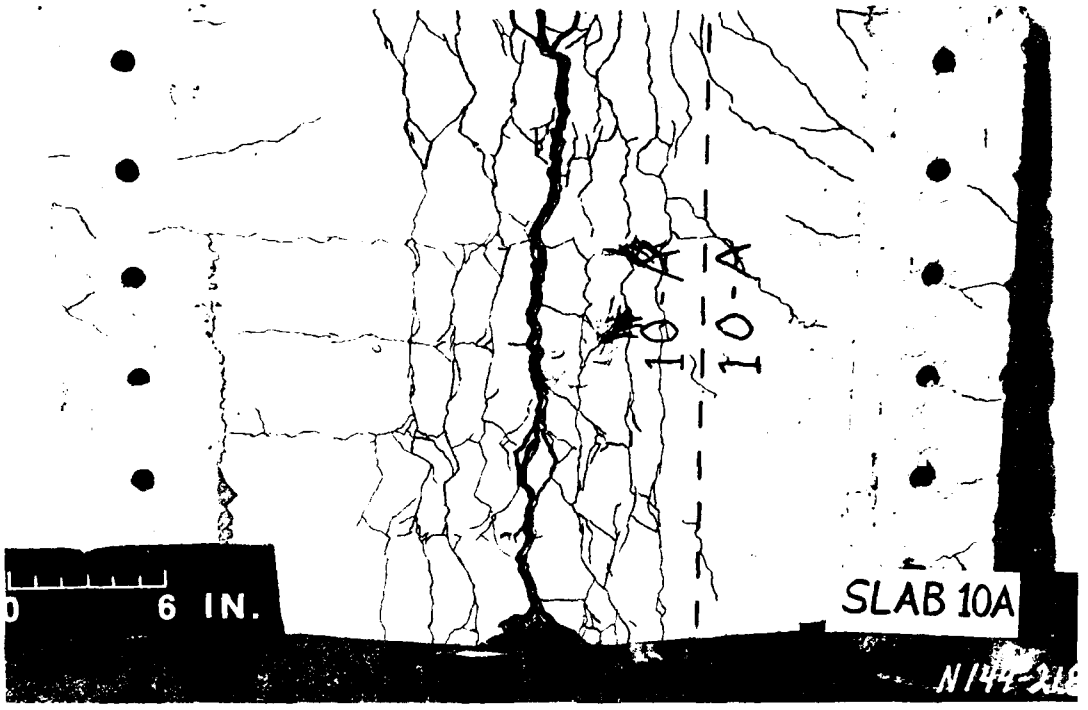

FIG. II.27.-Posttest Bottom View of Slab 10A

FIG. II.28.-Posttest Top View of Slab 10A

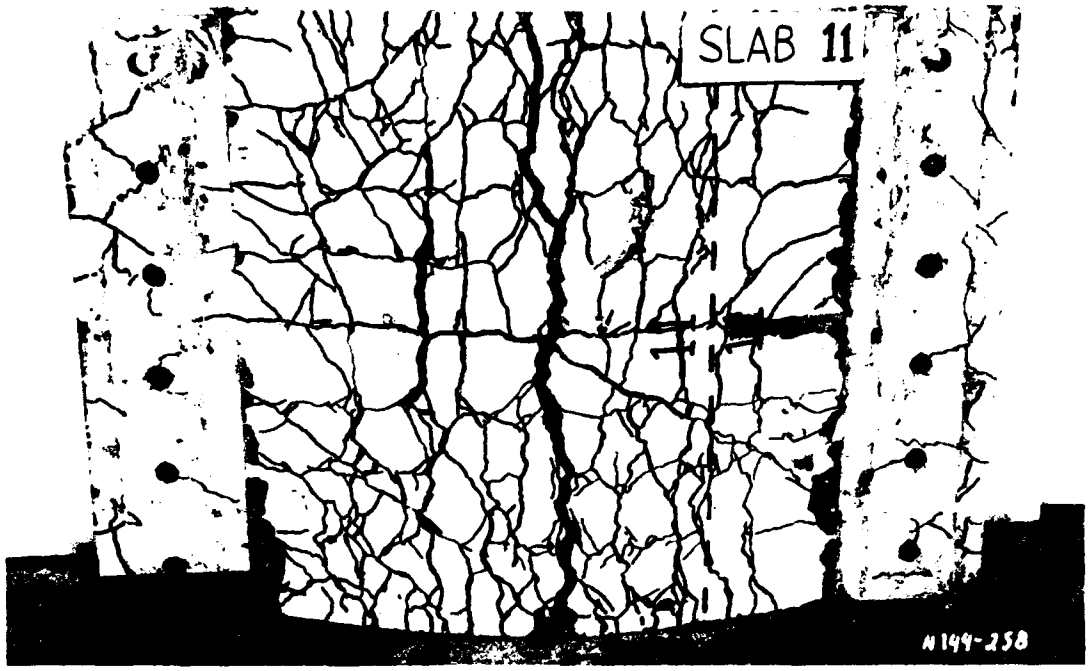

FIG. II.29.-Posttest Bottom View of Slab 11

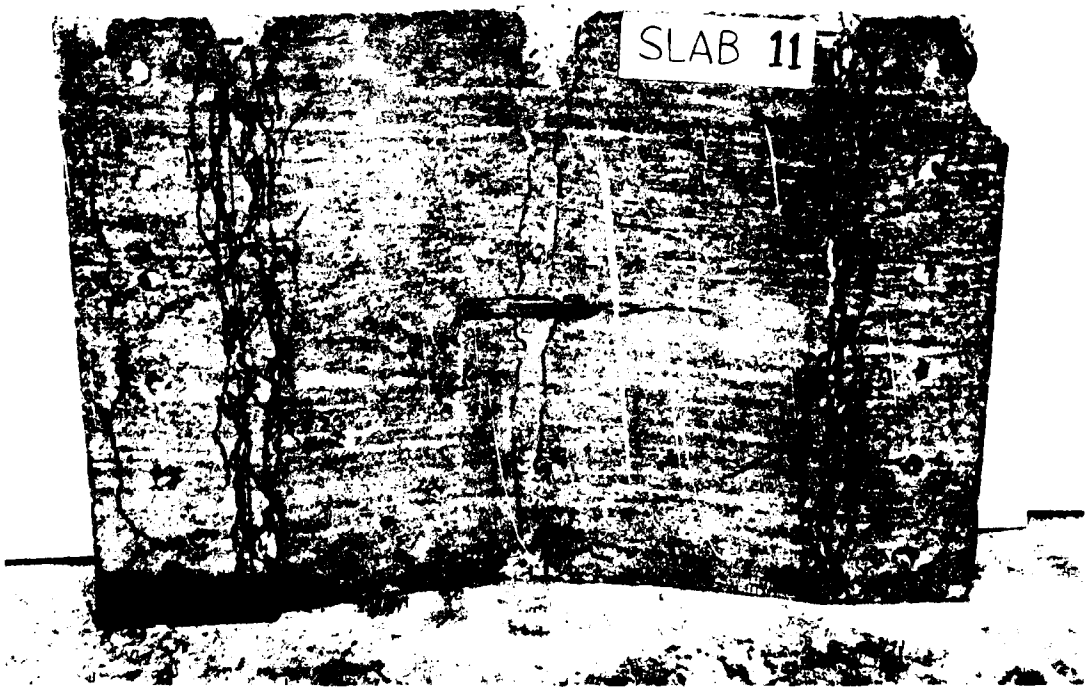

FIG. II.30.-Posttest Top View of Slab 11

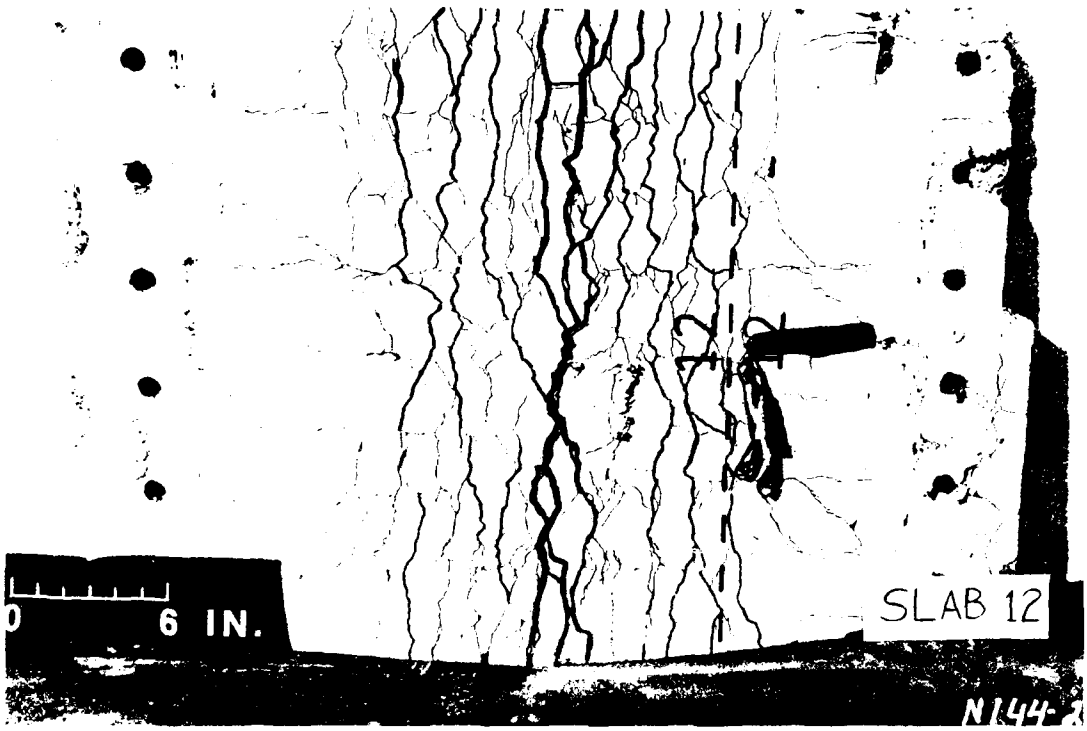

FIG. II.31.-Posttest Bottom View of Slab 12

FIG. II.32.-Posttest Top View of Slab 12

APPENDIX III

NOTATION

AD-A174 597 BEHAVIOR OF PARTIALLY RESTRAINED REINFORCED CONCRETE SLABS(U) ARMY ENGINEER WATERWAYS EXPERIMENT STATION VICKSBURG MS STRUCTURES LAB L K GUICE SEP 86 3/3

UNCLASSIFIED WES/TR/SL-86-32 F/G 13/3 NL

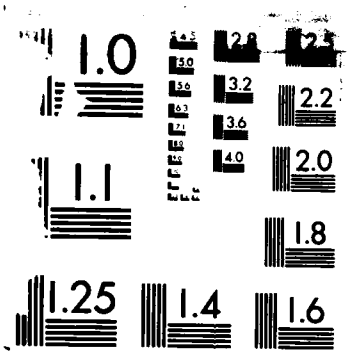

MICROCOPY RESOLUTION TEST CHART
STANDARDS 1963-A

The following symbols are used in this paper:

A = gross cross-sectional area of the slab strip;

a = depth of Whitney's stress block; half slab length;

B = slab width;

C_c, C_{cm}, C_{cs} = Compressive force in concrete, at midspan, and at supports, respectively;

C_s, C_{sm}, C_{ss} = Compressive force in steel, at midspan, and at supports, respectively;

c, c_m, c_s = depth of neutral axis, at midspan, and at supports, respectively;

d, d' = depth from compression surface to tensile reinforcement and compressive reinforcement, respectively;

d_b = bar diameter;

E = modulus of elasticity for analytical model;

e = deformation in analytical model;

f'_c = compressive cylinder strength of concrete;

f_y = yield strength of steel;

h = slab thickness;

L = slab length;

l_x, l_y = long span length and short span length, respectively;

M_n, M_{nm}, M_{ns} = nominal moment of resistance along hinge lines, at midspan, and at supports, respectively;

N = total thrust;

P = equivalent vertical concentrated force;

p = applied surface forces;

Q, Q_L, Q_{NL} = total internal forces, linear and nonlinear portions, respectively;

q, q_1, q_2 = nodal displacement, in global x and y directions, respectively;

S = surface area of slab;

s, s_e = spacing of principal steel within slab strip and at the edge of the strip, respectively;

T, T_m, T_s = total tensile force carried by steel, at midspan and supports, respectively;

t = lateral support movement;

U = internal potential energy;

U_t = total potential energy;

$u(x)$ = displacement along axis of member;

u_1 = nodal displacement in local coordinates;

V = external potential energy; volume;

$v(x)$ = displacement perpendicular to axis of member;

v_1 = transverse nodal displacement in local coordinates;

W_{jf}, W_{js} = Johansen's load for fixed and simple supports, respectively;

W_u = ultimate load;

w = uniform pressure on the slab;

X, x = global and local coordinate directions, respectively; portion of slab length;

Y, y = global and local coordinate directions, respectively;

β = fraction of slab length to plastic hinge;

β_1 = Whitney's stress block relationship;

δ = midspan deflection;

∂ = differential operator;

ε = normal strain;

ε_c = strain in outer fiber of concrete;

ε_p = creep and shrinkage strain;

ε_u = ultimate strain in concrete;

σ = normal stress;

θ = rotation of slab element;

θ_i = initial inclination of slab model;

ϕ_m = midspan curvature;

DISTRIBUTION LIST

Director, Federal Emergency Management Agency
ATTN: Mr. Tom Provenzano (6 Cys)
500 C St. SW
Washington, DC 20472

Commander, US Army Engineer District, Wilmington
ATTN: Pat Burns/Library
PO Box 1890
Wilmington, N. C. 28402

Headquarters, Department of Energy
ATTN: Library/G-049 MA-232.2/GTN
Washington, DC 20545

National Bureau of Standards
ATTN: Mr. Samuel Kramer
Dr. Lewis V. Spencer
Washington, DC 20234

Associate Director, Natural Resources and
Commercial Services
Office of Science & Technology
ATTN: Mr. Phillip M. Smith
Executive Office Building
Washington, DC 20500

Director, Office of Administration
Program Planning and Control
Department of Housing and Urban Development
ATTN: Mr. Bert Greenglass
Washington, DC 20410

Director, Defense Nuclear Agency
ATTN: SPTD/Mr. Tom Kennedy
STTL/Technical Library
Washington, DC 20305

Director, Defense Intelligence Agency
ATTN: Mr. Carl Wiehle (DB-4C2)
Washington, DC 20301

Assistant Secretary of the Army (R&D)
ATTN: Assistant for Research
Washington, DC 20301

Office, Chief of Engineers,
Department of the Army
ATTN: DAEN-RDZ-A
DAEN-ECE-D
Washington, DC 20314

Sandia Corporation
ATTN: Dr. Clarence R. Mehl
Dept. 5230
Box 5800, Sandia Base
Albuquerque, N. Mex. 87115

Director, US Army Engineer Waterways
Experiment Station
ATTN: Dr. S. A. Kiger
Mr. Bill Huff
Mr. Stan Woodson
3 cys Library
5 cys WESSS/Mr. Les Guice
P. O. Box 631
Vicksburg, Miss. 39180

Defense Technical Information Center
12 cy ATTN: (DTIC-DDAB/Mr. Myer B. Kahn)
Cameron Station
Alexandria, Va. 22314

Commander, US Army Materials and Mechanics
Research Center
ATTN: Technical Library
Watertown, Mass. 02172

Command and Control Technical Center
Department of Defense
Room 2E312 Pentegon
Washington, DC 20301

Los Alamos Scientific Laboratory
ATTN: Report Library MS-364
PO Box 1663
Los Alamos, N. Mex. 87544

Director, Ballistic Research Laboratory
ATTN: (DRXBR-TBD/Mr. George Coulter)
Aberdeen Proving Ground, Md. 21005

Commanding Officer, Office of Naval Research
Department of the Navy
Washington, DC 20390

Commanding Officer
US Naval Civil Engineering Laboratory
Naval Construction Battalion Center
ATTN: Library (Code L08A)
Port Hueneme, Calif. 93043

Commander, Air Force Weapons Laboratory/SUL
ATTN: Technical Library
Kirtland Air Force Base, N. Mex. 87117

Civil Engineering Center
AF/PRECET
Tyndall AFB, Fla. 32403

University of Florida
Civil Defense Technical Services
College of Engineering
Department of Engineering
Gainesville, Fla. 32601

Technical Reports Library
Kurt F. Wendt Library
College of Engineering
University of Wisconsin
Madison, Wisc. 53706

Agbabian Associates
250 N. Nash Street
El Segundo, Calif. 90245

AT&T Bell Laboratories
ATTN: Mr. E. Witt
Whippany, N. J. 07981

James E. Beck & Associates
4216 Los Palos Avenue
Palo Alto, Calif. 94306

Chamberlain Manufacturing Corp.
GARD, Inc.
7449 N. Natchez Avenue
Niles, Ill. 60648

ITT Research Institute
ATTN: Mr. A. Longinow
10 West 35th Street
Chicago, Ill. 60616

H. L. Murphy Associates
Box 1727
San Mateo, Calif. 94401

RAND Corporation
ATTN: Document Library
1700 Main Street
Santa Monica, Calif. 90401

Research Triangle Institute
ATTN: Mr. Edward L. Hill
PO Box 12194
Research Triangle Park, N. C. 27709

Scientific Services, Inc.
517 East Bayshore Drive
Redwood City, Calif. 94060

US Army Engineer Division, Huntsville
ATTN: Mr. Paul Iahoud (13 cys)
PO Box 1600, West Station
Huntsville, Al 35807

BEHAVIOR OF PARTIALLY RESTRAINED REINFORCED CONCRETE SLABS, Unclassified, US Army Engineer Waterways Experiment Station, September 1986, 197 pp.

This study was performed in conjuction with a Federal Emergency Management Agency program to plan, design, and construct Keyworker blast shelters. Keyworker shelters are box-type shelters in which damage is more likely in the roof slab than in the walls or floor. This study investigates the effect of partial edge restraint on the strength, ductility, and failure mechanism of a slab. Sixteen one-way, reinforced concrete plate elements were tested in a specially designed reaction structure under uniform static water pressure. Facilities were designed and constructed to measure the slab end actions, including thrusts, moments, and rotations. The primary parameters investigated included the span-thickness ratio, reinforcement ratio, and degree of edge restraint. Most slabs were loaded until significant tensile membrane forces developed. Rotational restraint significantly influenced overall slab behavior. If a slab is to develop significant compressive membrane forces, both lateral and rotational restraint must be provided. Small rotational freedoms had a relatively small effect on the slab's compressive membrane response. With large rotational freedoms, however, the slabs generally snapped through to the tensile membrane stage before significant thrusts were developed. Thin slabs generally exhibited a much better tensile membrane response than thicker slabs and underwent larger deflections before collapse. Recommendations are presented and an analytical procedure which considers nonlinear geometric behavior is proposed for investigating total slab response.

BEHAVIOR OF PARTIALLY RESTRAINED REINFORCED CONCRETE SLABS, Unclassified, US Army Engineer Waterways Experiment Station, September 1986, 197 pp.

This study was performed in conjuction with a Federal Emergency Management Agency program to plan, design, and construct Keyworker blast shelters. Keyworker shelters are box-type shelters in which damage is more likely in the roof slab than in the walls or floor. This study investigates the effect of partial edge restraint on the strength, ductility, and failure mechanism of a slab. Sixteen one-way, reinforced concrete plate elements were tested in a specially designed reaction structure under uniform static water pressure. Facilities were designed and constructed to measure the slab end actions, including thrusts, moments, and rotations. The primary parameters investigated included the span-thickness ratio, reinforcement ratio, and degree of edge restraint. Most slabs were loaded until significant tensile membrane forces developed. Rotational restraint significantly influenced overall slab behavior. If a slab is to develop significant compressive membrane forces, both lateral and rotational restraint must be provided. Small rotational freedoms had a relatively small effect on the slab's compressive membrane response. With large rotational freedoms, however, the slabs generally snapped through to the tensile membrane stage before significant thrusts were developed. Thin slabs generally exhibited a much better tensile membrane response than thicker slabs and underwent larger deflections before collapse. Recommendations are presented and an analytical procedure which considers nonlinear geometric behavior is proposed for investigating total slab response.

BEHAVIOR OF PARTIALLY RESTRAINED REINFORCED CONCRETE SLABS, Unclassified, US Army Engineer Waterways Experiment Station, September 1986, 197 pp.

This study was performed in conjuction with a Federal Emergency Management Agency program to plan, design, and construct Keyworker blast shelters. Keyworker shelters are box-type shelters in which damage is more likely in the roof slab than in the walls or floor. This study investigates the effect of partial edge restraint on the strength, ductility, and failure mechanism of a slab. Sixteen one-way, reinforced concrete plate elements were tested in a specially designed reaction structure under uniform static water pressure. Facilities were designed and constructed to measure the slab end actions, including thrusts, moments, and rotations. The primary parameters investigated included the span-thickness ratio, reinforcement ratio, and degree of edge restraint. Most slabs were loaded until significant tensile membrane forces developed. Rotational restraint significantly influenced overall slab behavior. If a slab is to develop significant compressive membrane forces, both lateral and rotational restraint must be provided. Small rotational freedoms had a relatively small effect on the slab's compressive membrane response. With large rotational freedoms, however, the slabs generally snapped through to the tensile membrane stage before significant thrusts were developed. Thin slabs generally exhibited a much better tensile membrane response than thicker slabs and underwent larger deflections before collapse. Recommendations are presented and an analytical procedure which considers nonlinear geometric behavior is proposed for investigating total slab response.

BEHAVIOR OF PARTIALLY RESTRAINED REINFORCED CONCRETE SLABS, Unclassified, US Army Engineer Waterways Experiment Station, September 1986, 197 pp.

This study was performed in conjuction with a Federal Emergency Management Agency program to plan, design, and construct Keyworker blast shelters. Keyworker shelters are box-type shelters in which damage is more likely in the roof slab than in the walls or floor. This study investigates the effect of partial edge restraint on the strength, ductility, and failure mechanism of a slab. Sixteen one-way, reinforced concrete plate elements were tested in a specially designed reaction structure under uniform static water pressure. Facilities were designed and constructed to measure the slab end actions, including thrusts, moments, and rotations. The primary parameters investigated included the span-thickness ratio, reinforcement ratio, and degree of edge restraint. Most slabs were loaded until significant tensile membrane forces developed. Rotational restraint significantly influenced overall slab behavior. If a slab is to develop significant compressive membrane forces, both lateral and rotational restraint must be provided. Small rotational freedoms had a relatively small effect on the slab's compressive membrane response. With large rotational freedoms, however, the slabs generally snapped through to the tensile membrane stage before significant thrusts were developed. Thin slabs generally exhibited a much better tensile membrane response than thicker slabs and underwent larger deflections before collapse. Recommendations are presented and an analytical procedure which considers nonlinear geometric behavior is proposed for investigating total slab response.

END

1-87

DTIC